NTNU – Trondheim
Norwegian University of
Science and Technology

Analysis of Riser-induced Loading on Wellhead

André Lylund

Subsea Technology
Submission date: June 2015
Supervisor: Bernt Johan Leira, IMT

Norwegian University of Science and Technology
Department of Marine Technology

NTNU
Norwegian University of Science and Technology
Department of Marine Technology

Master Thesis, Spring 2015
of
Master Student Andre Lylund

Analysis of Riser-induced Loading on Wellhead

Analyse av stigerørs-induserte belastninger på brønnhode

Fatigue of the wellhead for subsea-completed wells is a growing problem. This is partly due to the often extended life of the well from the original plan, due to the drilling of side-wells and the considerable maintenance which is performed, etc. New Blow out Preventers are often larger and heavier and new hydraulic tension systems are applied in order to keep the riser in tension. Especially in shallow water the stress on the wellhead is significant because of the forces transferred from the riser. Cracks in the wellhead can result in leakage and loss of the well. It is therefore of great importance that the load is kept at an acceptable level to ensure the well's integrity.

The following subjects are to be examined in this master thesis:

1. The candidate shall give a general description of the main components of a drilling riser system.

2. The candidate shall perform a review of literature related to methods for global analysis of risers and the associated wellhead loading. Relevant computation models and potential mechanical failure modes of the wellhead are also to be discussed.

3. The candidate shall make himself acquainted with the computer program SIMA/Riflex, which is applied for static and dynamic response analysis of marine risers. A brief description of this computer program and its theoretical basis is also to be given.

4. A model of a particular surface vessel together with the corresponding riser system is to be established. As a first simplification, the top of the blowout preventer (BOP) can be considered a fixed point. Global response analyses are performed for a number of selected sea states by application of SIMA/RIFLEX.

5. A simplified model for calculation of the loads, which are transferred to the wellhead, is to be established. This model should consider sea states, which contribute to the accumulation of fatigue damage. A simple estimate of the fatigue life of the well should be done. This model is to be applied to the results, which were obtained in item four. Parametric variations are subsequently to be performed to the extent that time allows.

The work scope may prove to be larger than initially anticipated. Subject to approval from the supervisor, topics may be deleted from the list above or reduced in extent.

In the thesis the candidate shall present his personal contribution to the resolution of problems within the scope of the thesis work.

Theories and conclusions should be based on mathematical derivations and/or logic reasoning identifying the various steps in the deduction.

The candidate should utilise the existing possibilities for obtaining relevant literature.

The thesis should be organised in a rational manner to give a clear exposition of results, assessments, and conclusions. The text should be brief and to the point, with a clear language. Telegraphic language should be avoided.

The thesis shall contain the following elements: A text defining the scope, preface, list of contents, summary, main body of thesis, conclusions with recommendations for further work, list of symbols and acronyms, references and (optional) appendices. All figures, tables and equations shall be numbered.

The supervisor may require that the candidate, in an early stage of the work, presents a written plan for the completion of the work.

The original contribution of the candidate and material taken from other sources shall be clearly defined. Work from other sources shall be properly referenced using an acknowledged referencing system.

The thesis shall be submitted in 3 copies:

- Signed by the candidate
- The text defining the scope included
- In bound volume(s)
- Drawings and/or computer prints which cannot be bound should be organised in a separate folder.

Supervisor: Professor Bernt J. Leira
Deadline: June 28th 2015

Trondheim, January 10th, 2015

Bernt J. Leira

Abstract

When riser systems are connected to subsea wells, large forces and moments are transmitted to the wellheads. This is due to the large weight of the blowout preventer and the environmental excitation forces that are transmitted to the wellhead. These loads can lead to fatigue of the wellhead.

In this thesis a global model of a drilling riser system is analysed in the computer program RIFLEX. The loads that are particularly interesting, are the loads that accumulate fatigue damage to the wellhead. The sea states given in a scatter diagram for the North Sea are investigated in order to find which sea states that contributes most to the accumulation of fatigue damage.

Results from a local analysis of the well is provided by Statoil. These results includes important input parameters which are used in the fatigue assessment in this thesis. For that reason, the results from the fatigue assessment concluded in this thesis, are highly dependent on the input parameters from Statoil.

The thesis can be divided into two parts. The first part is a literature review that gives background knowledge on the subject. The literature review begins with a presentation of a typical drilling riser system and its main components. Thereafter, an introduction to the analysis and simulation software RIFLEX is given. RIFLEX is used for static and dynamic analyses of the drilling riser system. Methods for global riser analyses are then presented. Relevant theory for fatigue design is also discussed in this part.

The second portion of the thesis begins with a presentation of the case studied in this thesis. This includes the local model, provided by Statoil, and a global model, which is established in RIFLEX. Static and dynamic analyses of the RIFLEX model is then performed, and the results are post processed and presented in the result section of the thesis. Parameter studies on soil stiffness, current, and blowout preventer (BOP)-size are also conducted. Since results from the local model is provided, the author has not been able to update the parameters studied in the local model. This is a limitation that may have caused some unexpected tendencies in results for the parameter studies.

In this thesis, the fatigue damage accumulated during the initial construction phase of the well, is studied. This phase involves connection of a heavy drilling rig to the well. This

operation may have a duration of a month or so. After the connection is completed, the well must have sufficient fatigue capacity to operate throughout its estimated lifetime.

Sammendrag

Det kan oppstå store krefter og momenter som følge av at en borerigg er koblet på brønnhodet. Dette er på grunn av det tunge boreutstyret, og på grunn av laster som følge av bølger, strøm og vind. Disse lastene kan over tid føre til utmatting av brønnhodet.

I denne masteroppgaven er det gjort en global analyse av et borestigerør med overflatefartøy i dataprogrammet RIFLEX. Lastene som er av størst interesse, er lastene som bidrar til utmatting. Alle sjøtilstandene i en typisk frekvenstabell fra Nordsjøen (Ekofisk) er analysert for å finne ut hvilke som bidrar mest til utmatting.

For å undersøke utmatting er det også nødvending å ha resultater fra en lokal analyse av brønnen, dette er gitt av Statoil. Disse resultatene inneholder viktige inputparametere til utmattingsberegningene. På grunn av dette, vil resultatene av utmattingsberegningene i stor grad være avhengig av resultatene som er gitt av Statoil.

Masteroppgaven kan deles i to deler. Den først delen er en litteraturstudie, som er ment for å gi teoribakgrunn om emnet. Litteraturstudiet begynner med en presentasjon av en typisk borerigg, og hovedkomponentene i borestigerørsystemet. Deretter blir simuleringsprogrammet RIFLEX presentert. Dette programmet blir brukt til statiske og dynamiske analyser av systemet. Metodikken for stigerørsanalyse blir også presentert i denne delen av oppgaven. Til slutt i første del, er det gitt en innføring i relevant utmattingsteori.

Andre del av masteroppgaven begynner med en presentasjon av det spesifikke tilfellet som videre blir analysert. Dette inkluderer både den lokale modellen som er gitt av Statoil, og den globale modellen som er opprettet i RIFLEX. Statisk og dynamisk analyse blir så utført, og resultatene blir deretter bearbeidet og presentert. Det er blitt utført parameterstudie på jordstivhet, strømningsprofiler og BOP masse. På grunn av at resultatene fra lokalmodellen er gitt som input fra Statoil, er det ikke mulig å oppdatere disse i lokalmodellen for parameterstudiene. Dette er en begrensning som muligens fører til uventede tendenser i noen av resultatene for parameterstudiene.

I denne masteroppgaven blir det fokusert på utmatingsskaden som oppstår i første fasen av brønnens levetid, altså når en borerigg er koblet på. Denne operasjonen varer typisk kun en måned, og etter denne måneden må brønnen ha stor nok utmattingskapasitet til at den varer resten av dens forventede levetid. For å konkludere om brønnen har tilstrekkelig

utmattingskapasitet, er det derfor nødvendig å undersøke utmatingsskade i de andre fasene av brønnens levetid.

Preface

This report is a result of my master thesis, which is my final work as an MSc student at NTNU Marine Technology. I am specialising in subsea technology; therefore, a project with a subject related to the oil industry was important. I wanted to use the project as an opportunity to learn more about the industry in which I intend to work. Professor Bernt J. Leira proposed the subject.

I want to say thanks to my supervisor, Professor Bernt J. Leira. Thanks for helping me find an interesting subject and for good guidance during both the project and master period. I want to say thanks to Andreas Amundsen at MARINTEK for the help with RIFLEX and the provided relevant examples. I want to say thanks to Guttorm Grytøyr from Statoil, who provided results from a local model. Lastly, I want to thank my fellow students for collaboration and social company.

Trondheim, June 28th 2015

André Lylund

André Lylund

Notation

Abbreviations

2D	Two-dimensional
3D	Three-dimensional
BOP	Blowout Preventer
CPU	Central Processing Unit
DFF	Design Fatigue Factor
DNV	Det Norske Veritas
DOF	Degree Of Freedom
FE	Finite Element
FEA	Finite Element Analysis
ISO	International Standard Organisation
JONSWAP	Joint North Sea Wave Project
LMRP	Lower Marine Riser Package
LWRP	Lower Workover Riser Package
MODU	Mobile Offshore Drilling Unit
RAO	Response Amplitude Operator
RLWI	Riserless Light Well Intervention
SCF	Stress Concentration Factor
TLP	Tension Leg Platform
WAMIT	Wave Analysis Massachusetts Institute of Technology
WH	Wellhead
XT	Christmas tree

Greek symbols

ρ	Density of sea water
σ	Stress
$\Delta\sigma$	Stress range
δ_m	Maximum misalignment

Roman symbols

a	Crack depth
a_1	Acceleration in surge
C_D	Drag coefficient
C_M	Mass coefficient
D	Diameter
$\boldsymbol{D}$	Damping matrix
D_{fat}	Accumulated fatigue damage
f_M	Moment to stress factor
f_Q	Shear force to stress factor
Hs	Significant wave height
K	Stress intensity factor
$\boldsymbol{K}$	Stiffness matrix
k	Thickness exponent
k_{sb}	Number of stress blocks
m	Mass per unit length
M	Moment wellhead
$\boldsymbol{M}$	Mass matrix
n	Number of cycles in a stress block
N	Number of cycles
S_m	Mean stress
S_{max}	Maximum stress in a cycle
S_{min}	Minimum stress in a cycle
S_Y	Yield stress
t	Thickness
t_{ref}	Reference thickness
Tp	Peak period
u_C	Velocity current
u_W	Velocity wave
Q	Shear force wellhead

Contents

List of figures

List of tables

1 Introduction

Wellhead fatigue is an old problem that has received growing attention in recent years. Continuous development of methods and technologies within the petroleum industry has made it possible to expand existing well lifetimes. Higher requirements for safety and efficiency result in more and often heavier equipment connected on the top of the wellhead. During drilling, workover, plug, and abandonment operations, environmental excitation forces are absorbed and transmitted to the subsea wellhead by the mobile offshore drilling unit (MODU), blowout preventer (BOP), and riser (Statoil, 2014). This results in a high number of cyclic loadings that may not have been considered when the wellhead was initially designed.

The scope of work for this project is to conduct a literature study of relevant theory and to perform dynamic analysis of a realistic riser model. Together with results from the local analysis provided by Statoil, these results can be used to investigate fatigue on the wellhead and conductor housing.

The literature study presents a typical drilling riser system and explains its main components. Relevant literature related to methods for global analysis of risers and associated wellhead loading will be presented. Theory of fatigue is also presented. The computer program SIMA/RIFLEX, which is applied for static and dynamic response analysis, is presented, and its theoretical basis is explained.

A model of the surface vessel with the corresponding riser system is established in RIFLEX. The environmental excitation forces that are transferred to the wellhead as a function of time are stored. Results from a local model show the hot spots on the wellhead and conductor housing. The fatigue life of these hot spots is investigated in this thesis.

1.1 Organisation of Thesis

Chapter 2 – Description of the main components in a marine drilling riser system.

Chapter 3 – Description of RIFLEX and theory for nonlinear static and dynamic analyses.

Chapter 4 – Description methods for riser analysis and loading on wellhead.

Chapter 5 – Relevant fatigue theory.

Chapter 6 – Flow chart of wellhead fatigue analysis.

Chapter 7 – Important information from the local model is presented.

Chapter 8 – The global model is described.

Chapter 9 – The results of the fatigue assessment.

Chapter 10 – Parametric studies on soil stiffness, current velocity, and BOP weight.

Chapter 11 – Discussion the limitation in the thesis.

Chapter 12 – Conclusion.

2 Marine Drilling Riser System

In this chapter, an overview of the main components in a marine drilling riser system is presented. The overview is based on the project thesis (Lylund, 2015). For more details or information concerning smaller parts in the riser system see (Norsk-Standard, 2009). Figure 2-1 is a simplified illustration that includes the main components in a marine drilling riser system.

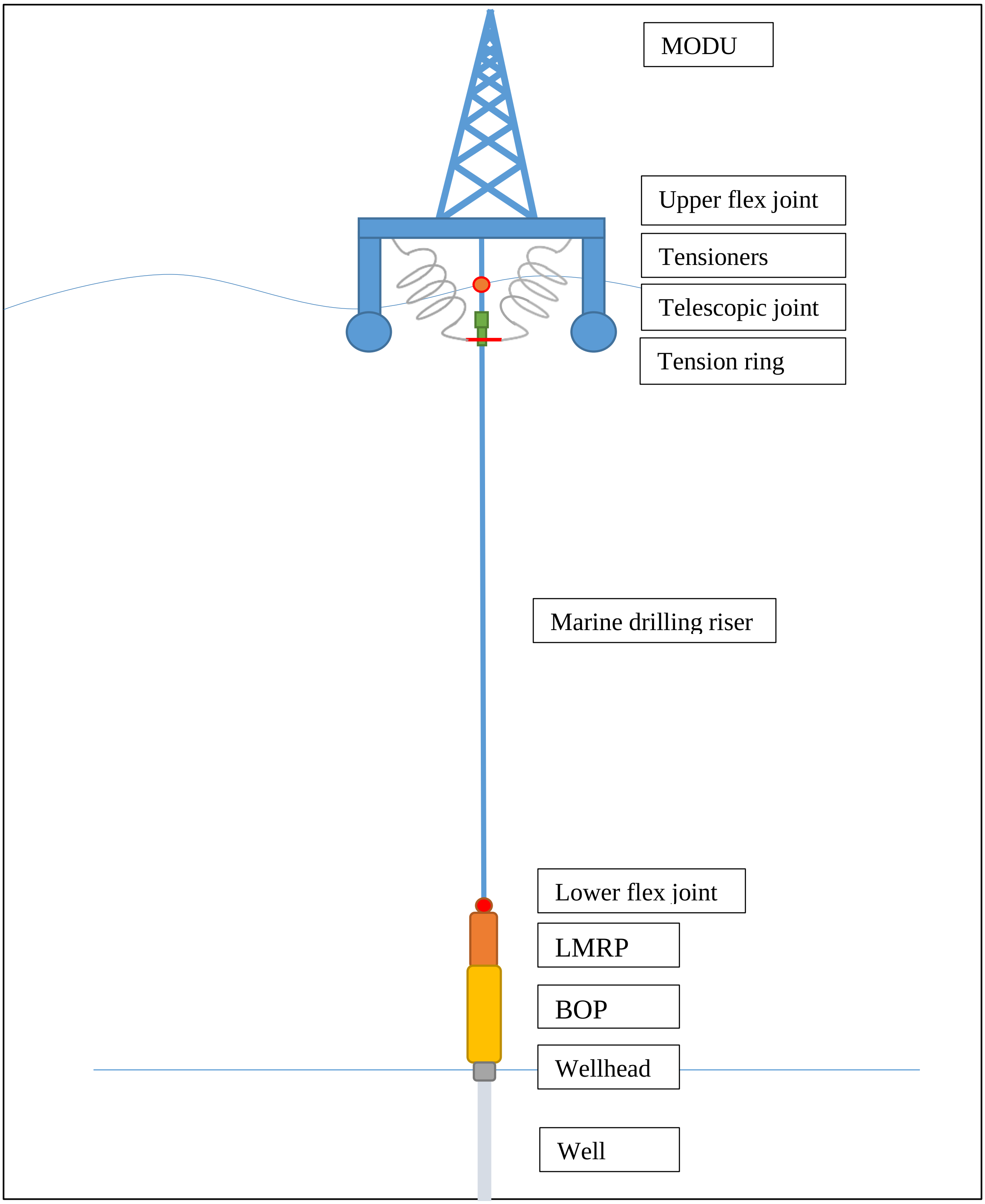

Figure 2-1 Sketch of main components in a drilling riser model. The illustration is not to scale.

2.1 Mobile Offshore Drilling Units

A MODU is a mobile rig or vessel used to drill offshore wells. Today, the following four types of MODUs are used:

- Submersible,
- Jackup rig,
- Semi-submersible, and
- Drillship.

The four types of MODUs are seen in Figure 2-2. The reason there are several types of MODUs is to satisfy the following requirements: technical, economical, governmental, and safety.

The jackup has the ability to jack up and stand on its own legs, while the submersible is lowered onto the seafloor; both types of MODUs rest on the seabed while drilling. This is an advantage, as drilling operations are sensitive to motions, especially heave motions. However, both types of MODUs are limited to shallow water depths.

Both semi-submersibles and drillships float during drilling operations and use dynamic positioning systems and/or mooring lines in order to maintain a specific position. The semi-submersible has a low water plane area and a high eigenperiod, which reduces the effects of first order wave forces. Because of this, the semisubmersible is more suitable in harsher environments than the drilling ship. A drillship may have other advantages, such as being faster and having better mobility (PetroWiki, 2013).

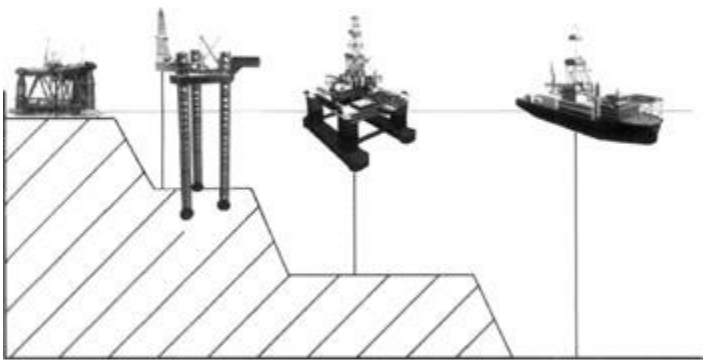

Figure 2-2 Types of MODU from left to right: submersible, jackup, semi-submersible, and drillship (iHS, 2014).

2.2 Flex Joint

Conventionally, there are two flex joints in the drilling riser system, the upper and lower flex joints. The upper flex joint is located at the top of the drilling riser column, while the lower flex joint is located on the top of the lower marine riser package (LMRP). A flex joint gets its flexibility from bonded laminations of elastomers between stacks of spherically shaped steel rings (Norsk-Standard, 2009). The flex joint is designed to have a specified stiffness and damping. The purpose of these joints is to allow the riser column to have a deflection angle, which occurs when the MODU moves laterally. The riser will also have some movement due to environmental loads. If there are no flexible parts in the riser system, the result is larger stresses and bending moments present in the system.

2.3 Telescopic Joint

The telescopic joint, also referred to as the slip joint, is located at the top of the riser column. The purpose of this joint is to compensate for the change in riser length due to vessel motions. As the name implies, the joint uses the same principles as a telescope. The telescopic joint consists of an outer barrel that is connected to the drilling riser and an inner barrel that is connected to the MODU (Norsk-Standard, 2009). The two barrels slide relative to each other when heave motions occur. Seals that ensure integrity are located between the two barrels.

A large variation in the tension is applied to the riser without the telescopic joint. Since the riser is elastic, tension will elongate the riser and compression will compress the riser. A long slender pipe starts to buckle when subjected to compression. Hence, buckling must be avoided, as this leads to large stresses in the pipe and can; in the worst-case scenario, this leads to failure of the riser.

2.4 Tensioner Ring

The tensioner ring is located on the lower part of the telescopic joint. The hydraulic tensioner is connected to this ring and is illustrated in red in Figure 2-1. Since the tensioner ring is the connection point between the telescopic joint and hydraulic tensioners, the ring must handle large forces from the tensioners.

2.5 Marine Riser Tensioner

The marine riser tensioners are large hydraulic springs, which are illustrated by two grey springs in Figure 2-1. The function of this system is to hold a constant tension in the marine drilling riser. Since the MODU is subjected to heave motions, the tension system must be able to dynamically vary the tension in order to counteract the tension effects that occur because of the heave motions.

The tension system requires large amounts of energy to provide the tension. However, the system that provides the energy is passive, which means that no electricity is necessary to vary the tension. The system uses large air-filled accumulators on the topside, which pressurise the piston system that provide hydraulic power to the hydraulic springs. Without this passive system, large amounts of electric energy are needed, and such amounts of electric energy are difficult to produce on a MODU. Other reasons for using the passive system are related to safety as well as restrictions on the voltage systems on a MODU.

There are several reasons pre-tension in the drilling riser column is necessary. As discussed in Section 2.2, buckling may occur if there is no pre-tension in the riser. Pre-tension will help prevent buckling, as it will provide additional geometric stiffness to the riser column.

Another reason for having top tension in the riser is that it will influence the eigenfrequency of the riser column and, therefore, the motion of the riser when subjected to external forces. This is due to the increase in geometric stiffness; according to general eigenfrequency formulas, higher stiffness will also increase the eigenfrequency of the riser. This indicates that pre-tension is an important tool to avoid dynamic amplification between the riser and the waves. The pre-tension will, therefore, influence the riser-induced forces on the wellhead. It is also important to mention that since the riser is in pre-tension, this will reduce the weight to which the wellhead is subjected.

Lastly, pre-tension is required for an emergency disconnect. During an emergency disconnect, the tensioners will pull up the riser column and lift the LMRP off the BOP stack.

2.6 Marine Drilling Riser

A drilling riser column is a series of large diameter pipes (referred to as drilling riser joints) that are coupled. One of the functions of the drilling riser column is to connect the BOP stack to the MODU. A picture of drilling riser joints is depicted in Figure 2-3.

There are two types of drilling risers used in the offshore oil and gas industry today: 1) high-pressure drilling risers and 2) low-pressure drilling risers. The main difference between the two types of drilling riser configurations is that, for the high-pressure drilling riser, the BOP is located on the drill floor and, for the low-pressure drilling riser, the BOP is located on the sea bottom. This thesis will focus on the low-pressure drilling riser since the BOP is located on the seafloor.

For low-pressure drilling riser joints, there are additional buoyancy elements, kill lines, choke lines, power cables, and signal cables to control the BOP on the outside of the pipe joint.

The main pipe is usually a low-pressure pipe. This is sufficient for drilling operations, as the mud will partly balance the high pressures in the well. It is also beneficial because a very large wall thickness is necessary to ensure a large diameter pipe will be able to withstand high pressures. This means greater weight and corresponding larger buoyancy elements are required to make the drilling riser naturally buoyant. Therefore, the outside diameter of the high-pressure drilling riser is often larger. Since wave and current forces exerted on the riser joints are proportional to the total diameter of the riser joints, the forces exerted on the riser will be higher.

Figure 2-3 Drilling riser joints with buoyancy elements (Wikipedia, 2013).

2.7 Lower Marine Riser Package

The LMRP is the upper part of the BOP stack. According to (Norsk-Standard, 2009), the LMRP comprises hydraulic connectors, annular BOP, flex joint, riser adapter, jumper hoses for the choke, kill, and auxiliary lines, and subsea control pods. It can be considered a mini BOP and can be disconnected from the BOP if the MODU loses position.

2.8 BOP Stack

According to (Norsk-Standard, 2009), a BOP stack comprises well control equipment including BOPs, spools, valves, hydraulic connectors, and nipples that connect the BOP to the subsea wellhead. A BOP is a safety valve located on the top of the well. The purpose of this valve is to ensure pressure control of the well while a drilling riser is connected. If the drilling crew loses control of the formation fluids, the BOP can immediately close the well to ensure a safe condition. Since drill pipe, casing, or tubing are lowered through the BOP and down into the well, the BOP needs to be able to cut or seal around such equipment. For this purpose, the BOP is equipped with shear rams and annular sealing devices (Schlumberger, 2014).

2.9 Christmas Tree

The Christmas tree (XT) consists of a set of valves, fittings, and spools. The main purpose of the XT is to direct and control the flow from the well. There are predominantly two types of XTs used in the industry today, horizontal (HXT) and vertical (VXT) (Schlumberger, 2014).

2.10 Wellhead

The wellhead is located on the topmost part of the wellbore. A connector called the H4-connector, which ensures sealing between the wellhead and BOP or the XT, is located on the outside of the wellhead. This connector is hydraulically operated and, therefore, can be operated from the MODU. The wellhead is also a well barrier and has structural purposes. A section from the upper part of the well is shown in Figure 2-4.

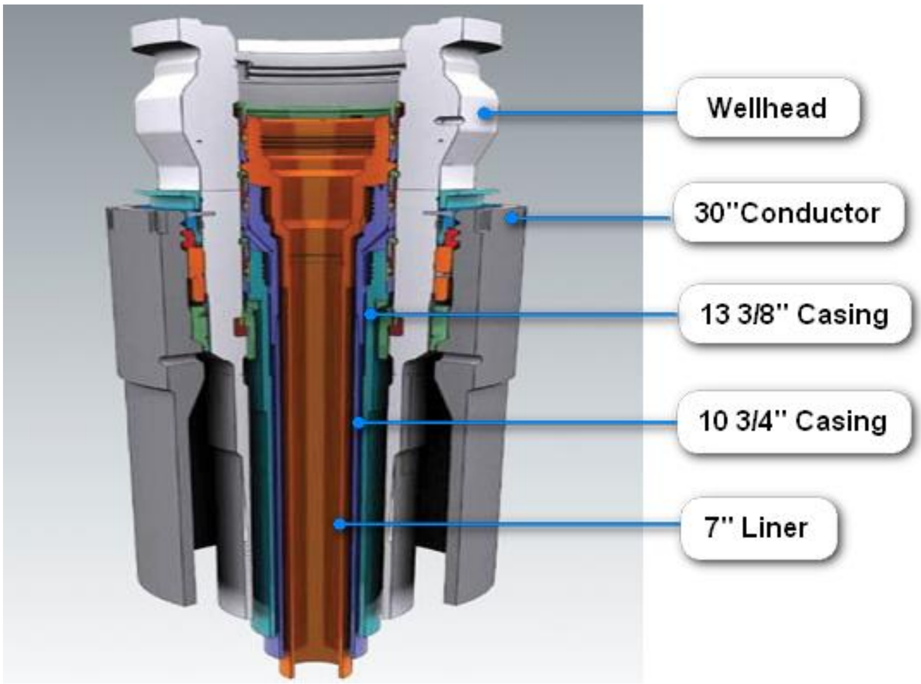

Figure 2-4 Upper part of the well (Cameron, 2012).

2.11 Drilling, Completion, and Workover Configurations

The drilling riser model is illustrated in Figure 2-1. In addition to this model, two other models are commonly used in the industry. According to Det Norske Veritas (DNV, 2011), these two are the completion configuration and workover configuration. These will not be discussed in detail; however, the main differences are shown in Figure 2-5. In the first phase, when the well is drilled, a drilling model is used. Since this is a preproduction phase, no XT is installed. This means that the BOP and LMRP are connected on top of the wellhead. In the second phase, called completion, the XT is installed on the wellhead. Therefore, the BOP and LMRP are installed on top of the XT. In the workover phase, a different configuration is used. Instead of the BOP and LMRP, a lower workover riser package (LWRP) is used. On top of the LWRP is a stress joint.

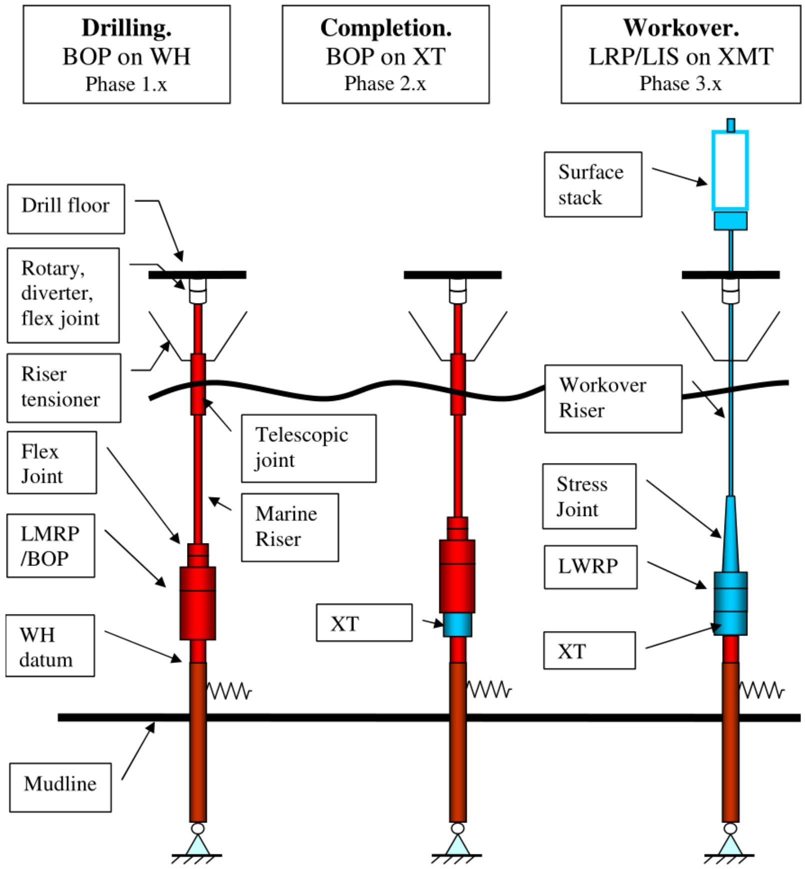

Figure 2-5 Sketch of the three different riser models and their main components (DNV, 2011).

3 Analysis and Simulation Software RIFLEX

SIMA is an advanced software tool for simulating scenarios regarding marine technology. The software was developed by MARINTEK and has been used in the industry by (for instance) DNV. The purpose of the software is to give the users an intuitive tool from modelling and running analyses to finally visualising the results using advanced 2D and 3D graphics. The SIMA software is divided into several modules. Each module is tailored to handle a specific area within the marine industry. The module relevant for riser systems is RIFLEX. This module is designed for static and dynamic analyses of slender marine structures. This means that RIFLEX is suitable for many marine structures, such as risers, mooring lines, tension leg platform (TLP) tendons, and umbilical and loading hoses to name a few. RIFLEX can model the environment by simulating waves and currents in a realistic way. A variety of load models can be used, for instance, hydrodynamic pressure effects or hydrodynamic loads described by Morrison's equation. The slender marine structures can be modelled based on the finite element method, and typical elements that are used are beam or bar elements. Non-linear material properties are supported, which often are of importance when analysing slender marine structures. Further, RIFLEX is based on non-linear theory in the time domain and is calibrated according to model testing to render accurate results (DNV/MARINTEK, 2004) (DNV-GL, 2014).

3.1 The Structure of RIFLEX

The basic structure of RIFLEX is shown in Figure 3-1. The figure shows that RIFLEX is divided into five modules. A well-developed file system is provided to ensure good communication between the modules. In the *INPMOD* module, the input data is read and organised. This can be input data for the wave induced vessel motion, which typically is a file containing response amplitude operator (RAO) data for the specific MODU. It can also be input data regarding wave spectrum and current and how this will influence the water particle velocities and accelerations. In addition, it can be input data that describe the system configuration. The benefit of having all input data read and sorted into one module is that the other modules can easily access this for further analysis. In the next module, called *STAMOD*, several types of static analyses are performed. In this module, the finite element model of the system is generated; this includes the element mesh and data concerning the stress-free configuration. The data gathered in this module is necessary for parameter studies and dynamic analysis. The dynamic analyses are performed in the *DYNMOD* module. A dynamic analysis describes the response of the system as a function of time. The dynamic analysis can also calculate frequencies and mode shapes. The eigenfrequency of the riser is one interesting frequency to calculate. Mode shapes describe how the riser oscillates when subjected to external forces. In the next module, *FREMOD*, the analysis can be performed in the frequency domain. The frequency domain is used for linear analysis; this means that there will not be variations by time. It is not possible to characterise non-linear systems by simple frequency (Langen & Sigbjornsson, 1979). In the *OUTMOD* module, post processing of selected results can be performed. This includes plots, 2D and 3D graphics, and exports to other analysis programs (MARINTEK, 2014d).

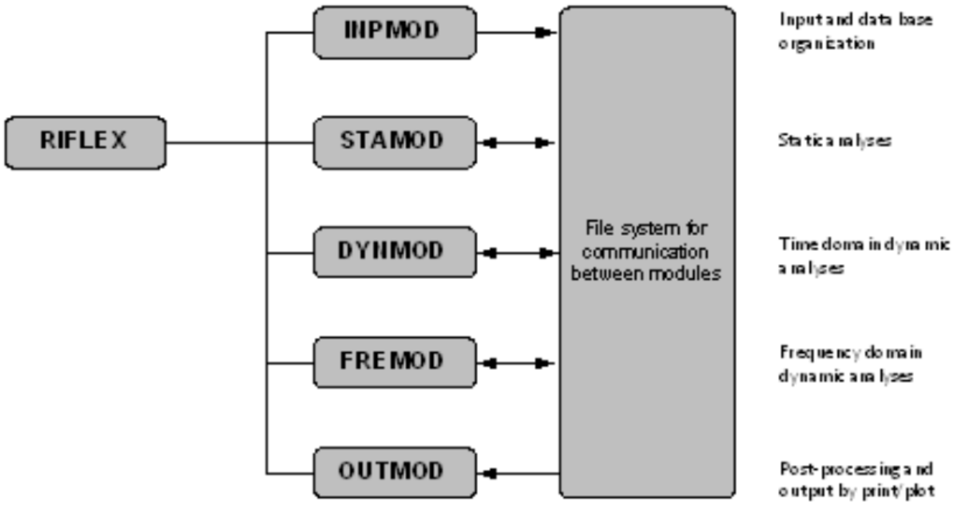

Figure 3-1 Structure of RIFLEX (MARINTEK, 2014d).

3.2 Modelling in RIFLEX

The general way to model a riser system will be briefly presented in this section. The riser system is a slender system and can, therefore, be modelled by bar or beam elements. The principle is illustrated in Figure 3-2. The super nodes define the boundary conditions of the structure. The line represents the structure itself and can be created between two super nodes. A segment is a part of the line and is assigned cross-section properties and element length. The segments are then divided into the desired number of bar or beam elements.

Components that have special properties or are not slender structures can be imported from the RIFLEX database and assigned the desired properties. This includes, for example, the flex joints, tensioner ring, or internal fluid.

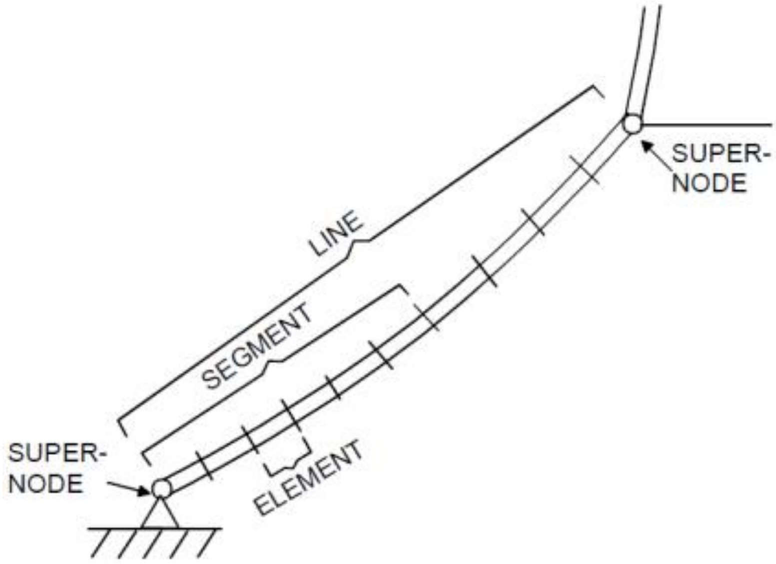

Figure 3-2 Modelling slender systems in RIFLEX (MARINTEK, 2014a).

3.3 Theory for Non-linear Static Analysis

RIFLEX enables non-linear static analysis. This can be studied in detail in (MARINTEK, 2014a) Chapter 4 and in (Moan, 2003). The reason the static analysis is non-linear is that the displacements and corresponding forces are not linear functions. Instances of non-linearity that cause this behaviour are typically associated with geometry, material, and boundary conditions. An example of geometrical non-linearity is that a slender marine structure often is subjected to large displacements. An example of material non-linearity can be that these large displacements cause the material to transfer from elastic to plastic behaviour. An example of non-linearities associated with boundary conditions is two bodies that are in contact with each other. Several techniques have been developed in order to solve non-linear static response. In (Moan, 2003), three main categories are described as follows:

- Incremental or stepwise procedures,
- Iterative procedures, and
- Combined methods.

3.3.1 Non-linear Equations

The finite element model for the static analysis is completely defined by the nodal displacement vector. In the static analysis, the solution is found when the resultant external force R is in equilibrium with the resultant internal structural reaction force $\mathrm{R_{int}}$:

$$\boldsymbol{R}_{int} = \boldsymbol{R} \tag{3.1}$$

This means when external forces are applied to the model, it will lead to displacements at the nodes. Since the model has stiffness according to the stiffness matrix, the displacements will cause internal structural reaction forces that contract the external forces. The resulting internal structural reaction forces can be found by summation of the topology matrices $\boldsymbol{a^i}$ for $\boldsymbol{i}$ elements multiplied by the internal nodal forces $\boldsymbol{S^i}$:

$$\boldsymbol{R_{int}} = \sum_{\boldsymbol{i}} (\boldsymbol{a}^i)^{\boldsymbol{T}} \boldsymbol{S}^i \tag{3.2}$$

In non-linear analysis, the relationship between the incremental stiffness $\boldsymbol{K_I(r)}$, the external load R, and the displacement vector $\boldsymbol{r}$ is:

$$\boldsymbol{K_I}(\boldsymbol{r})d\boldsymbol{r} = d\boldsymbol{R} \tag{3.3}$$

Since the incremental stiffness is a function of the displacement vector, various techniques are developed for solving the non-linear problem, which are presented in the following section.

3.3.2 Load Incremental Methods

In the load incremental method, the external load is stepwise applied. For each step, the displacements increase and a new stiffness matrix $\boldsymbol{K_I}$ is calculated. This method is called the Euler-Cauchy method, and an illustration of the principle is given in Figure 3-3.

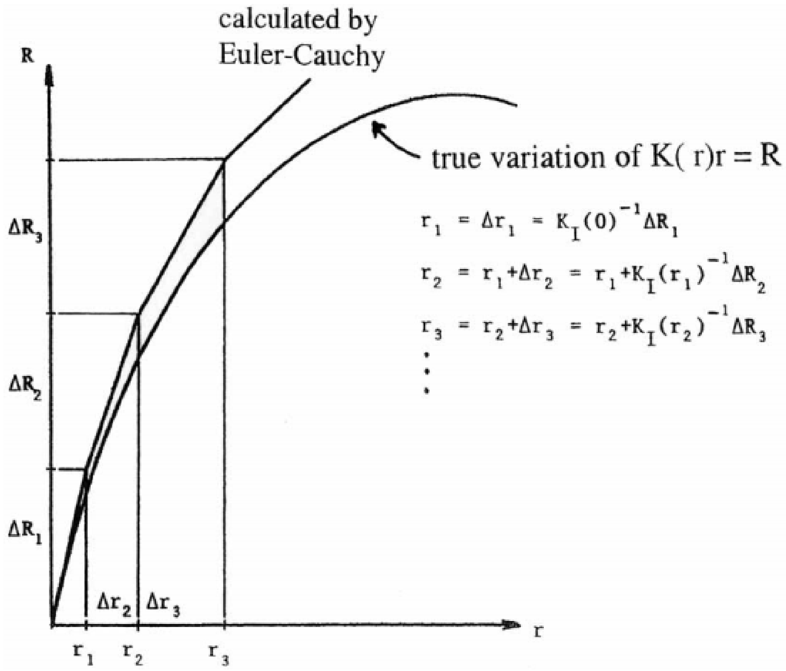

Figure 3-3 Euler-Cauchy incrementing (Moan, 2003).

As Figure 3-3 demonstrates, the results using the Euler-Cauchy method diverge from the true variation because the solution does not fully satisfy the total equilibrium between internal and external forces. The results can partly be improved by reducing the load steps. A better improvement would be to add equilibrium correction for each load step. The principle is that a reduction in external loads is included after each load step so that the global equilibrium is maintained. This is illustrated in Figure 3-4.

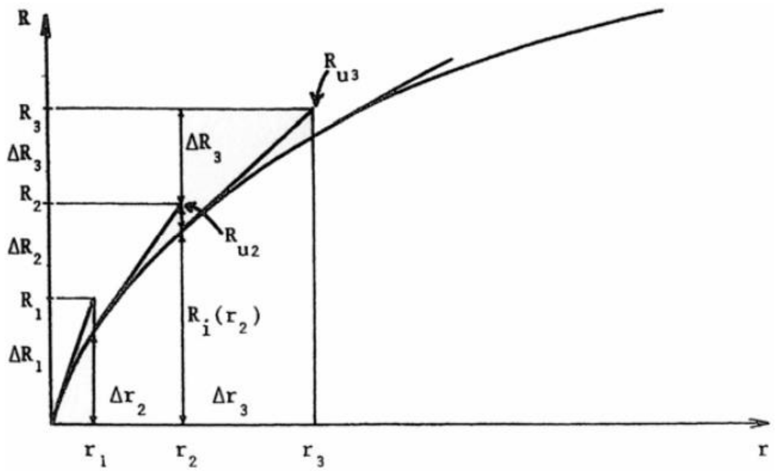

Figure 3-4 Euler-Cauchy procedure with equilibrium correction (Moan, 2003).

3.3.3 Iterative Methods

The most common iterative method is the Newton-Raphson method. The method is built upon an algorithm to solve x for the problem $f(x) = 0$:

$$x_{n+1} = x_n - \frac{f(x_n)}{f'(x_n)} \tag{3.4}$$

where $\boldsymbol{f'(x_n)}$ is the derivative of $\boldsymbol{f(x_n)}$ with respect to x, at $\boldsymbol{x = x_n}$, and

$$\frac{\boldsymbol{f(x_n)}}{\boldsymbol{tg\theta}} = \frac{\boldsymbol{f(x_n)}}{\boldsymbol{f'(x_n)}} \tag{3.5}$$

In Figure 3-5, the above formula is plotted and then $\boldsymbol{K_I(r)}$ is found as the generalisation of $\frac{\partial f}{\partial x}$.

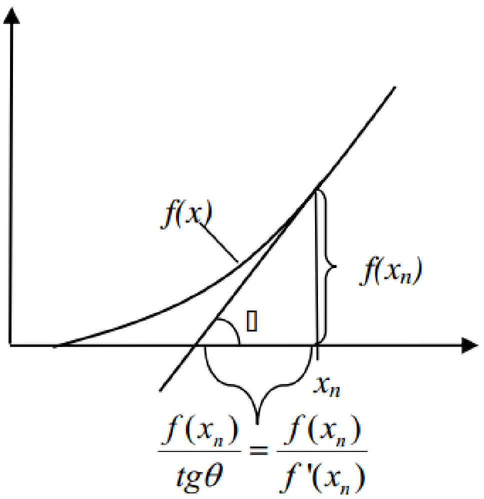

Figure 3-5 Newton-Raphson algorithm (Moan, 2003).

Then, the iteration equation is given in (3.6):

$$\boldsymbol{r}_{n+1} = \boldsymbol{r}_n - \boldsymbol{K}_{\boldsymbol{I}}^{-1}(\boldsymbol{r}_{\boldsymbol{n}}) \ (\boldsymbol{R}_{\boldsymbol{int}} - \boldsymbol{R}) \tag{3.6}$$

An example of this iteration process on a single degree of freedom (DOF) system is illustrated in Figure 3-6.

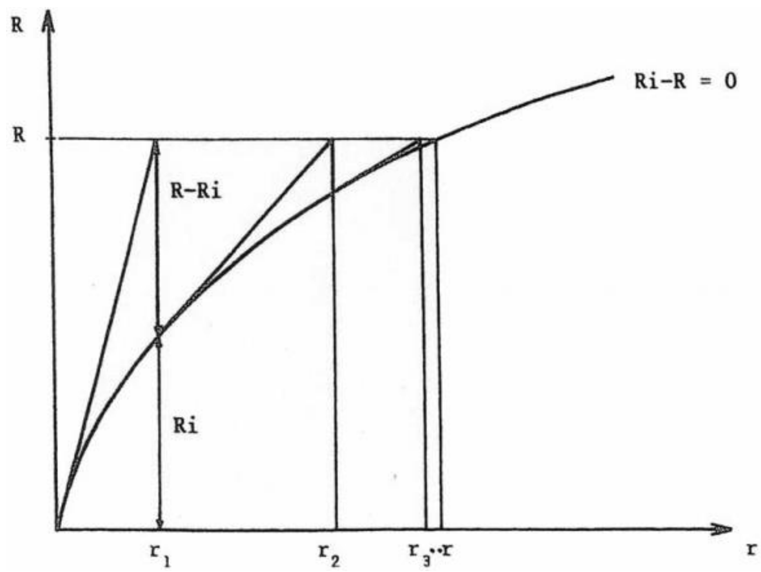

Figure 3-6 Newton-Raphson iteration (Moan, 2003).

3.3.4 Combined Methods

As the name implies, these methods are often combinations of incremental and iterative methods. For instance, the loads can be applied according to the Euler-Cauchy method, and the Newton-Raphson iteration can be performed after each step. This is illustrated in Figure 3-7.

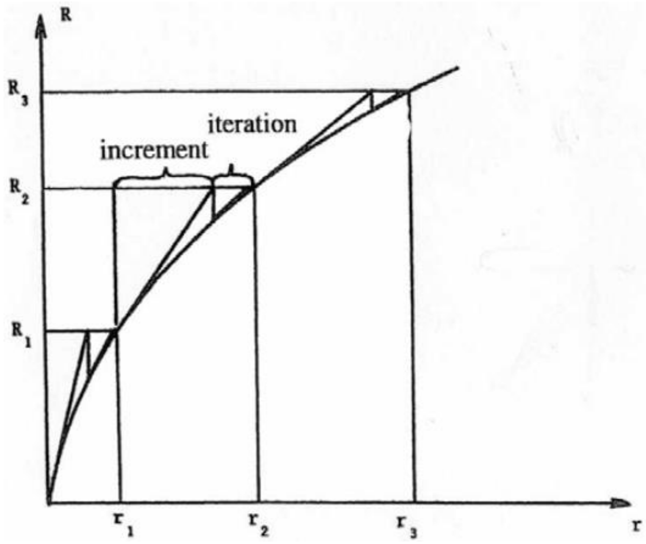

Figure 3-7 Combined incremental and iterative solution procedures (Moan, 2003)

3.4 Theory for Dynamic Analysis

Dynamic analysis is used to solve problems that are varying in time. Compared to static problems, dynamic problems have time as an additional dimension. Therefore, the dynamic behaviour of the construction is described by accelerations, velocities, and displacements. The dynamic effects can, in some cases, be accounted for by including a dynamic amplification factor (DAF) in the static calculations.

The theory and equations that are presented in this section are found in the work of (Langen & Sigbjornsson, 1979). The dynamic equilibrium equation that is given in Equation (3.7) describes the dynamic behaviour of constructions. The factors that govern the dynamic behaviour of the construction are as follows (Bergan, Larsen, & Mollestad, 1981):

- The stiffness properties of the system, which are given by the stiffness matrix $\boldsymbol{K}$,
- The size and the distribution of the mass and added mass, which is given by the mass matrix $\boldsymbol{M}$,
- The damping in the system, which is given by the damping matrix $\boldsymbol{C}$, and
- The load intensity and distribution as function of time $\boldsymbol{Q}(t)$:

$$\boldsymbol{M\ddot{r}} + \boldsymbol{C\dot{r}} + \boldsymbol{Kr} = \boldsymbol{Q}(t), \tag{3.7}$$

where $\boldsymbol{\ddot{r}}$, $\boldsymbol{\dot{r}}$, and $\boldsymbol{r}$ are the acceleration, velocity, and displacement vectors, respectively. The term $\boldsymbol{M\ddot{r}}$ represents the inertia forces. An accelerating system will experience inertia forces due to the acceleration of mass and added mass. The second term $\boldsymbol{C\dot{r}}$ represents the damping forces. Damping forces occur due to energy dissipation from the system. Typical examples of damping are friction, plastic deformation in material, or hydrodynamic damping. To simplify, it is often assumed that the damping is proportional to velocity, but damping can, in many cases, be non-linear with respect to the velocity. The term $\boldsymbol{Kr}$ represents the restoring force and is proportional to the displacement. The load vector $\boldsymbol{Q}(t)$ represents the excitation force and can be periodic or non-periodic. Examples of non-periodic forces are wind gusts or impulse loading (explosions).

3.4.1 Stepwise Numerical Integration of Nonlinear Systems

To solve non-linear problems in the time domain, RIFLEX uses stepwise numerical integration of non-linear systems. The equilibrium equation for the non-linear system at an arbitrary time is shown in Equation (3.8).

$$\boldsymbol{F}^I(t) + \boldsymbol{F}^D(t) + \boldsymbol{F}^S(t) = \boldsymbol{Q}(t, \boldsymbol{r}, \boldsymbol{\dot{r}}) \tag{3.8}$$

where $\boldsymbol{F}^I(t)$ is the inertia force, $\boldsymbol{F}^{\boldsymbol{D}}(t)$ is the force due to damping, and $\boldsymbol{F}^S(t)$ is the elastic force due to stiffness. If the mass is constant, the inertia force can be written as in Equation (3.10). In a hydrodynamic environment, the damping forces are typically non-linear with respect to velocity, and the elastic force may, in many cases, be non-linear with respect to displacement.

$$\boldsymbol{F}^I(t) = \boldsymbol{M\ddot{r}} \tag{3.9}$$

The solution is obtained by dividing the period of the dynamic problem into smaller intervals. The time is discretised such that $t_k = kh$, where h is the length of each time interval and k is interval number. The equilibrium equation for time instant t_k is given in Equation (3.10)

$$\boldsymbol{F}_k^I + \boldsymbol{F}_k^D + \boldsymbol{F}_k^S = \boldsymbol{Q}_k \tag{3.10}$$

The equilibrium equation for the next time instant t_{k+1} is given in Equation (3.11)

$$\boldsymbol{F}_{k+1}^I + \boldsymbol{F}_{k+1}^D + \boldsymbol{F}_{k+1}^S = \boldsymbol{Q}_{k+1} \tag{3.11}$$

The time between t_k and t_{k+1} is equal to h, which indicate that t_k and t_{k+1} represent the time at the beginning and end of the same time interval. By subtracting Equation (3.10) from Equation (3.11) the equation of motion on incremental form is obtained. The result of the subtraction is given in Equation (3.12):

$$\Delta \boldsymbol{F}_k^I + \Delta \boldsymbol{F}_k^D + \Delta \boldsymbol{F}_k^S = \Delta \boldsymbol{Q}_k \tag{3.12}$$

The incremental displacement, velocity, and acceleration can be written as in Equation (3.13 a-c):

$$\Delta \boldsymbol{r}_k = \boldsymbol{r}_{k+1} - \boldsymbol{r}_k \tag{3.13a}$$

$$\Delta \dot{\boldsymbol{r}}_k = \dot{\boldsymbol{r}}_{k+1} - \dot{\boldsymbol{r}}_k \tag{3.13b}$$

$$\Delta \ddot{\boldsymbol{r}}_k = \ddot{\boldsymbol{r}}_{k+1} - \ddot{\boldsymbol{r}}_k \tag{3.13c}$$

The inertia, damping, and elastic force can be written as in Equation (3.14 a-c):

$$\Delta \boldsymbol{F}_k^I = \boldsymbol{M} \Delta \ddot{\boldsymbol{r}}_k \tag{3.14a}$$

$$\Delta \boldsymbol{F}_k^D = \boldsymbol{C}_{Ik} \Delta \dot{\boldsymbol{r}}_k \tag{3.14b}$$

$$\Delta \boldsymbol{F}_k^S = \boldsymbol{K}_{Ik} \Delta \ddot{\boldsymbol{r}}_k \tag{3.14c}$$

The mass matrix $\boldsymbol{M}$ of the structure can be considered constant. The stiffness matrix $\boldsymbol{K}$ and the damping matrix **C** are varying as functions of time. Therefore, a linearisation of these must be done within the increment. The results are $\boldsymbol{K}_{Ik}$ and $\boldsymbol{C}_{Ik}$, which are the average values within the interval as illustrated in Figure 3-8 a) and b). It is necessary to do an iteration process since the displacement and velocity at the end of the interval are based on $\boldsymbol{K}_{Ik}$ and $\boldsymbol{C}_{Ik}$.

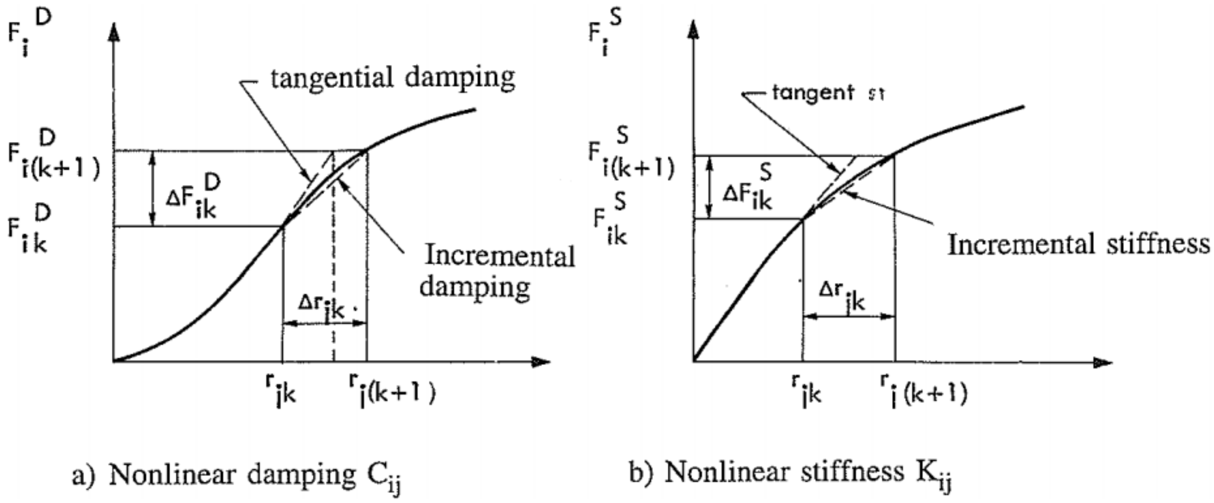

Figure 3-8 Incremental damping and stiffness (Langen & Sigbjornsson, 1979).

By inserting Equation (3.14 a-c) into Equation (3.12), Equation (3.15) is obtained as follows:

$$\boldsymbol{M}\Delta\ddot{\boldsymbol{r}}_k + \boldsymbol{C}_{Ik}\Delta\dot{\boldsymbol{r}}_k + \boldsymbol{K}_{Ik}\Delta\ddot{\boldsymbol{r}}_k = \Delta\boldsymbol{Q}_k \tag{3.15}$$

Equation (3.15) can be used to find a stepwise solution where the tangential modulus is employed. This corresponds to the solution of the initial value problem by Euler's method and is illustrated in Figure 3-9 a). Note that the same solution methods can be applied for both static and dynamic problems. The difference is that in dynamic problems, the solution methods also include damping and inertia terms. The linearisation within each time step introduces residual forces that will cause an error that will increase for each time step. To obtain a more accurate solution, an equilibrium correction can be done after each time step, and the result is shown in Figure 3-9 b).

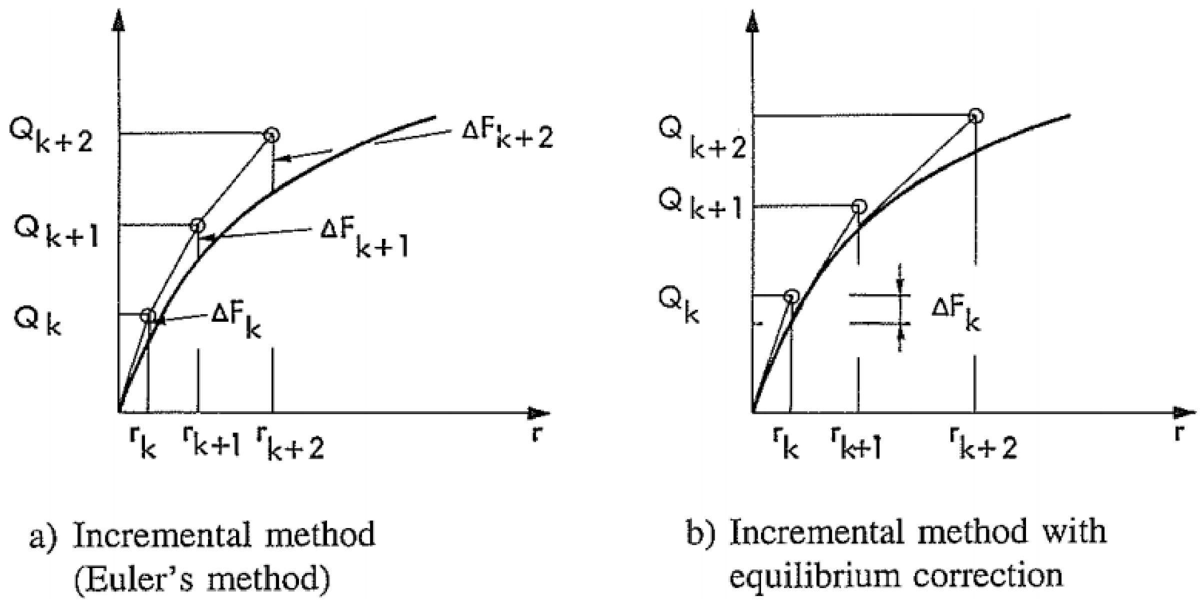

Figure 3-9 Incremental (stepwise) solution(Langen & Sigbjornsson, 1979).

The equilibrium correction requires an iteration procedure on the error in order to attain the balance between the internal and external forces. This can be done by the Newton-Raphson iteration or modified Newton-Raphson iteration. This is illustrated in Figure 3-10.

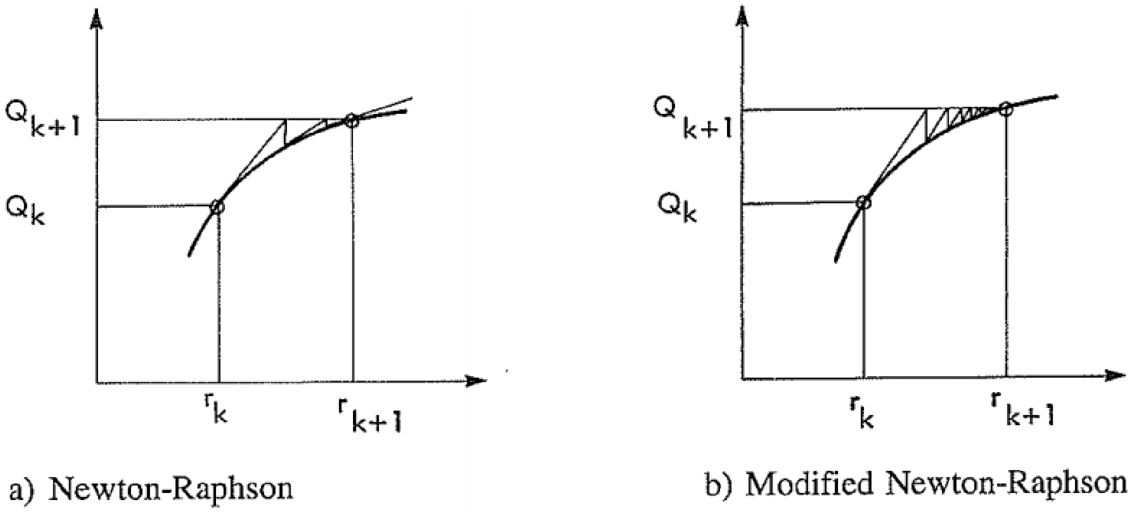

Figure 3-10 Equilibrium iteration within a time step (Langen & Sigbjornsson, 1979).

4 Methodology of Global Analysis of Riser Systems

The purpose of the global load analysis is to collect information on the load history on the wellhead system. The results should provide time series of the moments and shear forces acting on the wellhead, and the results are strongly dependent on environmental conditions (DNV, 2011). Therefore, it is important to collect correct information about the weather and sea states during operation. If the operation is weather restricted for certain sea states, these sea states shall not be included. In order to attain accurate results, it is important to include all the relevant forces acting on the system. It is also important to establish a realistic model of the system.

4.1 Important Parameter for Riser Analysis

As listed in the DNV guidelines for the wellhead fatigue analysis method (DNV, 2011), important parameters to include in the global analysis are as follows:

- Buoyancy,
- Weight,
- Effective tension and geometric stiffness,
- Hydrodynamic loads from waves and currents,
- MODU motion due to waves,
- The non-linear characteristics of the lower flex joint, and
- The characteristic response of the riser tension system, which ensures correct tension variation in the system due to MODU heave.

These data should be quality controlled and provided by the operator.

In order to be able to model the system in a practical way, the following assumptions are made (DNV, 2011):

- The MODU is assumed to be in nominal offset (i.e., positioned directly over the WH),
- All loads are in one plane, and
- Long-crested waves are used.

4.2 Lower Boundary Condition

The lower boundary condition for the global analysis is considered to be at the wellhead datum. Since the wellhead and the rest of the well are supported by the soil beneath the seafloor, the lower boundary condition is not completely fixed. The support in the lateral direction will be of importance for the global analysis. The soil effects in the lateral direction can be considered non-linear springs. The principle of how this can be done is illustrated in Figure 4-1. Each soil layer has different properties that are represented with different springs. The stiffness of the springs can be described using Equation (4.1):

$$k = K_{Soil} \cdot \Delta z \tag{4.1}$$

Here, k is the stiffness of the spring, K_{Soil} is the soil stiffness of the soil layer, and Δz is the height that the spring supports.

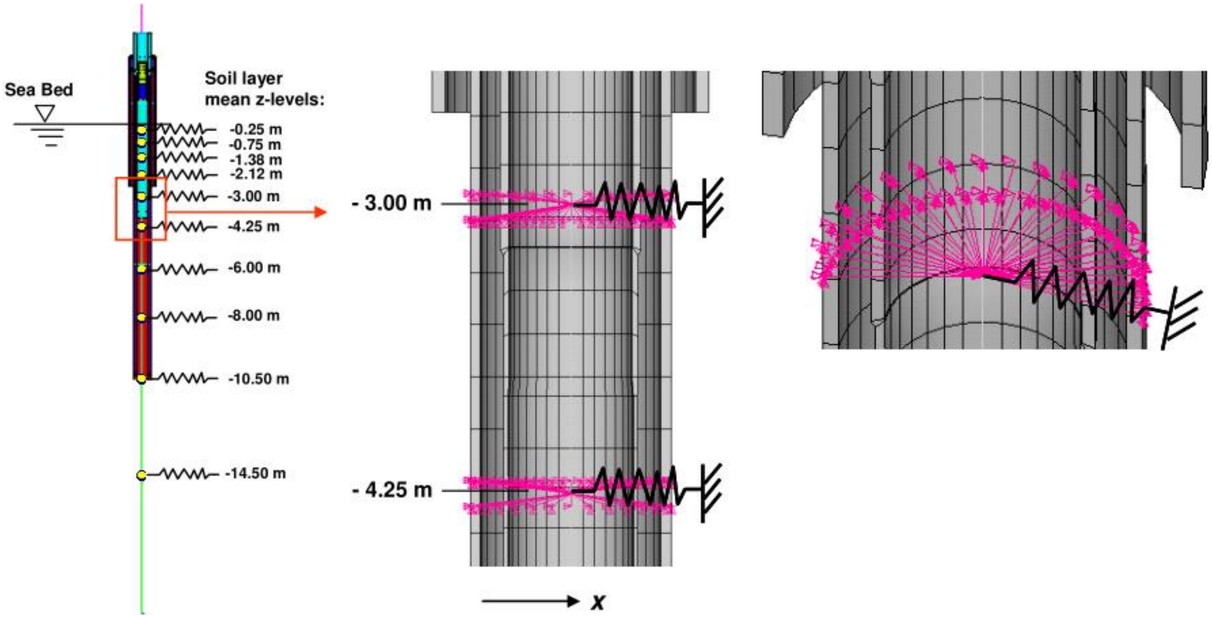

Figure 4-1 Example of non-linear springs that represent the lateral soil support of the well (DNV, 2011).

The study of the soil support is subject to the local analysis part and will, therefore, not be covered in more detail here. The spring values that represent the lateral support of the well are important input in the global analysis. The spring values are given from the local analysis. For the global analysis, the lower boundary condition will be modelled as a beam with bending stiffness *EI*, beam length *H*, and springs with non-linear stiffness. The top of the beam will represent the lateral stiffness of the wellhead datum. This is illustrated in Figure 4-2.

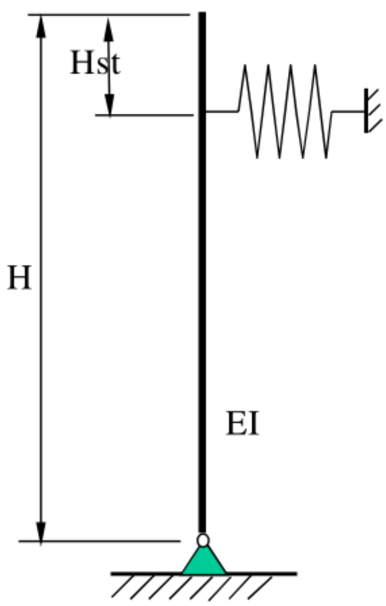

Figure 4-2 Lower boundary condition for global load analysis. Top of the beam is at wellhead datum and will be connected to the lower part of the riser model (DNV, 2011).

4.3 Upper Boundary Condition

The upper boundary consists of the MODU, which is located directly above the wellhead. This includes the diverter, rotary table, and tensioning systems (DNV, 2011). The floating MODU will have motions that are dependent on the RAO functions. An RAO function is a transfer function that gives the vessel motion as a function of wave amplitudes. The RAOs are vessel specific, and the difference in motions between two differently designed MODUs can vary greatly in the same sea state. In order to simulate the vessel motions for a specific sea state in RIFLEX, the RAO functions for the vessel must be provided and are considered input data for the analysis. This data can be found by conducting model tests on the MODU.

The tensioner system will dynamically attempt to compensate for the MODU motion. Hence, information about the tensioner system must be included in the model. The tensioner system can be modelled as springs that are connected between the MODU and the upper flex joint. According to DNV (DNV, 2011), it is recommended to model all riser tensioners instead of simplifying the tensioners to a single point load. This is to ensure the correct top tension and righting moment of the riser system. Since the top tension of the riser will influence the bending moments on the wellhead, it is important to attain a realistic description of the top tensioners. In reality, the top tension will vary, which will result in a varying axial load on the wellhead. This variation in axial load will not be of importance in the fatigue assessment since axial loads will be neglected. However, the change in tension will influence the behaviour of the riser and, hence, the riser induced loads on the wellhead.

4.4 Modelling of Riser

For drilling and completion operations, there is usually a drill string or completion riser inside the marine drilling riser, a ‘pipe-in-pipe’ problem. This will have an effect on the behaviour of the riser system since both pipes have axial stiffness, bending stiffness, and mass per unit length. Therefore, both the riser and the internal pipe must be accounted for in the global analyses. To do this, there are two models used: 1) pipe-in-pipe model and 2) lumped model.

In the pipe-in-pipe model, both pipes are modelled separately. The lumped model combines the properties from both pipes into a lumped riser. The bending stiffness, axial stiffness, and mass per unit length of the lumped riser will be the sum of the marine riser and internal pipe. The applied top tension on the lumped riser should also be the sum of the top tension that is applied to the marine riser and the internal pipe. However, since the length of the internal pipe will vary with the depth of the drilled well, it is not constant. In order to be on the conservative side, it is recommended to take the maximum drill string tension.

The advantages of the lumped model are that it is simpler to model and results in less computational time. The lumped model will also give slightly more conservative results since there will be a small dead band in the flex joint angle. Figure 4-3 illustrates the difference between the two models.

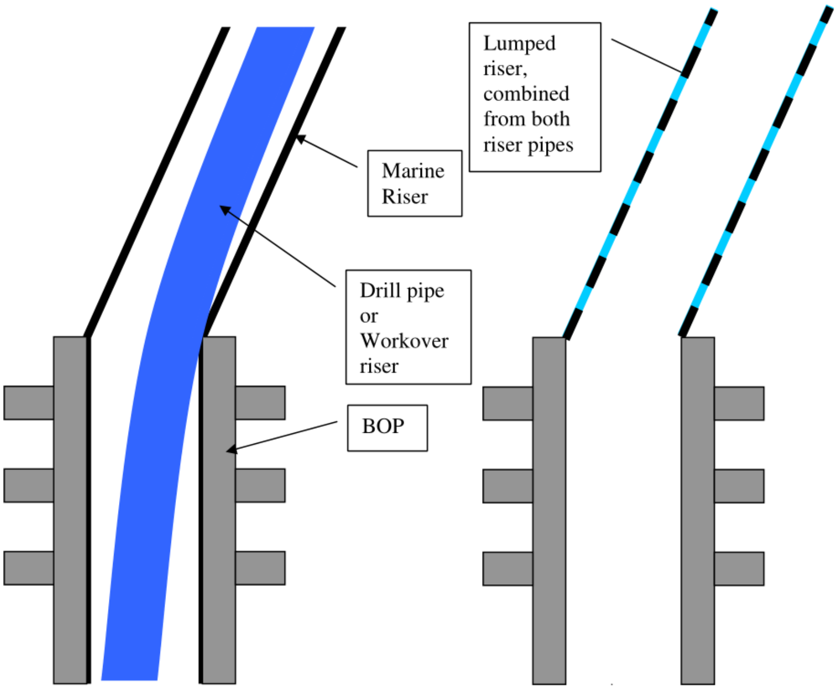

Figure 4-3 Pipe-in-pipe (left) and simplified lumped model (right) (DNV, 2011).

4.5 Modelling of the Flex Joint

The flex joint should be modelled to have a non-linear bending stiffness. According to (DNV, 2011), a flex joint with linear stiffness is non-conservative. This is illustrated in Figure 4-4. The red line includes both the static non-linear moment curve and the dynamic stiffness. This can be modelled by two rotational springs in series. The flex joint also has a damping term due to the material properties, which can be included in one of the springs.

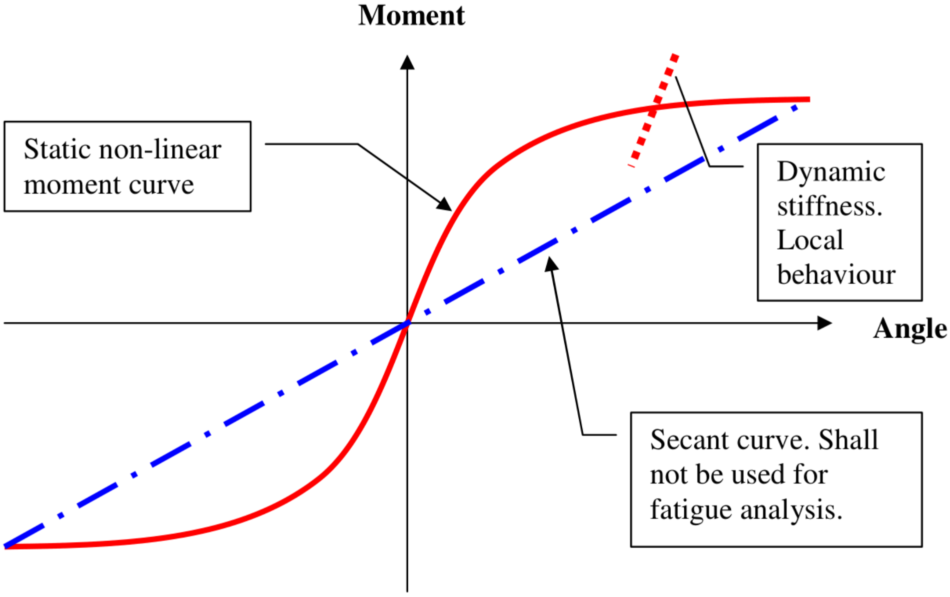

Figure 4-4 Illustration of linear (blue) and non-linear (red) stiffness of a flex joint (DNV, 2011).

4.6 Environmental Loads on the Riser

The environmental loads that are acting on the system are predominantly wind, current, and waves as seen Figure 4-5. Wind loads are acting directly on the components above the sea surface. The wind can also generate waves that exert loads on the components below the water surface. The MODU has a large area above the water surface and will, for that reason, be subjected to wind forces. Since most of the length of the riser is submerged, the wind loads exerted on the riser will be negligible compared to the hydrodynamic loads. However, the wind will indirectly affect the riser since the riser is connected to the MODU.

Because of currents and waves, the water particles will have velocity and acceleration. When relative velocity or acceleration between the system components and the water particles exist, forces will occur. The sea consists of many irregular waves. The type of sea state depends on many factors, such as geographical location, time of the year, water conditions, and so on. A sea spectrum is used in order to attain information of the sea states in the actual area. A sea spectrum gives information about how much energy is distributed through different wave frequencies. The spectrum is based on statistical data and is gathered over a long period. In order to describe the sea states in the North Sea, the joint North Sea wave project (JONSWAP) spectrum is used. Parameters of importance are significant wave height H_S and the spectral peak period T_P. In addition, H_S is the average of the one-third highest waves, and T_P is the period with the greatest energy.

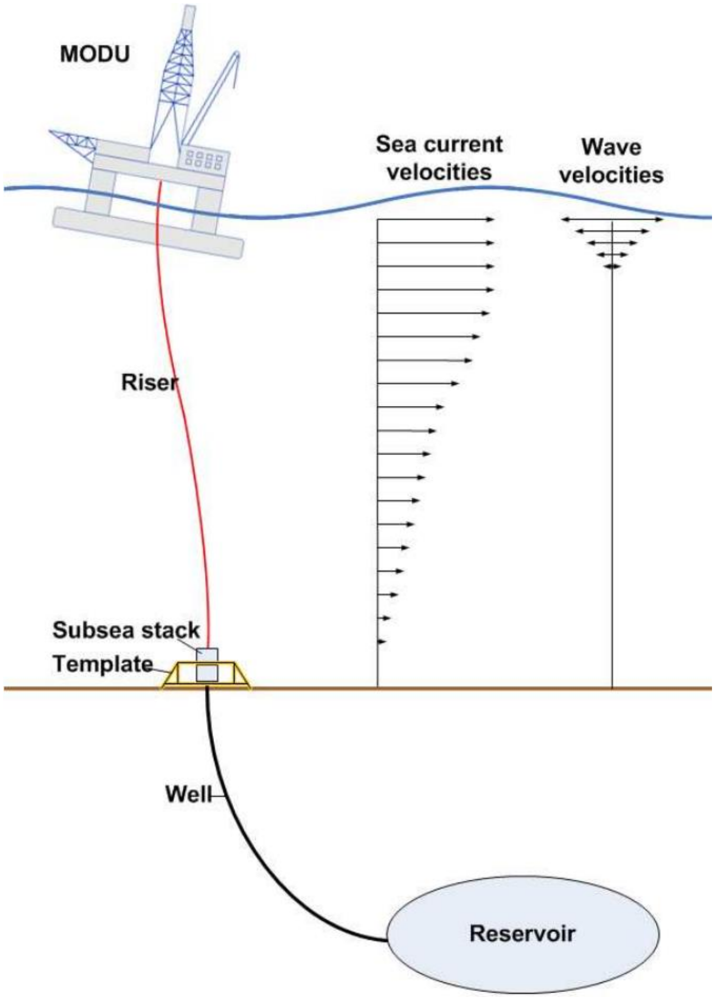

Figure 4-5 System overview (DNV, 2011).

4.7 Morrison's Equation

In order investigate the forces that are acting on the riser, it is necessary to know the geometry of the riser. The riser has a cylindrical geometry and a very small diameter compared to typical wavelengths in the North Sea. As described in (Faltinsen, 1990), this means that the diffraction forces will be relatively small compared to mass and viscous drag forces. Therefore, it is reasonable to assume that Morrison's equation can be used to calculate the horizontal forces that are acting on the riser. Since the riser is very long compared to its diameter, the riser will oscillate and not remain fixed when subjected to horizontal forces. In Figure 4-5, each strip of the riser will have a horizontal motion. In order to attain a good approximation of the horizontal forces, it is necessary to consider the relative velocities and accelerations between the riser and the water particles. Morrison's equation is suitable for a fixed pile without horizontal motions, so the equation must be modified in order to account for the oscillating behaviour. Since the oscillating behaviour will affect the relative velocity and accelerations, these terms must be changed. This can be done according to (Larsen, 2005), and the results are described in Equations (4.2), (4.3), and (4.4).

According to Morison's equation, the horizontal wave and current force per unit length for a rigid pile can be written as in Equation (4.2):

$$dF = \rho \frac{\pi D^2}{4} C_M a_1 + \frac{\rho}{2} C_D D (u_C + u_W)|u_C + u_W| \tag{4.2}$$

where ρ is seawater density, D is the riser diameter, C_M is the mass coefficient, a_1 is the horizontal particle acceleration, C_D is the drag coefficient, u_C is the current velocity, and u_W is the horizontal particle velocity.

By taking the relative motion between the oscillating riser and the water particles into account, the equation becomes the following (4.3):

$$dF = \rho \frac{\pi D^2}{4} C_M a_1 + \frac{\rho}{2} C_D D (u_C + u_W - \dot{\eta}_1)|u_C + u_W - \dot{\eta}_1| \tag{4.3}$$

where $\ddot{\eta}_1$, $\dot{\eta}_1$, and η_1 are, respectively, the horizontal acceleration, velocity, and displacement of the riser.

Since the riser is oscillating, it will also affect the added mass term, which is on the left side of the equation. The total dynamic equation per unit length will therefore be (4.4):

$$\left(m + \rho \frac{\pi D^2}{4}(C_M - 1)\right)\ddot{\eta}_1 + c\dot{\eta}_1 + k\eta_1 = \rho \frac{\pi D^2}{4} C_M a_1 + \frac{\rho}{2} C_D D (u_C + u_W - \dot{\eta}_1)|u_C + u_W - \dot{\eta}_1| \tag{4.4}$$

where *m* is the dry mass per unit length, *c* is the damping per unit length, and *k* is the stiffness per unit length.

4.8 Load on Wellhead

Environmental loads are absorbed by the MODU and the riser and are transmitted to the wellhead through the riser system. This will result in shear forces and bending moments in the wellhead. In addition to the environmental loading, the weight of the BOP and LMRP will cause bending moments and axial loading on the wellhead. The internal pressure will also cause imposed forces on the wellhead.

Modern MODUs are typically equipped with a dynamic positioning system. This system will attempt to hold the MODU directly above the wellhead. If the MODU experiences a lateral offset position, there will be an increase in the forces and moments on the wellhead. This is due to an increase in the deflection angle that the riser experiences on the flex joint located on the top of the LMRP. This is illustrated in Figure 4-6. Typically, this deflection angle can be a maximum of five to six degrees before the LMRP disconnects. This corresponds to an MODU offset in the horizontal plane of about 10% of the water depth (Sangesland, 2014).

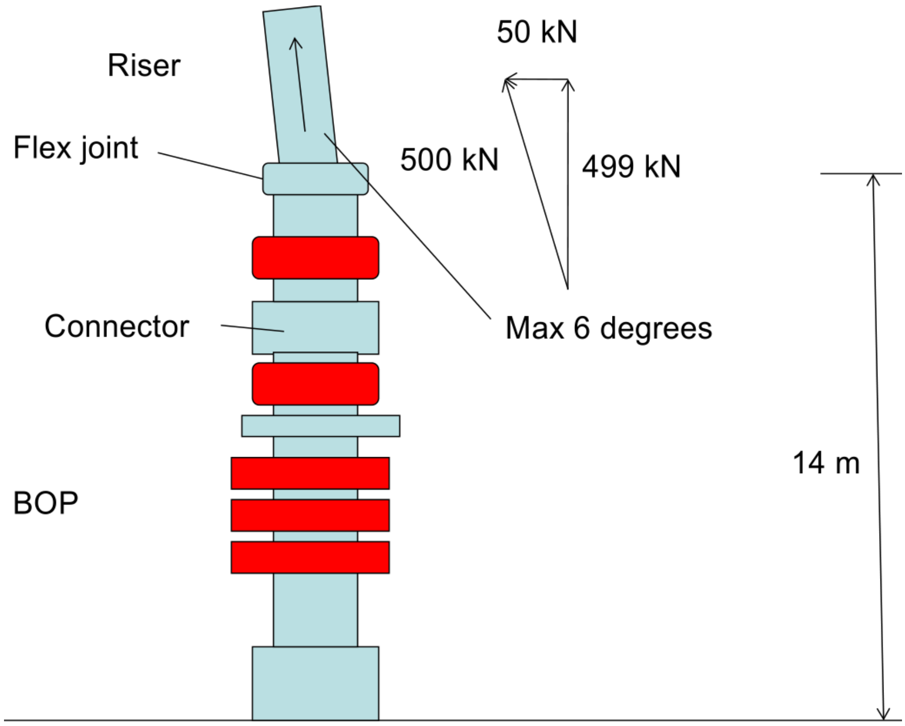

Figure 4-6 Deflection angle of the flex joint causes moment on the subsea wellhead (Sangesland, 2014).

4.9 Converting Loading to Stress

With regard to fatigue calculation, it can be convenient to convert the load amplitudes to stress ranges. RIFLEX cannot calculate stress directly, so forces and moments must be converted to stress by external methods. In principle, this can be done by the simple formula given in Equation (4.5). The relationship between the moments and stresses are typically linear in the high cycle fatigue region. The formula shows how the moment M and shear force Q on the wellhead can be converted to stress by a moment factor f_M and a shear factor f_Q. It is necessary to perform a local analysis of the wellhead in, for instance, ABAQUS in order to find these factors. The factors can be calculated by applying forces and moments to the wellhead and reading the corresponding stresses from ABAQUS (Sævik, 2015)

$$\sigma = f_M \cdot M + f_Q \cdot Q \tag{4.5}$$

4.10 Support of the Wellhead

The support of the wellhead will play a significant role in how the wellhead handles loads. The degree of support of the wellhead depends on many factors. For example, the soil properties around the well are important. In some areas where the seafloor is very soft, the well can be installed inside a suction anchor. This can increase the stiffness of the well. Another important factor to consider is the cement job of the well. Sometimes there can be a lack of cement between the surface casings or conductor. There can also be a lack of grout outside the conductor or a combination of these issues. These examples are considered to be poor cement jobs and result in less support of the wellhead. In Figure 4-7, four different support scenarios are illustrated.

1. Base Case

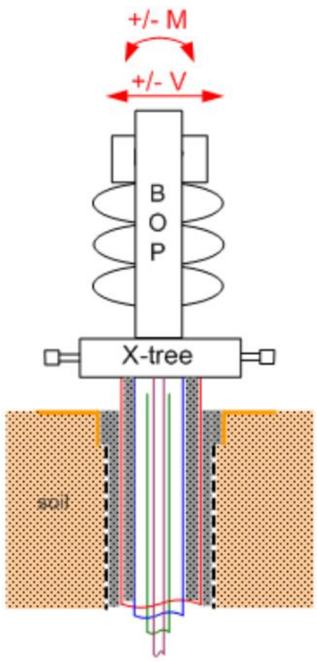

2. Cement shortfall between 20” and 30”

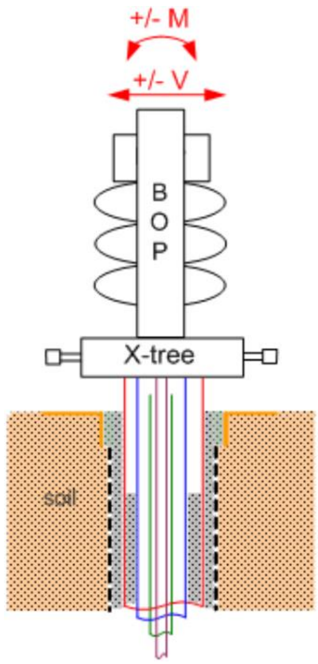

3. Lack of grout outside 30”

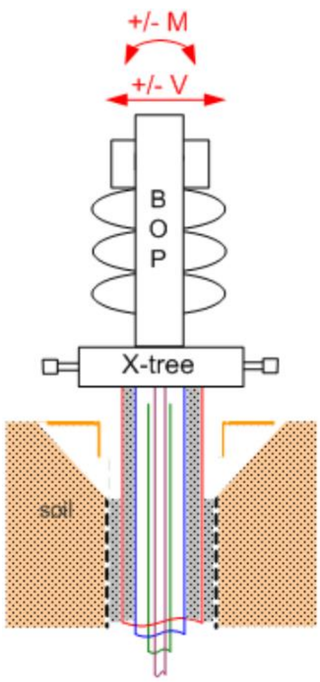

4. Lack of grout and cement shortfall

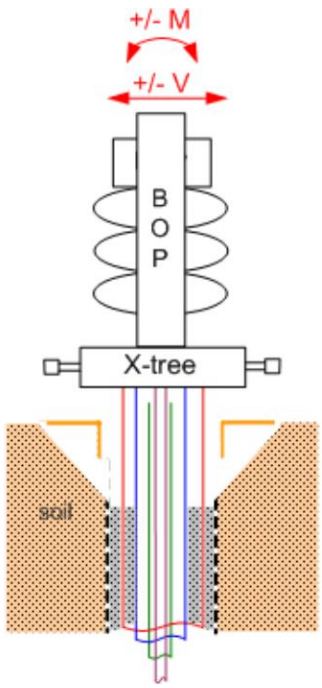

Figure 4-7 Four examples of how the well can be supported (DNV, 2011).

4.11 Failure Modes of the Wellhead

According to (Berge, 2006), marine structures are subjected to dynamic loads. The cumulative effect of varying loads may initiate fatigue cracks. The fatigue cracks typically start to grow at the weld toe because the welding process causes micro defects, such as slag and undercut. At the initiation of the crack, the crack grows slowly. As the crack length increases, the crack growth accelerates. When the cracks reach a certain length, the wellhead may start to leak. Depending on the brittleness of the material, the crack may start to grow uncontrollably, which can lead to total failure of the wellhead and a possible blowout. Oil and gas will rise to the surface and potentially cause an environmental disaster and may cause fire or explosions on the MODU.

Extreme weather conditions can cause very high loads on the structure. If the von Mises stress in the structure becomes close enough to the material yield stress, the structure may fail due to material yielding.

If problems occur with the positioning system, the MODU can experience a drift off. Normally, an emergency system disconnects the LMRP from the BOP if this happens. This system will typically disconnect when the lower flex joint angle exceeds five to six degrees. If, for some reason, a problem with the disconnecting system occurs, the wellhead could be subjected to large lateral forces and bending moments. This may lead to yielding of the material and can cause large plastic deformations of the components in the riser system and upper well. This can, in the worst scenario, threaten the integrity of the well and lead to a blow out.

Figure 4-8 shows an illustration of a failure assessment of the riser system. The green area illustrates the acceptable region of failure. If the failure occurs in this region, the BOP and LMRP closes in order prevent a blow out. If the failure occurs below the LMRP, the failure is unacceptable and may lead to a blow out.

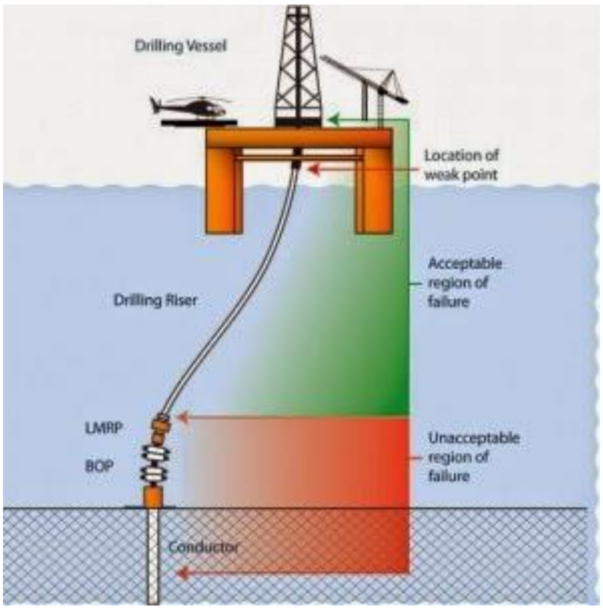

Figure 4-8 Riser failure assessment (MECF, 2014).

5 Theory of Fatigue Design

Fatigue includes crack initiation and crack growth that occurs in a material when subjected to cyclic stress variations over a long period. Small cracks grow together and create larger cracks. This process continues until the material collapses. Offshore structures are generally exposed to fatigue due to environmental loading, such as waves, which implies cyclic loading to the structures. According to (Berge, 2006), a typical time span of fatigue life on offshore structures is 20 years, which corresponds to the order of 10^8 cycles.

The first phase of fatigue is a crack initiation. Local yielding at the surface of the material causes this phase. This typically occurs where the crystal grains in the material are orientated so that slip bands are formed (DNV, 2011). The second phase is crack growth or crack propagation. This phase is described by Paris' law:

$$\frac{da}{dN} = C(\Delta K)^m \tag{5.1}$$

where a is the crack depth, N are the number of cycles, C and m are material parameters, and ΔK is the difference in stress intensity $K_{max} - K_{min}$.

According to (DNV, 2011), the fatigue assessment of a wellhead is mainly based on the SN-curve and Miner–Palmgren hypothesis. Fracture mechanics can also be used in some cases.

5.1 Fracture Mechanics

Fracture mechanics is a subgroup of solid mechanics, where the purpose is to quantify the relations between the following (Roylance, 2001):

- Crack length,
- The materials inherent resistance to crack growth, and
- The stress at which the crack rapidly propagates to cause structural failure.

Fracture mechanics is divided into linear elastic fracture mechanics (LEFM), which applies to linear problems and elastic-plastic fracture mechanics (EPFM), which applies to non-linear problems. Linear problems are often characterised by a relatively small plastic zone ahead of the crack tip compared to characteristic dimensions like plate thickness and crack size. This is characteristic for brittle materials. In addition, the state of stress ahead of the crack tip should be in plain strain. Non-linear problems are characterised by a larger plastic zone ahead of the crack tip, and the state of stress is plain stress. These problems will have plastic behaviour before failure

Empirically, it is found that the state of stress ahead of the crack tip can be decided by Equation (5.2):

$$t, a \geq 2.5\left(\frac{K}{S_Y}\right)^2 \tag{5.2}$$

where t is the plate thickness, a is the crack length, K is the stress intensity factor, and S_Y is the yield stress.

5.2 SN-curves

Fatigue data is typically based on testing, and a common method to present the results is in SN-diagrams. An SN diagram is a stress-life diagram that plots the stress ranges as a function of the number of cycles until failure of the component of interest. A typical example of test specimens and the corresponding SN-diagram is illustrated in Figure 5-1. As seen in the figure, it is convenient to use a log-log format on the SN diagram because the mean life curve tends to follow a log-linear relationship in the high cycle range. This region typically ranges from 10^5 to 10^8 cycles and the mean curve in this region can be described by Equation (5.3):

$$N(\Delta\sigma)^m = Constant \tag{5.3}$$

where N is the number of cycles to failure, $\Delta\sigma$ is the stress range, and m is the exponent in crack growth relation.

In the low cycle region, typically below 10^5 cycles, the failures tend to scatter and do not follow a trend line because the stress ranges in the low cycle region are very high and may cause plasticity in the material (ductility and strain hardening). Therefore, methods other than the SN-diagram are used in the low cycle region. In the threshold region above 10^8 cycles, the stress ranges are usually so small that the test specimens experience no fracture during testing. It is also seen that other factors like microstructure, mean stress, and environment have a large influence on the fatigue life. Therefore, there will be many uncertainties in this region.

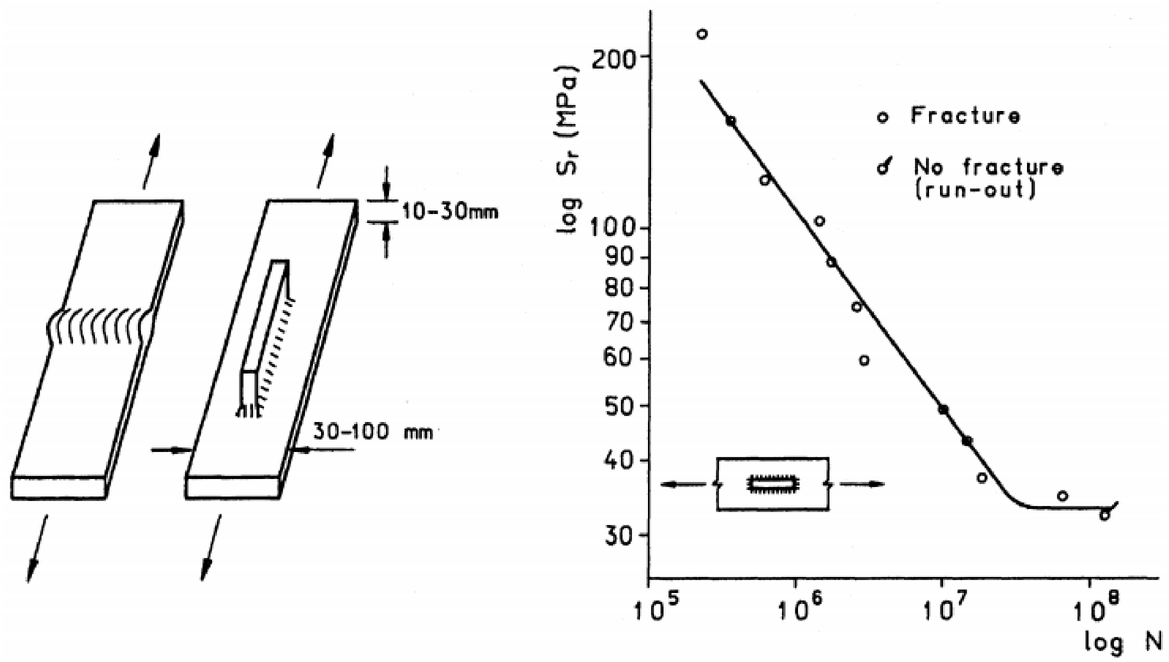

Figure 5-1 Typical specimens and SN data for welded joints (Berge, 2006).

5.3 Design SN-curves

As seen in Figure 5-1, the fractures tend follow the mean curve. The fractures are not exactly on the curve, that is, some are above, and some are below the curve. The testing conditions are identical, so the variations are due to small deviations in the microstructure of each of the respective test specimens. To be on the conservative side, the design curve must be below all the fractures. The variations around the mean curve tend to follow a normal distribution, and the design curve is, therefore, defined to be the mean curve minus two standard derivations. This is illustrated in Figure 5-2.

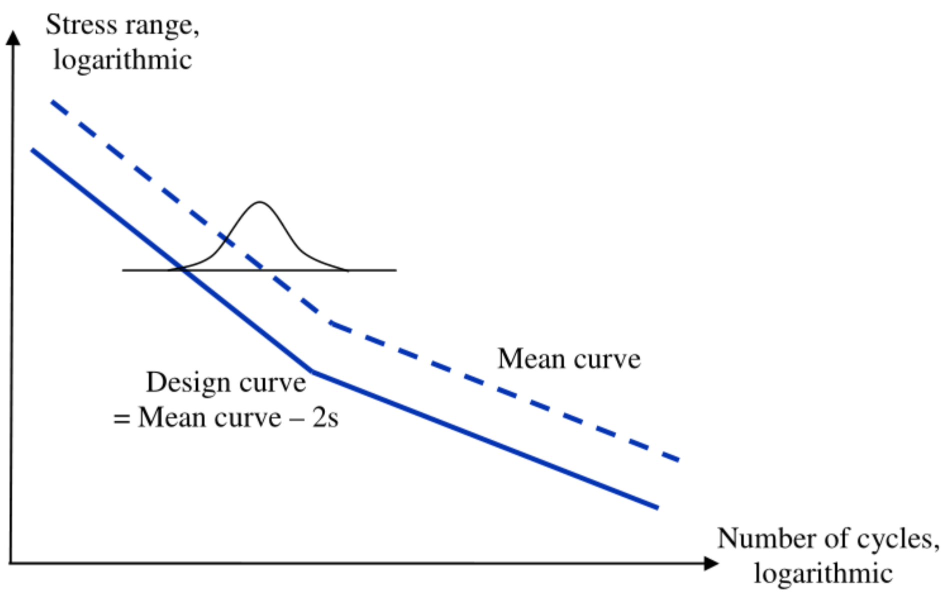

Figure 5-2 Design SN-curve equals to mean SN curve minus two standard derivations (DNV, 2011).

5.4 Constant and Variable Amplitude Loading

In a marine environment, the structures are exposed to variable amplitude loadings, such as waves and wind. However, most methods for fatigue assessment are based on constant amplitude loading. Variable amplitude load history must, therefore, be converted to an equivalent constant amplitude load history (Berge, 2006).

5.4.1 Constant Amplitude Loading

Figure 5-3 Fatigue load history and symbols (Berge, 2006) as well as the principle of constant amplitude loading and relevant terms, where S_{max} is the maximum stress in a cycle, S_{min} is the minimum stress in a cycle, and S_m is the mean stress in a cycle. The stress range ΔS is defined as the difference between S_{max} and S_{min}.

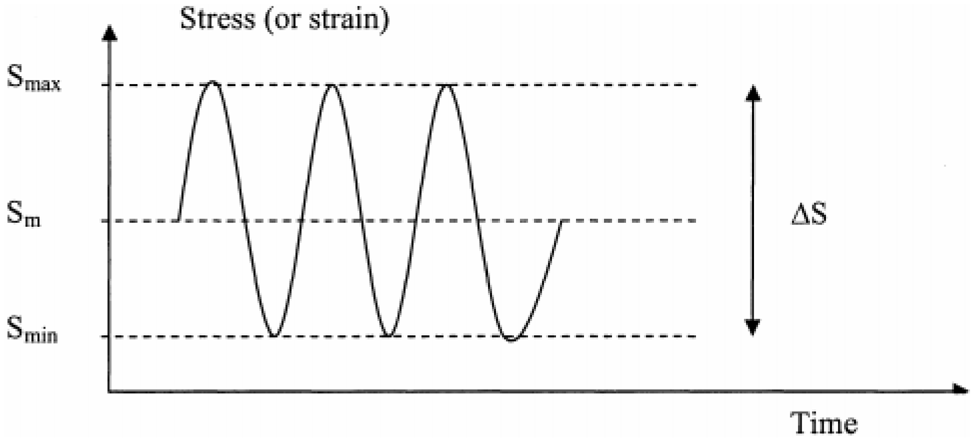

Figure 5-3 Fatigue load history and symbols (Berge, 2006).

5.4.2 Variable Amplitude Loading

Figure 5-4 illustrates an irregular load history and basic parameters related to fatigue and cycle counting. Irregular load history means that the cycles have a varying load range (double amplitude). The load range is defined as the difference between the peak and the valley of each cycle. The following definitions are taken from american society for testing and materials (ASTM, 2011). A valley is defined as the point at which the first derivative of the load-time history changes from a negative to a positive. A peak is defined as the point at which the first derivative of the load-time history changes from a positive to a negative. A reversal is defined as the point at which the first derivative of the load-time history changes sign. A mean crossing is defined as when the load-time history crosses the mean-load level with a positive slope and/or negative slope (as specified).

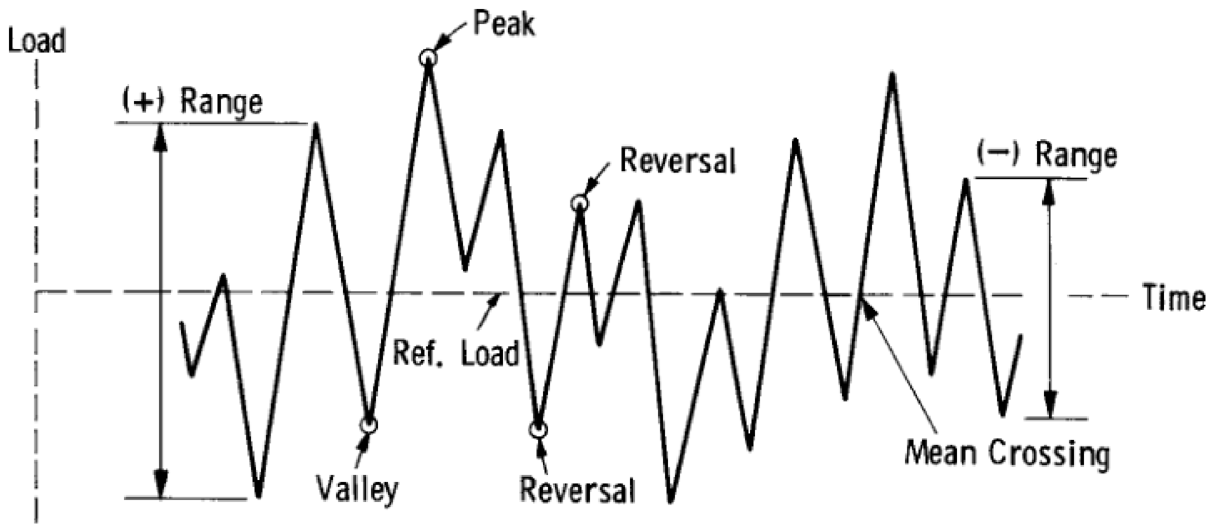

Figure 5-4 Illustration of irregular load-time series with basic fatigue loading parameters pointed out (ASTM, 2011).

5.4.3 Cycle Counting Methods

The purpose of cycle counting is to count cycles of various sizes in an irregular load-time history. Typical load parameters in a time history can be force, stress, strain, and torque acceleration or deflection (ASTM, 2011). There are many different methods of cycle counting; some of the most known are listed below:

- Level crossing counting,
- Peak counting,
- Simple-range counting,
- Range pair counting, and
- Rainflow counting.

The main difference between the methods is how the cycles are defined. The methods generally give similar results for narrow-banded time histories. However, for very wide banded load histories with a low irregular factor, the methods provide scattering results. For that reason, the choice of counting method is important in these cases. According to (Berge, 2006) rainflow counting has proven to be reliable in these cases. The rainflow-counting method is, therefore, widely used as a counting method. An introduction to the principle of the rainflow-counting method will be presented. For further details about the other methods, (ASTM, 2011) or (Berge, 2006) can be studied.

Figure 5-5 a) shows a strain history where the peaks and valleys are marked with numbers, while Figure 5-5 b) shows the corresponding stress-strain response. It can be seen that each time a loop is closed another cycle is counted. These closed loops are called closed hysteresis loops and are shaded in the figure. It can also be seen that not all of the cycles make closed loops. These are counted as half cycles. A more detailed explanation of the rainflow-counting procedure is explained below Figure 5-5.

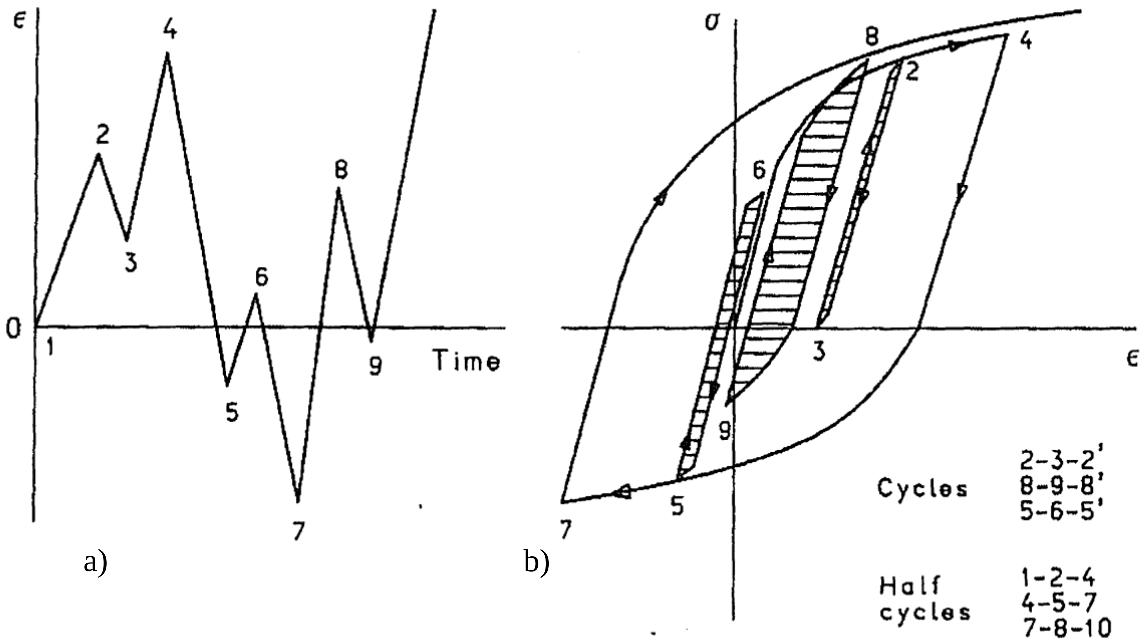

Figure 5-5 a) Strain history and b) the corresponding stress-strain response (Berge, 2006).

The rainflow cycles are counted according to the following rules. The strain history from Figure 5-5 a) is rotated ninety degrees clockwise in Figure 5-6. This is to make it easier to understand the principle of how the cycles are defined. The strain history is visualised as a pagoda roof and the cycles as water that is dripping down. The rules are cited from (Berge, 2006):

1. Rain will flow down the roof, initiating at the inside of each peak or valley. When it reaches the edge, it will drip down.
2. The rain is considered to stop, and a cycle is completed, when it meets another flow from above.
3. Starting from a peak, the flow also stops when it arrives opposite a more positive peak than that from which it started. Starting from a valley, the flow stops when it arrives opposite a more negative valley than that from which it started.

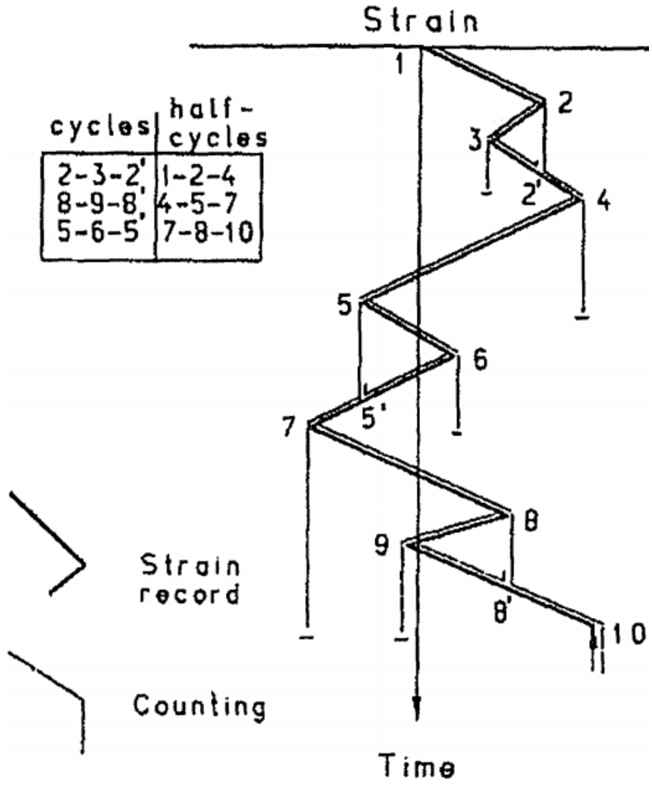

Figure 5-6 Illustration of the cycles are counted by rainflow-counting method (Berge, 2006).

5.5 Rainflow Counting

All the cycles in the load history can be counted and sorted in terms of load range. This is done in order to give a picture of which load ranges are most common. The principle of this process is illustrated in Figure 5-7.

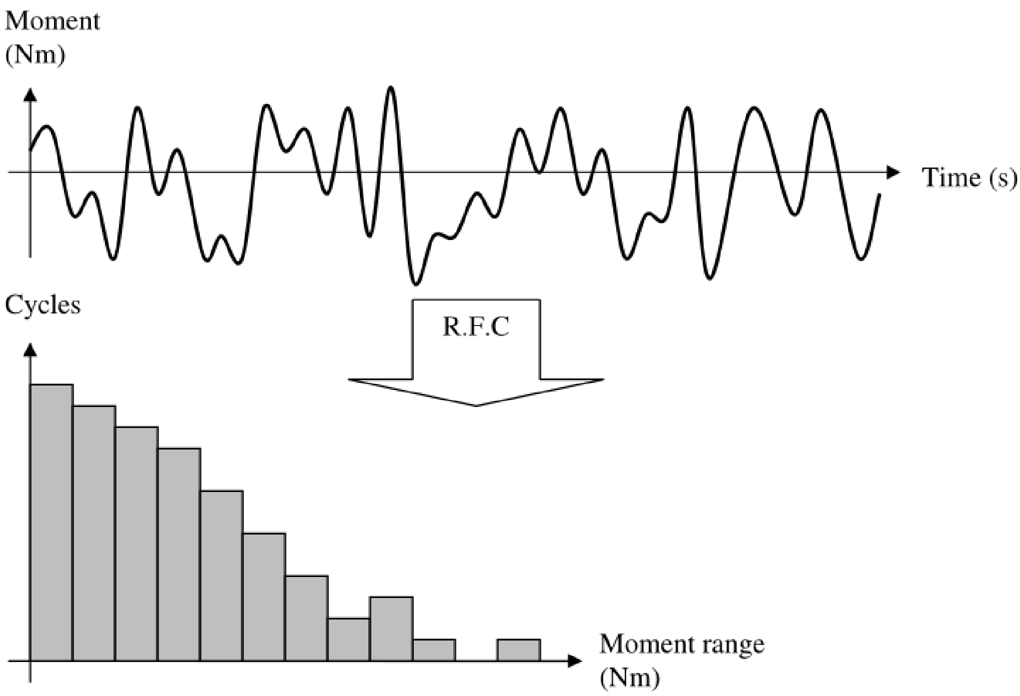

Figure 5-7 Principle of counting and sorting cycles in terms of moment range (DNV, 2011).

The rainflow-counting procedure is done for all individual sea states in a relevant scatter diagram. The result is many short-term load histograms that can be weighted into a long-term load histogram. The weighting process is done according to the probabilities from a relevant scatter diagram. An illustration of this procedure is shown in Figure 5-8.

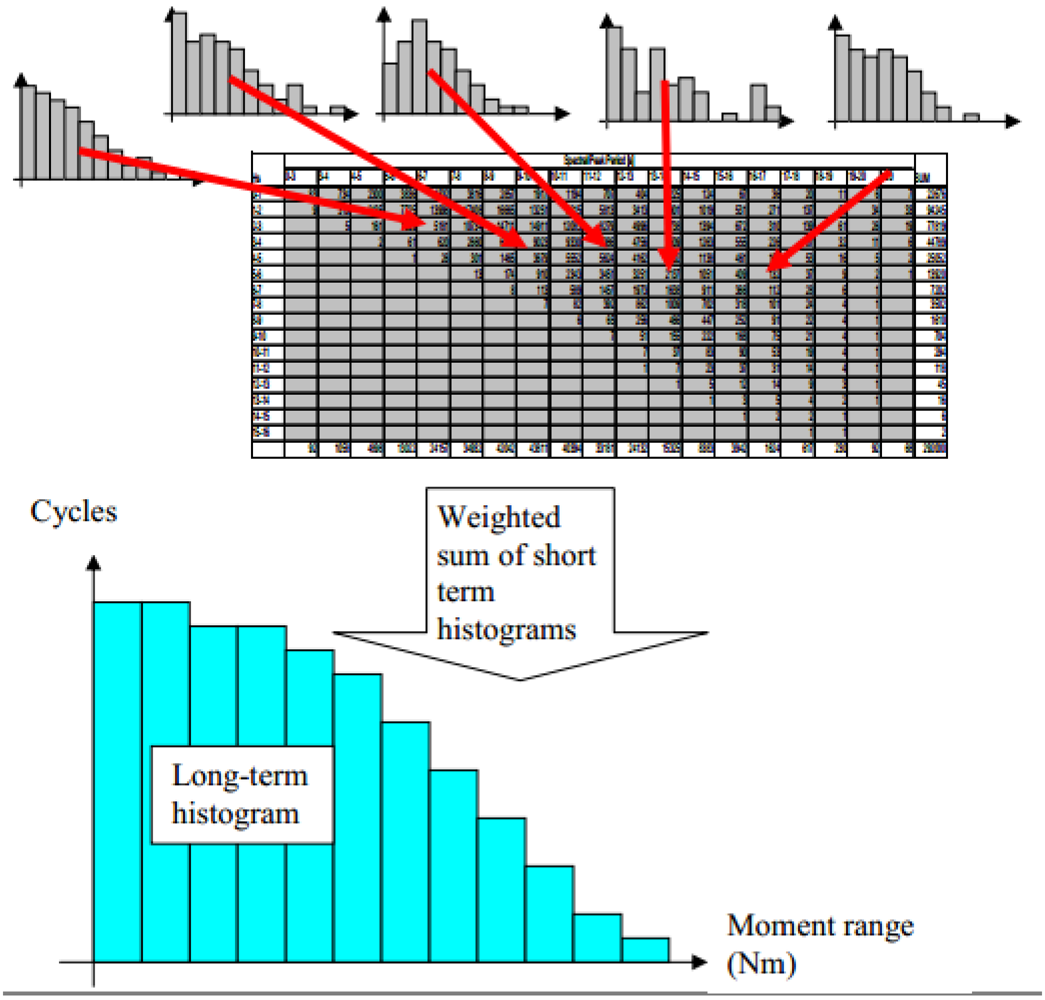

Figure 5-8 Principle of counting the moment range in each sea state and sorting these into a longterm histogram (DNV, 2011).

One of the advantages of storing the data as loads (forces and moments) instead of stress is that the loads will not be affected if the size or geometry of the wellhead changes. For that reason, the load history can be used directly for future screening analysis.

5.6 Fatigue design criterion

The formulas in this section are found in (DNV, 2011). Equation (5.4) states that failure occurs if the total fatigue damage is more or equal to one.

$$D_{fat} \cdot DFF \leq 1.0 \tag{5.4}$$

where D_{fat} is the accumulated fatigue damage from the Miner-Palmgren rule and DFF is the design fatigue factor. The choice of DFF is based on safety classes that are listed in Table 5-1. For drilling operations, a high safety class must be considered.

Table 5-1 Design fatigue factors DFF (DNV, 2010).

Safety class		
Low	*Normal*	*High*
3.0	6.0	10.0

$$\log(N) = \log(\bar{a}) - m \log(\Delta\sigma) \tag{5.5}$$

where N is the predicted number of cycles to failure for stress range $\Delta\sigma$, m is the negative inverse slope of the SN-curve, and $\log(\bar{a})$ is the intercept of log N-axis by the design SN-curve.

The total fatigue damage can then be calculated by the Miner-Palmgren rule, which is given in Equation (5.6). The Miner-Palmgren rule sums up the contributions from the different stress ranges (DNV, 2011):

$$D_{fat} = \frac{1}{a} \sum_{i=1}^{k_{sb}} n \cdot (\Delta\sigma_i)^m \tag{5.6}$$

where a is a constant related the SN-curve, k_{sb} is the number of stress blocks, n is the number of cycles in the stress block with stress range $\Delta\sigma_i$, and m is the negative inverse slope of the SN-curve. Typical values of m are 3, 4, or 5.

5.7 Stress Concentration Factors

The formulas in this section are found in (DNV, 2011). The hot spot stress accounts for possible misalignments that can cause stress concentrations at the welds. This is done by multiplying the nominal stress by a stress intensity factor as given in Equation (5.7):

$$\Delta\sigma_{hot\ spot} = SCF \cdot \Delta\sigma_{nominal} \tag{5.7}$$

where $\Delta\sigma_{hot\ spot}$ is the hot spot stress, SCF is the stress concentration factor, and $\Delta\sigma_{nominal}$ is the nominal stress.

The stress concentration factor can be calculated according to Equation (5.8):

$$SCF = 1 + \frac{3\delta_m}{t} e^{-\sqrt{t/D}} \tag{5.8}$$

where δ_m is maximum misalignment, t is the pipe wall thickness, and D is the outer diameter of the pipe.

5.8 SN-data Offshore Steel Structures

Relevant SN-curves for fatigue design of offshore steel structures can be found in (DNV, 2012). Figure 5-9 shows twelve design SN-curves that can be used in the design of offshore steel structures with cathodic protection. The twelve design curves are for different welding classes. The upper weld classes, such as B and C curves, have a higher fatigue life than the lower curves, such as F, G, or W. The upper weld classes are typically of higher quality. Factors that can influence the categorisation of welds are welding geometry, residual stresses, tolerances, and post-weld treatment.

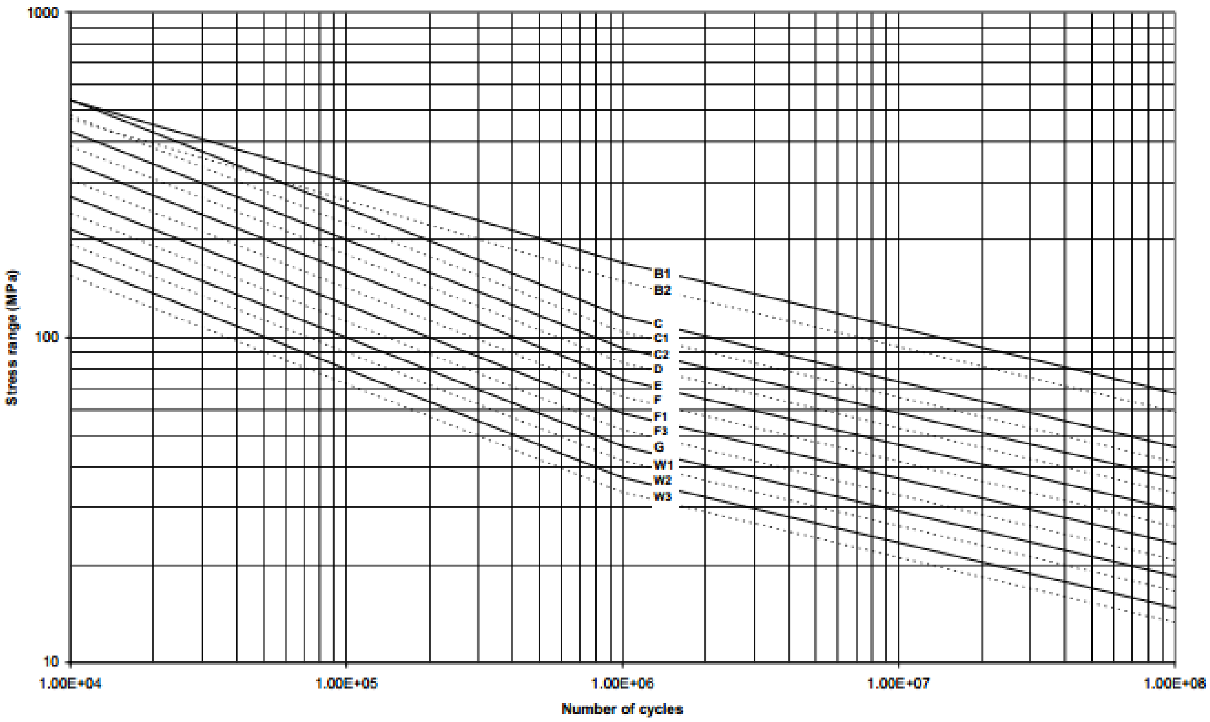

Figure 5-9 SN-curves in seawater with cathodic protection (DNV, 2012).

The most critical parts with respect to fatigue in the majority of the cases are the welds because they can have a more brittle structure and have faults in the material as a result of the welding process. Table 5-2 shows typical welding geometries and the corresponding design SN-curves.

Table 5-2 Classification of welds (DNV, 2012).

Description		*Tolerance requirement*	*S-N curve*	*Thickness exponent k*	*SCF*
Welding	*Geometry and hot spot*				
Single side	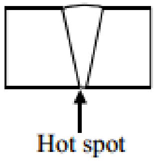	$\delta \leq$ min (0.15t, 3 mm)	F1	0.00	1.0
		$\delta >$ min (0.15t, 3 mm)	F3	0.00	1.0
Single side on backing	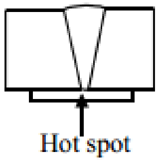	$\delta \leq$ min (0.1t, 2 mm)	F	0.00	1.0
		$\delta >$ min (0.1t, 2 mm)	F1	0.00	1.0
Single side	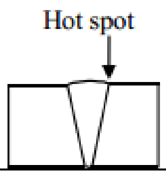		D	0.15	Eq. (2.10.1)
Double side	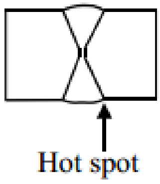		D	0.15	Eq. (2.10.1)

Several methods can improve the fatigue life of a weld. Grinding is one of the methods that are commonly used in order to improve fatigue life. Table 5-3 shows the classification of machine grinded welds. By comparing Table 5-2 and Table 5-3, it can be seen that machine grinding can have a significant improvement on the weld's fatigue life. As an example, the design life of a single side welding can be improved from category F1 to C1. By studying Figure 5-9 with a stress range of about 100 MPa, the number of cycles can be improved from roughly $2.0 \cdot 10^5$ to $1.0 \cdot 10^6$ cycles because machine grinding will leave a smooth surface without slag and other defects from which the cracks can start growing. Hence, the initiation phase of the fatigue life will be much longer (Berge, 2006). If grinding is used, there is a requirement that the weld shall be examined by non-destructive methods to ensure that the weld is of high quality.

Table 5-3 Classification of machine grinded welds (DNV, 2012).

Description		*S-N curve*	*Thickness exponent k*	*SCF*
Welding	*Geometry and hot spot*			
Single side	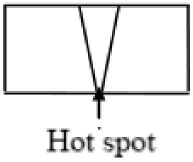	C1	0.15	Equation (6)
Single side	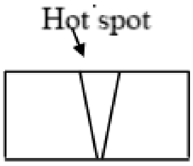	C1	0.15	Equation (6)
Double side	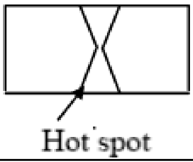	C1	0.15	Equation (6)

5.9 Thickness Effect

The effect of thickness is given in Equation (5.9).

$$\log(N) = \log(\bar{a}) - m \log\left(\sigma\left(\frac{t}{t_{ref}}\right)^{k}\right) \tag{5.9}$$

where t_{ref} is the reference thickness, which is typically 25 mm for girth welds in pipes, while t is the thickness through which the crack most likely will grow, and k is the thickness exponent on fatigue strength (DNV, 2011).

5.10 Typical Hot Spots on Wellhead and Casing

The information in this section is provided by (Fedem & Berbu, 2015). Typical hot spots on the conductor (blue) and wellhead (green) housings are illustrated in Figure 5-10. The areas below the swage radii and the 30in extension weld are hot spots on the conductor housing. The 20in extension weld is also a hot spot and is located below the narrowing portion on the wellhead. It is expected that these hot spots are the weak links with respect to fatigue, but the plain pipe casing should also be checked to verify this.

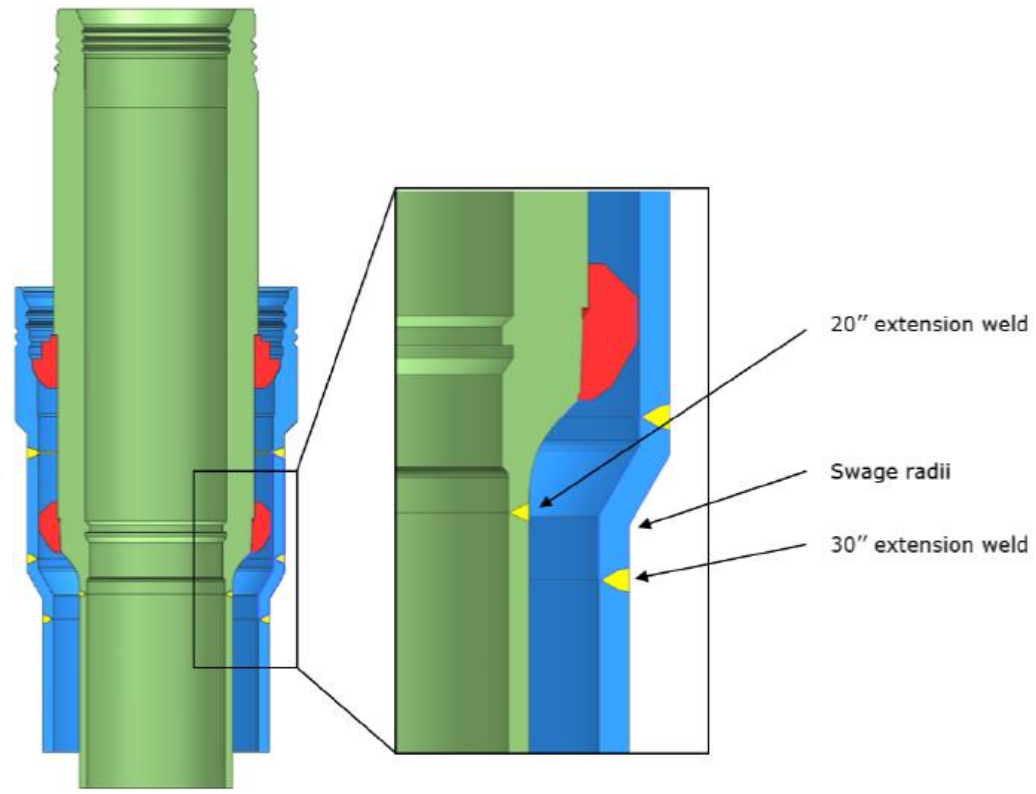

Figure 5-10 Hot spots in wellhead and conductor housing (Fedem & Berbu, 2015).

In addition to checking the wellhead and the conductor housing, the upper most 30 connector and the upper most 20in are checked for fatigue life. These connectors are located, respectively, 15.6 metres and 5.5 metres below the mud line. For the connector, both the welds and the base materials should be checked.

6 Procedure of Wellhead Fatigue Analysis

The flowchart in Figure 6-1 describes the procedure of wellhead fatigue analysis. This thesis focuses on global analysis. The results from the global analysis are primarily wellhead loads. These data are post processed for further fatigue calculations. Information on hot spots and corresponding load-to-stress functions and SCFs must be attained. Load-to-stress functions are found through local analysis of the wellhead system, casing, and soil model. The SCFs are found in a detailed finite element analysis (FEA) model. Results from a local analysis and SCFs are provided by Statoil and are considered input data for this thesis.

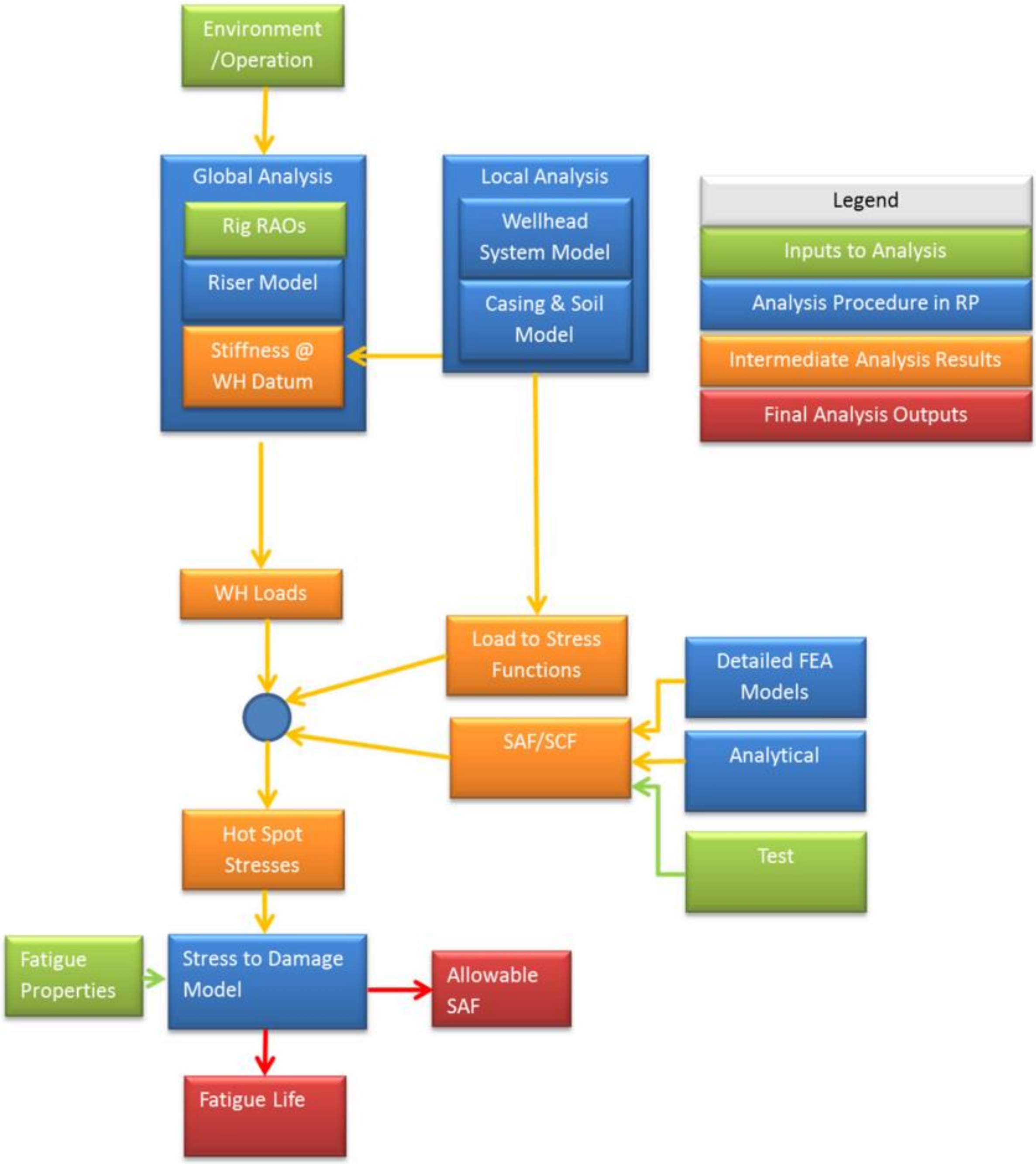

Figure 6-1Flowchart wellhead fatigue analysis method (DNVGL, 2015).

7 Results from Local Model

In this section, the results from the local analysis that are provided by Statoil are presented (Grytøyr, 2015c). This information is necessary, as the well is a complex structure and simplified analytical calculations will not give realistic results. Results of interest are load-to-stress functions at the various hot spots and corresponding SCF and SN-curves.

The results from the local model are provided by (Grytøyr, 2015c). The results are based on a benchmark study that Statoil uses as a training program for new employees. Input data for the local model of the wellhead can be studied in Appendix A, and the soil data can be studied in Appendix B.

7.1 Hot Spots

In Figure 7-1, the following eight hot spots are marked on the local model:

- Hot spot 10_1: wellhead extension weld (outside),
- Hot spot 10_2: wellhead extension weld (inside),
- Hot spot 11_1: surface casing connector,
- Hot spot 20_1: conductor housing extension weld (outside),
- Hot spot 20_2: conductor housing extension weld (inside),
- Hot spot 21_1: conductor casing connector,
- Hot spot 21_2: conductor casing connector weld (outside), and
- Hot spot 21_3: conductor casing connector weld (inside).

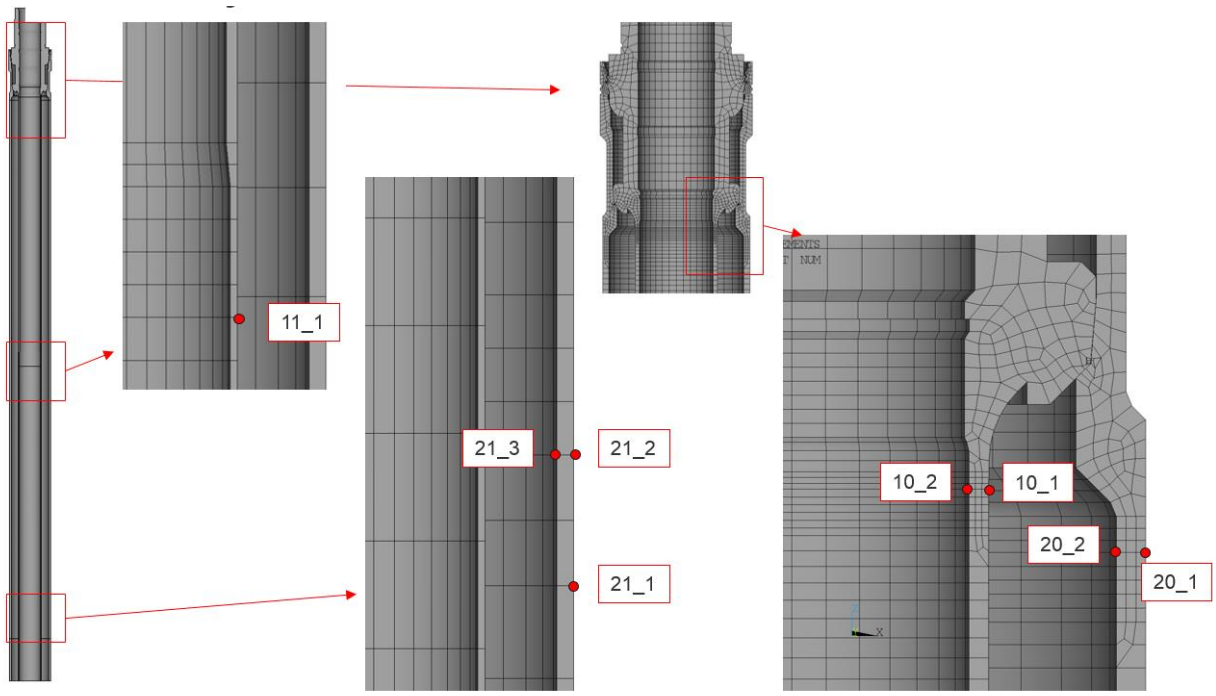

Figure 7-1 Overview of the hot spots from local analysis (Grytøyr, 2015c).

7.2 SCF and SN-curves

The choice of SCF and SN-curve for the fatigue calculations depends on the type of hot spot. In Table 7-1, the type of hot spot with corresponding SCF and design SN-curves are listed. Statoil provided this information, but the background of how this information was obtained is not specified. According to the theory discussed in Section 5.8, the selection of SN-curve will have a significant effect on the estimated fatigue life.

In general, SN-curve B1 is applicable to plain plates without welds, and C1 is applicable to machine flushed welds. In order to use B1 and C1 curves, the hot spots must be completely protected from the corrosive environment. This includes during transportation and storage phases. If this not is the case, SN-curve F3 should be considered. When using SN-curve F3, the weld is not sensitive to corrosion because the weld itself will be the weak link; therefore, if corrosion occurs on top of the weld, it will not have a significant effect on the fatigue life.

Table 7-1 SCF and design SN-curves for the hot spots (Grytøyr, 2015c).

Hot spot number	Hot spot description	SCF	SN curve	OD [inch]	WT [inch]
10_1	Weld OD Housing/Extension	1.197	C1	20	1
10_2	Weld ID Housing/Extension	1.197	C1	20	1
11_1	Connector	4.2	B1	20	0.635
20_1	Weld OD Housing/Extension	1.111	C1	36	1.5
20_2	Weld ID Housing/Extension	1.111	C1	36	1.5
21_1	Connector	5.0	B1	36	1.5
21_2	Weld OD Extension/Connector	1.111	C1	36	1.5
21_3	Weld ID Extension/Connector	1.111	C1	36	1.5

7.3 Load-to-stress Functions

The local analysis determines the stresses in the hot spots by applying moments at the wellhead datum. The results are transfer functions that obtain the correlation between the moment at the wellhead datum and the stresses at the hot spots.

Statoil provided text files with load-stress data for the hot spots. The data are plotted in Figure 7-2. In order to understand the naming procedure of the load-stress functions, the load-stress functions “STF_P11_10_1_case_0_0” and “STF_P11_20_1_case_31_0” are explained in the following bullet points:

- P11: The first numeral, 1, indicates that it is operation phase 1 (drilling phase where the BOP lands on the WH) and the second numeral, 1, indicates that one casing is installed (which is the surface casing in this case). The number of casings installed affects the down weight on the wellhead and, therefore, is an important parameter in the local analysis.
- 10_1 and 20_1: Indicate the hot spot numbering according to Figure 7-1.
- Case_0_0: Indicates that cement level is 0 and the grout (scour) level is 0. This case corresponds to the *base case,* which is illustrated in Figure 4-7.
- Case_31_0: Indicates cement level 31 and grout (scour) level 0. This case corresponds to the *cement shortfall between 20” and 30”,* which is illustrated in Figure 4-7.

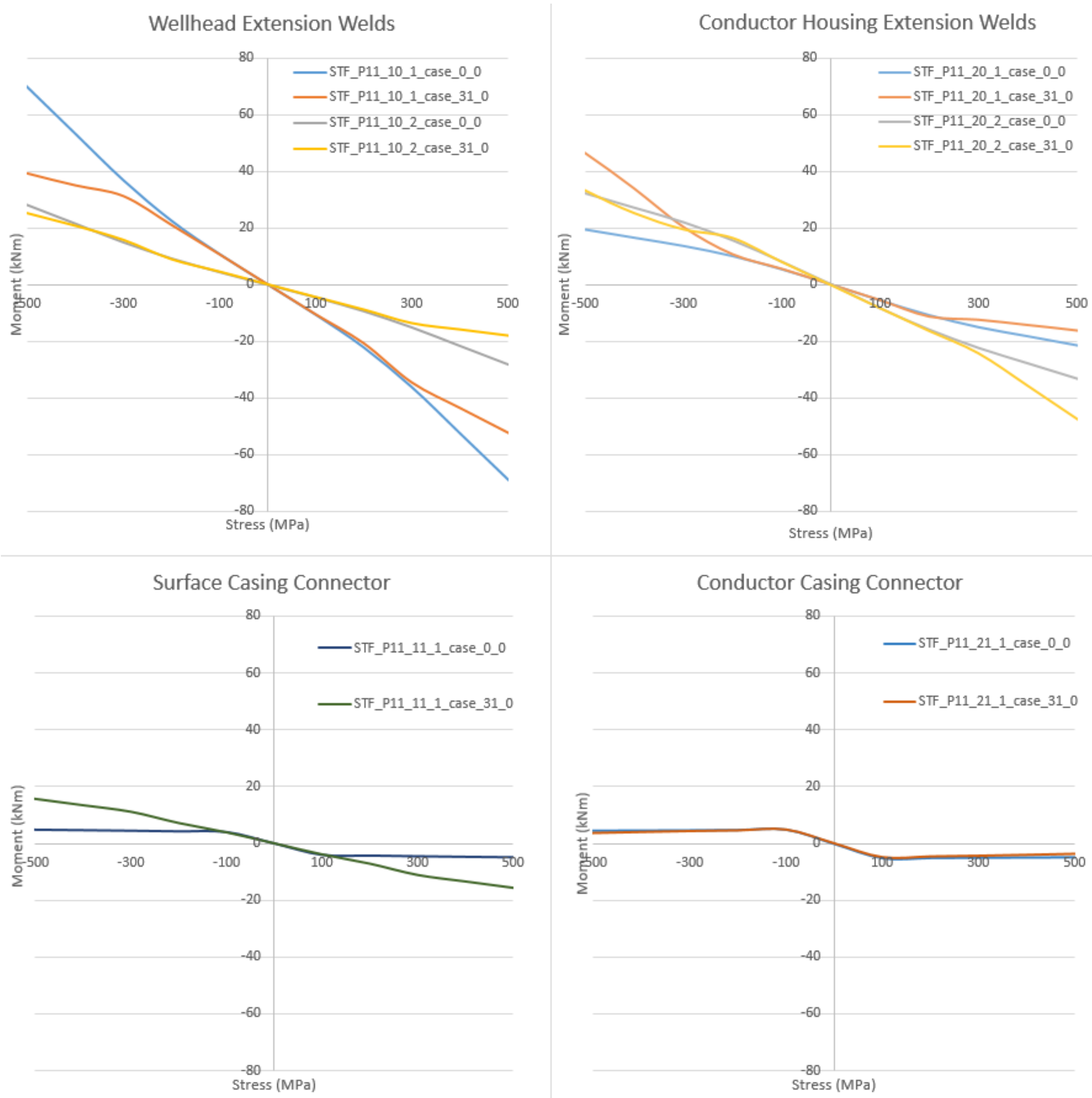

Figure 7-2 Transfer functions moment-to-stress for the hot spots.

By comparing case_31_0 and case_0_0, it is evident that the lack of cement between 20” and 30” results in higher stresses for all the hot spots except the conductor casing connector. This may be because the conductor casing connector is located at a distance below the other hot spots, which is located below the cement shortfall. It can also be seen that the plots have some non-linearities, especially for cement level “31”. One possible explanation for this could be that the parts glide relative to each other.

Note that load-stress data for the conductor casing connector weld (hot spots 21_2 and 21_3) was not included in the provided files. Therefore, these hot spots are not included in further analyses.

8 Presentation of the RIFLEX-model (Case Study)

8.1 General

In the following chapter, the RIFLEX model is presented. The model is based on the drilling riser example and the Njord drilling system example. Both of these models were provided by MARINTEK. The examples were then modified to suit the thesis. The configuration presented is a case study of a semi-submersible operating in weather conditions from the North Sea (Ekofisk-field).

8.2 RIFLEX Model

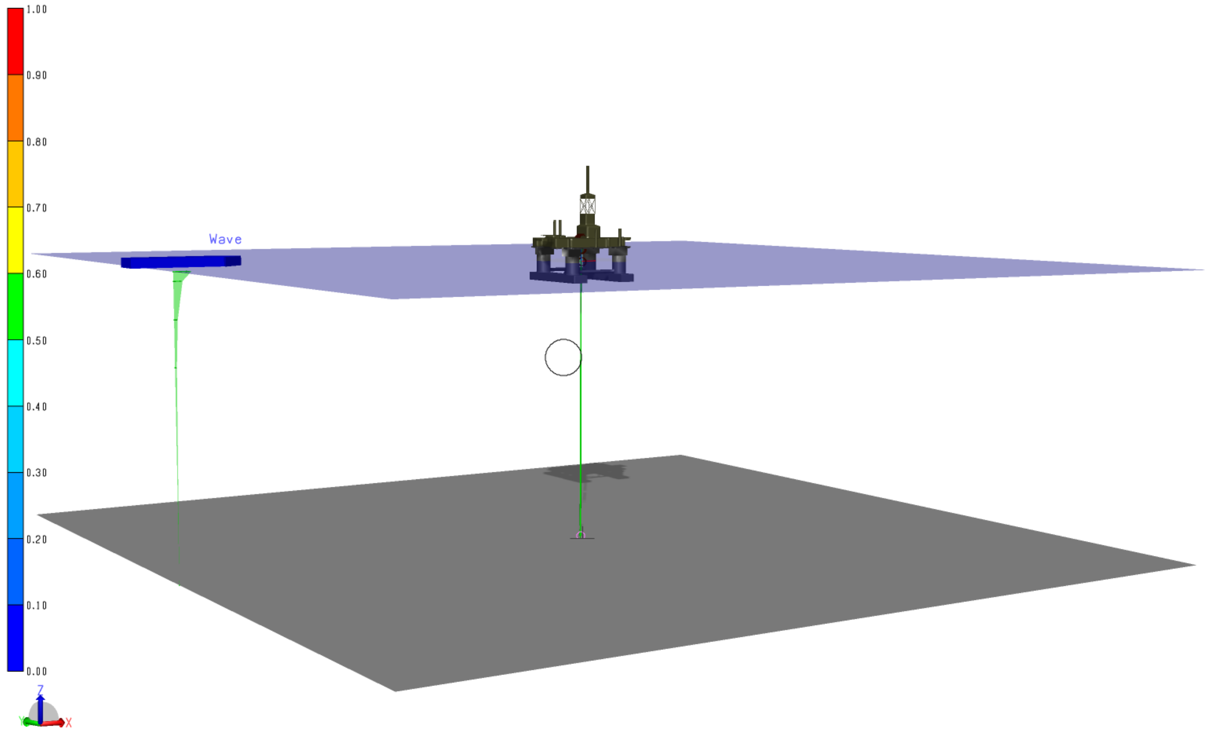

Figure 8-1 RIFLEX model in static condition.

Figure 8-1 shows a screenshot of the 3D model in RIFLEX. The grey and blue rectangle represents the seafloor and sea surface, respectively. The water depth is 330 metres. The vessel in the middle is a semi-submersible, and the green line beneath is the riser system. The blue arrow to the left indicates the wave propagation direction, and the green graph below indicates how the current varies with the water depth.

A more detailed view of the components in the upper part of the riser model is given in Figure 8-2. The figure shows the upper flex joint located on top of the riser column. There are six tensioners with a super node at each end. The telescopic joint is located below the upper flex joint.

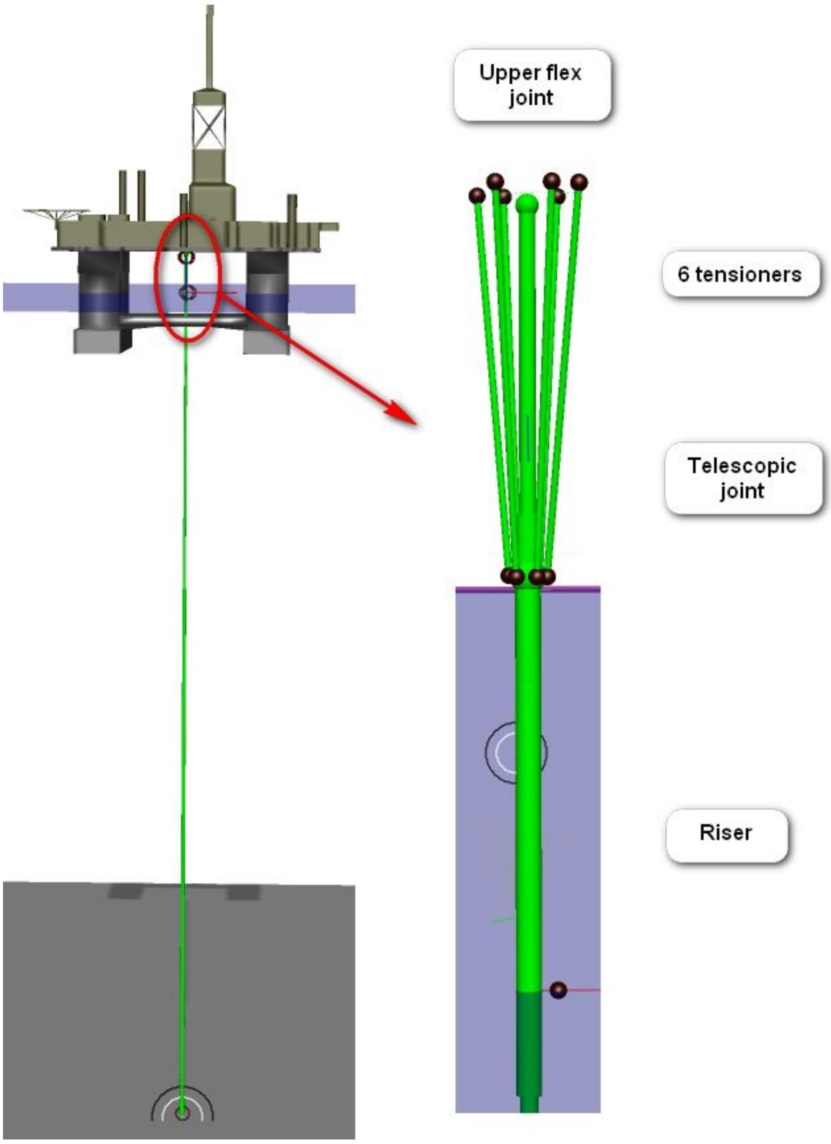

Figure 8-2 Detailed view of the upper part of the riser model (RIFLEX).

A more detailed view of the lower part of the riser model can be studied in Figure 8-3. This view includes the flex joint that is located in the upper part of the LMRP. The BOP is located below the LMRP. The wellhead is illustrated as a node below the BOP.

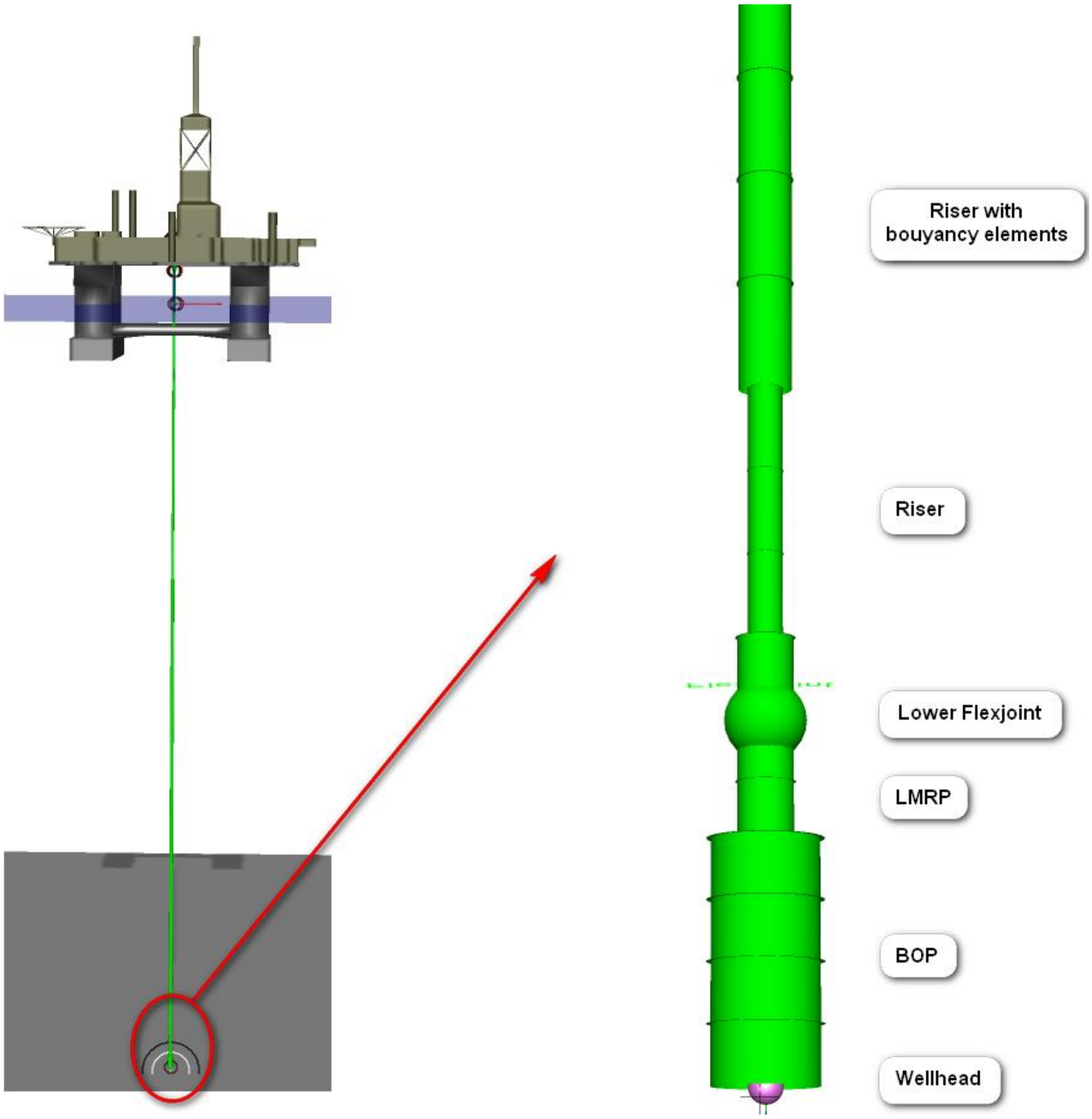

Figure 8-3 Detailed view of the lower part of the riser model (RIFLEX).

8.3 Structural Modelling in RIFLEX

8.3.1 MODU Transfer Functions

First order motion transfer functions are generally calculated in another program, such as wave analysis Massachusetts Institute of Technology (WAMIT) or Wadam. Therefore, these functions can be considered input parameters in this analysis. The wave heading is 0 degrees; therefore, surge and pitch motions are important in this analysis. These functions will describe the lateral displacement of the top of the drilling riser. The first order motion transfer function for surge and pitch is presented in Figure 8-4 and Figure 8-5. Heave motion is compensated for by the heave compensator system, and yaw motion is not important for the drilling riser.

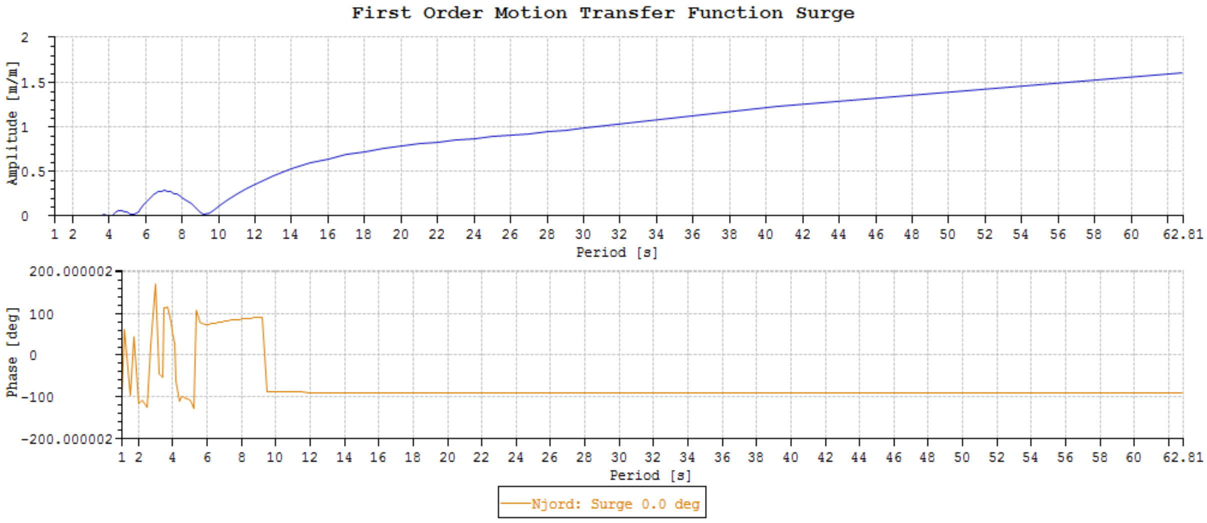

Figure 8-4 RAO Surge.

Roll, pitch, and yaw are dimensionless and given as rotation per wave slope (MARINTEK, 2014a).

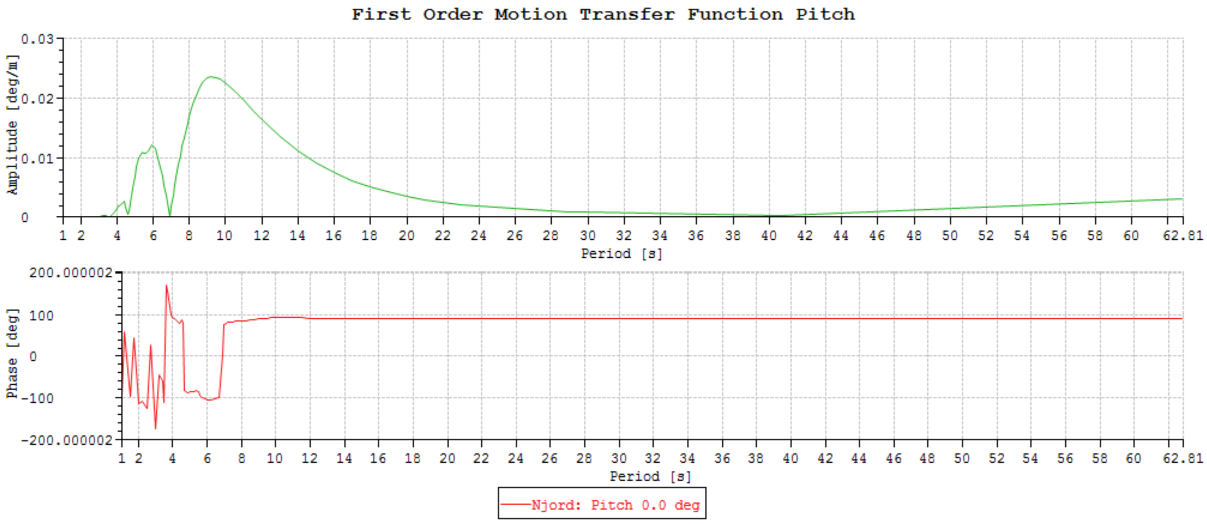

Figure 8-5 RAO Pitch.

8.3.2 Riser

The total length of the riser is 315 metres. The riser consists of four different riser joints with different cross-sectional properties. The upper and lower part of the riser consists of pup 20 ft and pup 15 ft joints. Pup joints are defined as riser joints that are shorter than the standard riser joint length (API, 2010). Table 8-1 illustrates that the lower pup joints (pup 15 ft) have a larger weight per unit length compared to the slick joint and the 20 ft pup joint. This may be because the lower section of the riser is a critical area and needs to be reinforced. The majority of the risers consist of slick joints (slick 50 ft) and riser joints with buoyancy elements (buoyancy 50 ft). A slick joint is defined as a special riser joint that is designed to prevent damage to the riser (API, 2010). As illustrated in Table 8-1, the hydrodynamic properties are the same for the pup and slick joints. The buoyancy elements have a larger hydrodynamic diameter, which will result in larger environmental forces acting on this section.

Table 8-1 Length and cross section properties for the riser joints.

Parameter	Pup20ft_cs	Slick50ft_cs	Buoyancy50ft_cs	Pup15ft_cs	Unit
Length	6.096	106.68	198.12	4.572	$[m]$
Internal diameter	527.0	502.0	527.0	527.0	$[mm]$
External diameter	792.8	750.0	1085.7	798.1	$[mm]$
Thickness	264.8	248.0	558.7	271.1	$[mm]$
Mass coefficient	442.91	361.09	558.01	503.06	$[kg/m]$
Submerged weight	161.7	111.0	-167.3	213.87	$[kg/m]$
Axial stiffness	$5.43{\cdot}10^9$	$5.43{\cdot}10^9$	$5.43{\cdot}10^9$	$5.43{\cdot}10^9$	$[Nm^2]$
Bending stiffness	$1.82{\cdot}10^8$	$1.82{\cdot}10^8$	$1.82{\cdot}10^8$	$1.82{\cdot}10^8$	$[Nm^2]$
Torsion stiffness	$1.41{\cdot}10^8$	$1.41{\cdot}10^8$	$1.41{\cdot}10^8$	$1.41{\cdot}10^8$	$[Nm^2]$
Hydrodynamic diameter	0.762	0.762	1.113	0.762	$[m]$
Drag coefficient	1.0	1.0	1.0	1.0	[-]
Added mass coeff.	0.822	0.822	1.1	0.822	[-]

8.3.3 Internal Fluid

The internal volume of the riser column contains drilling fluid. The drilling fluid has the following properties Table 8-2:

Table 8-2 Properties internal fluid.

Parameter	Fluid	Unit
Density	1600	$[kg/m^3]$
Volumetric flow rate	0	$[m^3/s]$
Inlet pressure	0	$[Pa]$
Pressure drop	0	$[Pa/m]$

8.3.4 BOP

The BOP is modelled using beam elements. It should be mentioned that the stiffness of the elements that make up the BOP is significantly greater than the elements that make up the riser. Therefore, the riser will have much greater deflections, and the BOP will have small deformations. Furthermore, the BOP is divided into two segments, with two elements per segment. The lower segment of the BOP is modelled by cross section bop_cs1 and the upper segment is modelled by cross-section bop_cs2. These two cross sections are, however, identical. It may seem redundant to define two identical cross sections, but it can be useful when conducting parametric studies on the BOP mass. Since the wellhead is part of the lower segment of the BOP, this segment must be kept constant during parameter studies. The cross section properties for the BOP are given in Table 8-3:

Table 8-3 Properties BOP.

Parameter	bop_cs1	bop_cs2	Unit
Length	2.214	2.214	[m]
Mass coefficient	19191	19191	$[kg/m]$
External cross section area	2.792	2.790	$[m^2]$
Internal cross section area	0.197	0.197	$[m^2]$
Height	4.282	4.282	$[m]$
Axial stiffness	$1.0{\cdot}10^{13}$	$1.0{\cdot}10^{13}$	$[Nm^2]$
Bending stiffness	$1.0{\cdot}10^{13}$	$1.0{\cdot}10^{13}$	$[Nm^2]$
Torsion stiffness	$1.0{\cdot}10^{13}$	$1.0{\cdot}10^{13}$	$[Nm^2]$
Hydrodynamic diameter	4.521	4.521	$[m]$
Drag coefficient	1.0	1.0	[-]
Added mass coefficient	1.1	1.1	[-]

8.3.5 LMRP

The LMRP is modelled similarly to the BOP. Beam elements with the same stiffness properties as the BOP are used. Furthermore, the LMRP is divided into three segments, with one element per segment. The cross-sectional properties for the LMRP are listed in Table 8-4.

Table 8-4 Properties LMPR.

Parameter	Lmrp_cs1	Lmrp_cs2	Lmrp_cs3	Unit
Mass coefficient	33039	5002	5002	[kg/m]
External cross section area	0.742	0.375	0.375	$[m^2]$
Internal cross section area	0.197	0.198	0.198	$[m^2]$
Height	1.0	1.092	1.478	[m]
Axial stiffness	$1.0{\cdot}10^{13}$	$1.0{\cdot}10^{13}$	$1.0{\cdot}10^{13}$	$[Nm^2]$
Bending stiffness	$1.0{\cdot}10^{13}$	$1.0{\cdot}10^{13}$	$1.0{\cdot}10^{13}$	$[Nm^2]$
Torsion stiffness	$1.0{\cdot}10^{13}$	$1.0{\cdot}10^{13}$	$1.0{\cdot}10^{13}$	$[Nm^2]$
Hydrodynamic diameter	4.521	4.521	4.521	[m]
Drag coefficient	1.0	1.0	1.0	[-]
Added mass coefficient	1.1	1.1	1.1	[-]

8.3.6 Telescopic Joint

The telescopic joint comprises two cylinders, the outer and inner barrel, that slide relative to each other. Therefore, the telescopic joint is modelled by two cylinders each consisting of one segment with one element per segment. The inner barrel has a smaller diameter than the outer barrel. The cross-sectional properties for the inner and outer barrel are listed in Table 8-5.

Table 8-5 Properties telescopic joint.

Parameter	**Inner barrel**	**Outer barrel**	**Unit**
Total mass	0	1728	$[kg]$
External cross section area	0.223	0.551	$[m^2]$
Internal cross section area	0	0	$[m^2]$
Height	10.549	2.085	[m]
Axial stiffness	10	$6.22{\cdot}10^9$	$[Nm^2]$
Bending stiffness	0	$2.74{\cdot}10^8$	$[Nm^2]$
Torsion stiffness	$1.405{\cdot}10^8$	$2.121{\cdot}10^8$	$[Nm^2]$
Hydrodynamic diameter	0	0.83	[m]
Drag coefficient	0	1.0	[-]
Added mass coefficient	0	1.0	[-]

8.3.7 Tensioners

There are six tensioners, and each tensioner is modelled separately in RIFLEX. Each tensioner consists of one segment with seven elements. The difference between the tensioners and the other slender systems in the riser system is the tensioners are the only components that are modelled by bar elements. This is because the tensioners only provide stiffness in the axial direction. The tensioners provide axial forces that are a function of the elongation and are plotted in Figure 8-6. The stiffness of the top tensioners can be can be varied depending on the top tension. There is also some friction and axial damping in the tensioners, which will not be discussed in any detail.

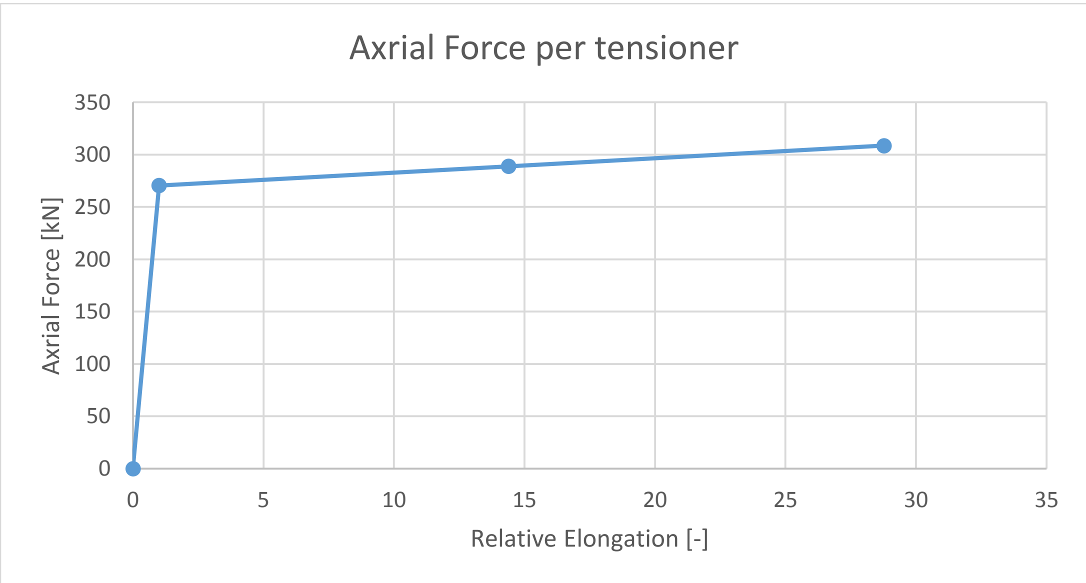

Figure 8-6 Axial force per tensioner.

8.4 Upper and lower flex joint

The upper and lower flex joints are inserted from the RIFLEX database. Their properties are listed in Table 8-6. Notice that only the lower flex joint has rotational damping. The lower flex joint also has non-linear stiffness in Y and Z rotations.

Table 8-6 Properties flex joints.

Parameter	Upper flex joint	Lower flex joint	Unit
Damping Rot Y	0	43280	$[Nms/deg]$
Damping Rot Z	0	43280	$[Nms/deg]$
Stiffness rotation X	Linear	Linear	
Stiffness rotation Y	Linear	Non linear	
Stiffness rotation Z	Linear	Non linear	

8.5 Wellhead and the Lower Boundary Conditions

The well line is modelled using beam elements and extends from the wellhead datum 16 metres down to the soil node. The beam elements are assigned mass and stiffness properties in order to represent the mass and stiffness of the well. Eleven soil springs are created in order to give a realistic representation of the lateral stiffness contribution from the soil. The boundary condition at the top of the well is free with respect to translations and rotations, while the boundary condition at the bottom of the well is fixed with respect to translations and free with respect to rotations. This means that the lateral displacement of the wellhead datum is strongly dependent on the soil springs that support the well. The model of the well, including the soil springs, is shown in Figure 8-7.

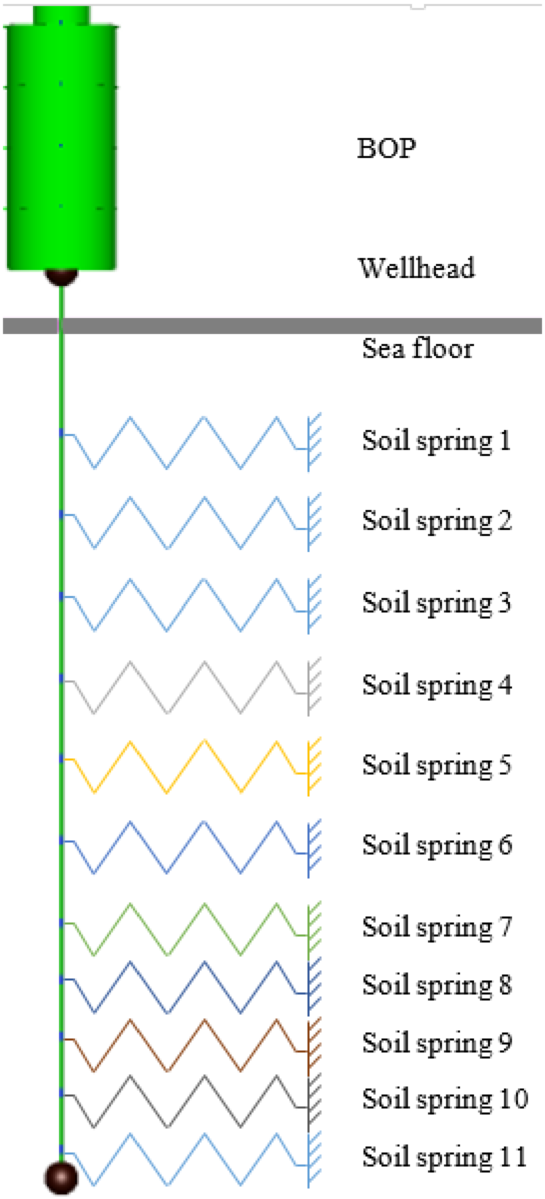

Figure 8-7 Model of the well and soil springs.

The eleven soil springs have non-linear stiffness in the XY plane and the force-displacement relation for the springs is plotted in Figure 8-8. The stiffness is the slope of the curves. Springs 1, 2, and 3 have the lowest stiffness. This is expected since the soil stiffness usually increases with distance below the mud line. It can also be seen that springs 8, 9, and 10 have a lower stiffness than springs 4, 5, 6, and 7. This is a bit unexpected but can partly be explained by the fact that the springs in the lowest section of the well are located closer to each other.

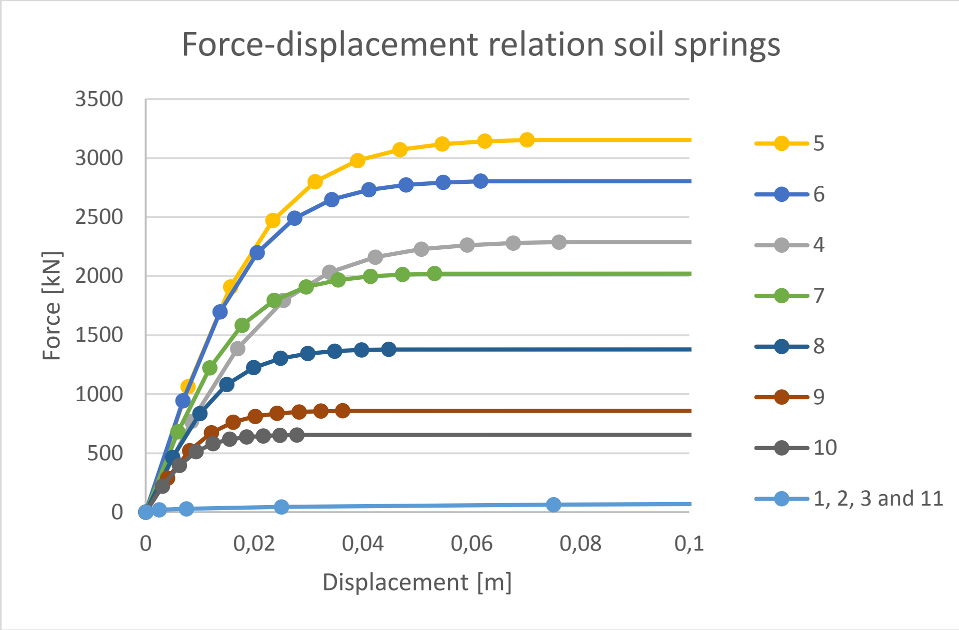

Figure 8-8 Lateral support of the wellhead with, non-linear spring.

8.6 Environment

The model is simulated under different environmental conditions. The sea consists of irregular waves in the real world. Therefore, simulations using irregular wave environments will attain the most realistic results. For parametric studies, all parameters are kept constant except the parameter that is studied. For parameter studies, it may be useful to use a regular wave environment.

8.6.1 Irregular Wave Environment

The irregular wave parameters in RIFLEX are given in Table 8-7. The direction indicates from which angle the waves are coming. The RAO file will provide the MODU different motions depending on the wave direction. Since the components in the riser system are circular, the wave direction will not affect the environmental forces that act on the riser system. As illustrated in Figure 8-1, a zero-degree angle corresponds to beam sea. The spreading of the wave is set to zero, which indicates a unidirectional sea. In addition to Hs and Tp, which were explained in Section 4.6, the seed is an important parameter for the irregular sea in RIFLEX. The seed parameter determines the phase angles that are generated. The principle is that the sea spectrum is divided into small parts. Each part is described by the sum of cosine and sine functions. Therefore, the phase angles in these functions will affect the results.

Table 8-7 Irregular sea parameters.

Parameter	**Value**	**Unit**
Direction	0	$[deg]$
Spreading code	Unidirectional	[-]
Spreading	0	[-]
Significant wave height	Variable	$[m]$
Spectral peak period	Variable	$[s]$
Seed	Variable	[-]
Gamma	3.3	[-]
Water depth		$[m]$

The analysis is run for all the sea states in the scatter diagram in Table 8-8. The scatter diagram is from the Ekofisk-field during 1980-1993. The sea states in the scatter diagram depend on the location. Therefore, a scatter diagram for another area may be very different.

Table 8-8 Scatter diagram for the Ekofisk-field (Myrhaug, 2007).

Hs / Tp	**<4**	**5**	**6**	**7**	**8**	**9**	**10**	**11**	**12**	**13**	**14**	**15**	**16**	**17**	**18**	**19**	**20**	**21**	
0.5	219	247	98	56	108	139	85	53	38	28	16	9	3	1	1	1			1102
1.0	462	1444	1332	551	394	409	362	255	153	126	66	73	28	20	9	4		1	5689
1.5	54	763	1991	1654	703	436	327	258	176	86	49	49	23	21	22	3	3	3	6621
2.0	1	114	994	2015	1329	583	260	246	193	91	37	20	10	16	14	3	1		5927
2.5		7	189	1122	1532	734	261	182	165	124	48	20	8	1	1	2	1		4397
3.0			14	329	1082	958	309	137	139	96	39	13	6			1	1	1	3125
3.5				59	533	983	382	140	87	72	33	15	4	2		1			2311
4.0				10	133	660	418	144	65	36	23	14	3	4					1510
4.5					28	313	417	149	41	25	7	10	4	1					995
5.0					2	113	271	190	40	19	8	6	2	1					652
5.5						23	154	136	49	23	7	12	4						408
6.0						4	61	109	52	26	4	6	4						266
6.5							20	58	35	14	6	4	5						142
7.0							6	23	35	14	5	2	1						86
7.5							2	21	16	13	4	3	2	1	1				63
8.0								4	8	9	3	1							25
8.5								2	8	3	2	3	2						20
9.0									2	5	2								9
9.5									1	5	1	3	2						12
10.0												1							1
10.5										2	1	1		1					5
11.0											1								1
11.5										1		1		1					3
12.0												1							1
	736	2575	4618	5796	5844	5355	3335	2107	1303	818	362	267	111	70	48	15	6	5	33371

An illustration of the JONSWAP-spectrum with $Hs = 6.0$ and $Tp = 12.0$ is given in Figure 8-9. The spectrum shows that most of the energy is concentrated around the peak period.

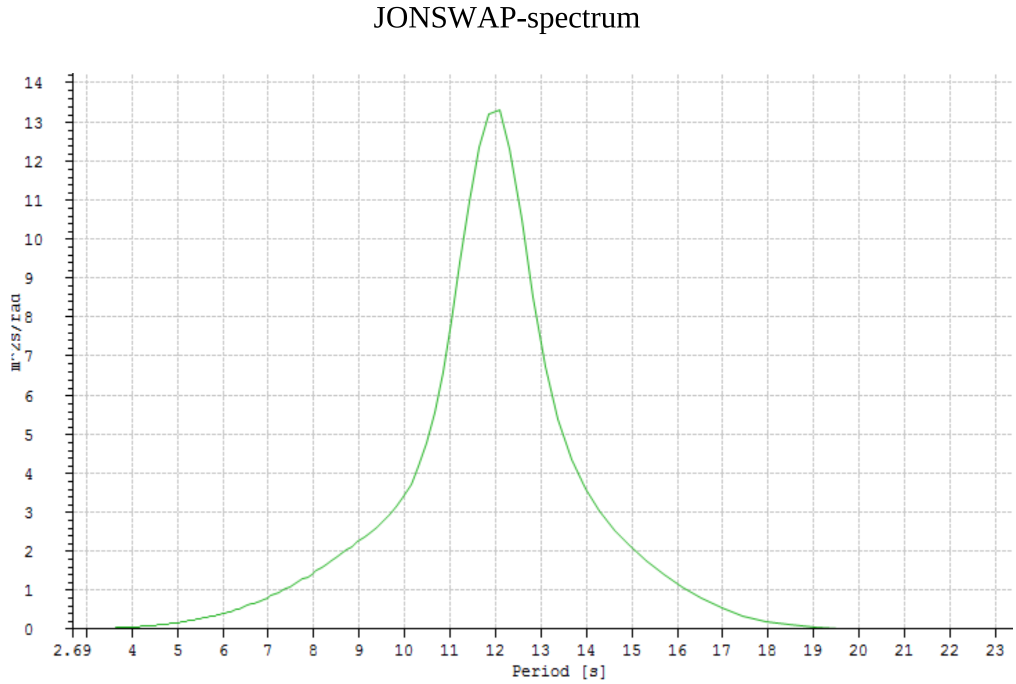

Figure 8-9 Example of JONSWAP spectrum, Hs=6.0 and Tp=12.0.

8.6.2 Regular Wave Environment

During a regular wave environment, identical waves are generated. This can be useful for parameter studies but is not as realistic as the irregular wave environment. Regular wave parameters are given in Table 8-9.

Table 8-9 Regular wave parameters.

Parameter	Value	Unit
Direction	Variable	$[deg]$
Phase	0.0	$[s]$
Period	Variable	$[s]$
Amplitude	Variable	$[s]$

8.7 Dynamic Calculation Procedure

The dynamic calculations are performed using a non-linear time domain analysis. The dynamic analysis must be done for all 208 sea states in the scatter diagram. In order to limit the processing time, a simulation time should not be longer than necessary. Simulation length is chosen as 20 minutes for each dynamic analysis. A twenty-minute simulation time is considered sufficient to give a good distribution of the load amplitudes in each time series. This is important in order give a good estimate of the fatigue damage.

The Newmark procedure was chosen since the Wilson procedure is not applicable to non-linear analyses. These methods are based on numerical integration. The integration and damping parameters are listed in Table 8-10.

Table 8-10 Integration and damping parameters for the dynamic calculation

Parameter	**Value**	**Unit**
Inverse Beta	3.9	[-]
Gamma	0.505	[-]
Theta	1.0	[-]
Stiffness damping	0.03479	[-]

The damping ratio is the ratio of the actual damping and the critical damping. The damping ratio as function of frequency is shown in Figure 8-10.

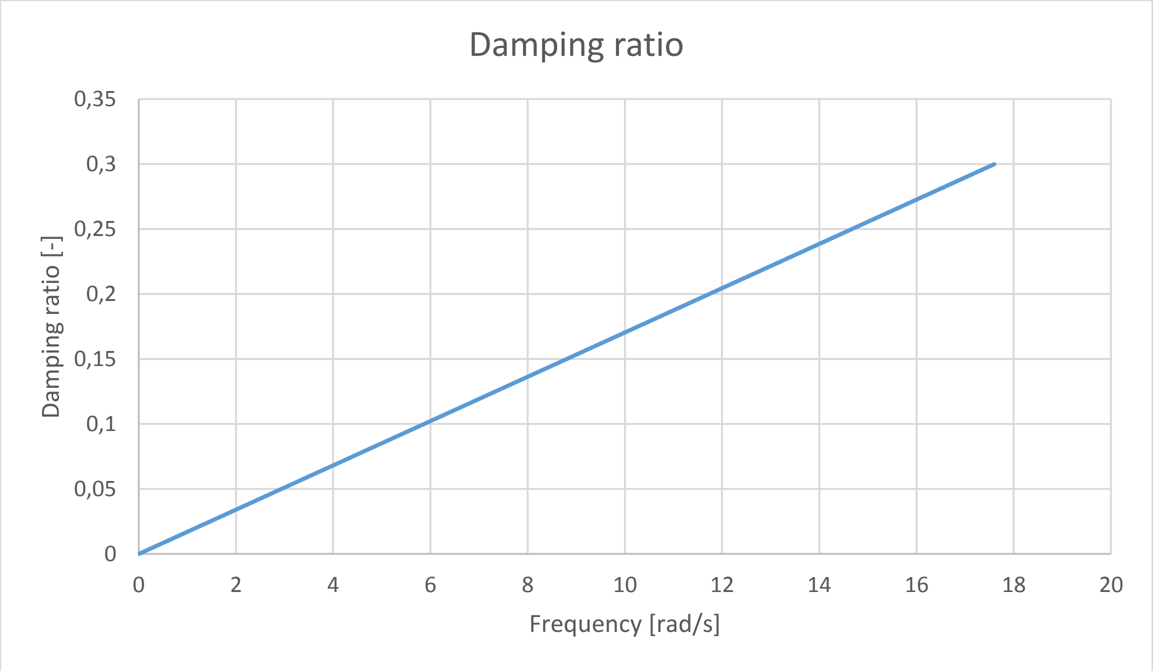

Figure 8-10 Damping ratio as a function of frequency.

The parameters for the non-linear integration procedure are listed in Table 8-11.

Table 8-11 Parameters for non-linear integration procedure.

Parameter	**Value**	**Unit**
Frequency of equilibrium iterations	1	[-]
Max iterations per step	10	[-]
Equilibrium accuracy	$1.0 \cdot 10^{-5}$	[-]
Time step subdivision	Automatic	[-]

9 Results

Matlab with the wave analysis for fatigue and oceanography (WAFO) package was initially used in order to post process the load time series and to calculate the fatigue damage by Miner's rule. To be able to analyse the load series by the WAFO package in Matlab, the load series must be exported from RIFLEX and imported as a rainflow matrix in Matlab. The matrix contains two columns where the first is the time and the second is the corresponding loads. It turns out that the process of exporting and importing results was very time consuming. Therefore, the integrated fatigue filter in the RIFLEX postprocessor was used instead. This filter is available in the new version of SIMA/RIFLEX. However, Excel and Matlab are used in order to systematise results and plot diagrams.

9.1 Study of Sea State Influence on Fatigue

In this section, the linear relationship between moment and stress is utilised. It should also be noted that drilling operations are typically restricted for sea states with Hs above a certain limit. This is not taken into account, and the whole scatter diagram is studied.

The scatter diagram in Table 8-8 contains a total of 208 sea states. Figure 9-1 provides an overview of how the damage on the wellhead varies for different sea states. It can be seen that the most extreme sea states, with Hs ranging from 10 to 12 metres and Tp from 13 to 17 seconds, excites the largest fatigue damage. It can also be seen that the damage increases with Hs. This is expected since larger waves typically excite larger forces. For a constant value of Hs, the damage increases slightly with decreasing Tp. This is not expected since long period waves typically excite forces at higher depths than waves with shorter periods. In addition, the RAO in surge, plotted in Figure 8-4, is observed to increase for longer wave periods. It was therefore expected an increase in fatigue damage for increasing Tp. However, the RAO function in pitch has a peak of around 6 to 14 seconds, this may partly be an explanation to why the damage increases with decreasing Tp. The phase angle may also explain this behaviour. The relative velocity between the riser and the water particles depends on whether the motion of the MODU and waves are in phase or anti-phase.

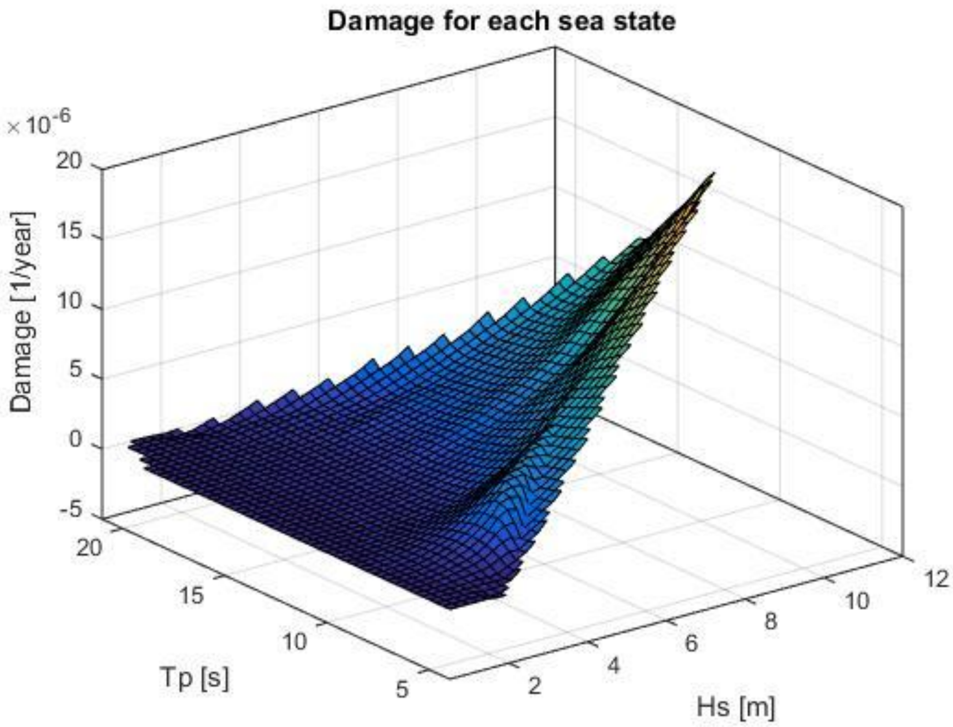

Figure 9-1 Damage for each sea state in the scatter diagram.

In Figure 9-2, the damage for each respective sea state is weighted with the corresponding probability of occurrence. It can be seen that even though the most extreme sea states result in greater damage; they do not contribute much to the accumulated fatigue damage because these sea states are very seldom. The sea states in the window of Hs = 1.5 to 3.5 metres and Tp= 7.0 to 12 seconds do only moderate damage, but due to their high probability of occurrence, they significantly contribute to the accumulated fatigue damage.

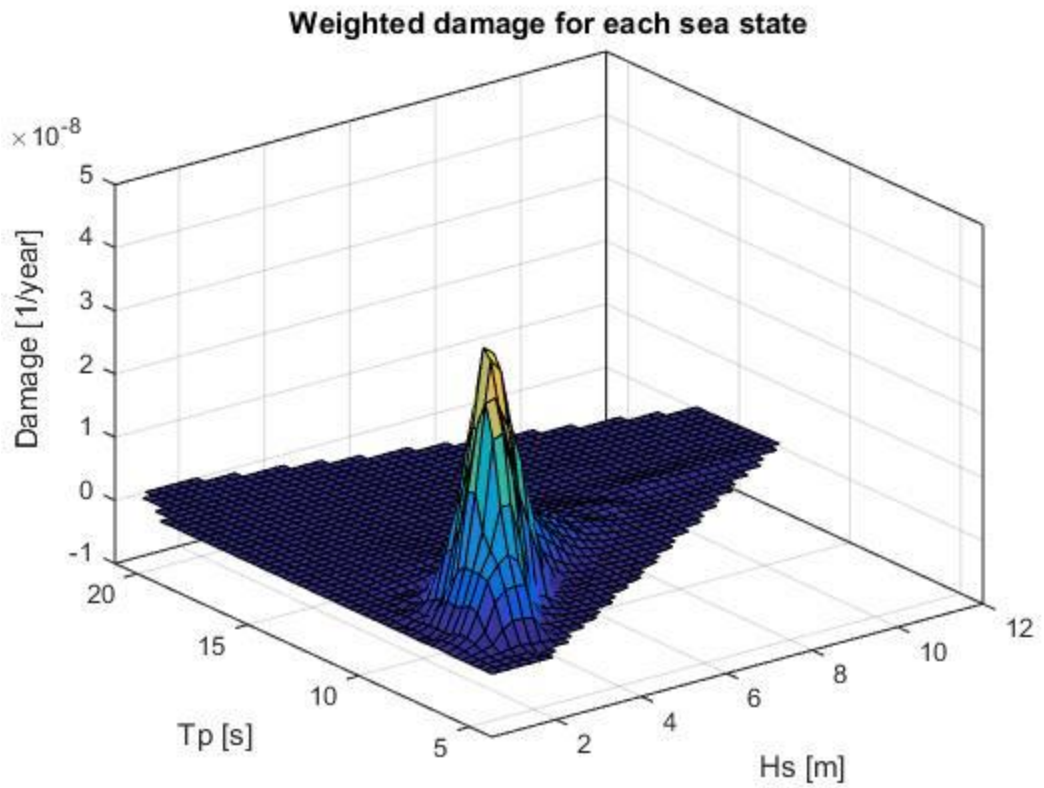

Figure 9-2 Weighted damage for each sea state in the scatter diagram.

The results from Figure 9-1 and Figure 9-2 can be summarised in Table 9-1. The sea states that individually imply greater damage are marked in green. The sea states that most contribute to the accumulation of fatigue damage are marked in yellow.

Table 9-1 Scatter diagram: Sea states with high damage (green) and high weighted damage (yellow).

Hs / Tp	<4	5	6	7	8	9	10	11	12	13	14	15	16	17	18	19	20	21	
0.5	219	247	98	56	108	139	85	53	38	28	16	9	3	1	1	1			1102
1.0	462	1444	1332	551	394	409	362	255	153	126	66	73	28	20	9	4		1	5689
1.5	54	763	1991	1654	703	436	327	258	176	86	49	49	23	21	22	3	3	3	6621
2.0	1	114	994	2015	1329	583	260	246	193	91	37	20	10	16	14	3	1		5927
2.5		7	189	1122	1532	734	261	182	165	124	48	20	8	1	1	2	1		4397
3.0			14	329	1082	958	309	137	139	96	39	13	6			1	1	1	3125
3.5				59	533	983	382	140	87	72	33	15	4	2		1			2311
4.0				10	133	660	418	144	65	36	23	14	3	4					1510
4.5					28	313	417	149	41	25	7	10	4	1					995
5.0					2	113	271	190	40	19	8	6	2	1					652
5.5						23	154	136	49	23	7	12	4						408
6.0						4	61	109	52	26	4	6	4						266
6.5							20	58	35	14	6	4	5						142
7.0							6	23	35	14	5	2	1						86
7.5							2	21	16	13	4	3	2	1	1				63
8.0								4	8	9	3	1							25
8.5								2	8	3	2	3	2						20
9.0									2	5	2								9
9.5									1	5	1	3	2						12
10.0												1							1
10.5										2	1	1		1					5
11.0											1								1
11.5										1		1		1					3
12.0												1							1
	736	2575	4618	5796	5844	5355	3335	2107	1303	818	362	267	111	70	48	15	6	5	33371

9.2 Fatigue Assessment of the Hot Spots from Local Model

The fatigue life of the hot spots on the wellhead and conductor housing (which is presented in Section 7.1) is presented in this section by importing the load-to-stress function, which was provided by Statoil, into the RIFLEX post processor. The SN-curves and SFC according to Table 7-1 are also implemented. There are high safety requirements for drilling operations, as there are great risks involved. Fatigue failure of the wellhead or the conductor implies a very high risk of loss of the well and an uncontrolled blowout. This could lead to human injury or death for the personnel on board the drilling rig. It also leads to extensive environmental pollution and large economical and political consequences. Therefore, a high safety class is chosen for the calculations. According to Table 5-1, DFF is equal to 10 for the high safety class. Details on the calculation can be found in submitted attachment (zip-file).

The fatigue life for each of the hot spots is illustrated in Figure 9-3. Note that the fatigue life calculated in this thesis assumes a continuously drilling operation until a fatigue failure occurs. This is not realistic since the duration of a drilling operation, is approximately only a month. A better way of presenting the results would have been to plot the remaining fatigue capacity as function of the well lifetime. It is observed that hot spot 10_1 is a critical hot spot. The fatigue lifetime for this hot spot is 3.6 years for case_0_0 (no lack of cement) and 5.1 years for case _31_0 (lack of cement between 20" and 30"). If the well have a fatigue lifetime of 3.6 year during continually drilling, it means that after one month of drilling, the well has 97.7% remaining fatigue capacity. It has only lost 2.3% (one month is 2.3% of the total time in 3.6 years) of its fatigue capacity during the first month of drilling. It is difficult to evaluate whether the wellhead is under-dimensioned or not, because this thesis only examines the fatigue damage that accumulated during a drilling operation.

Drilling operation typically last for a month in the initial construction phase of the well lifetime. After the construction phase is completed, the producing phase of the well is initiated. This phase will continue as long as the well is profitable. During the production phase several well intervention and work over operations are expected. In the last phase the well is plugged and abandoned. All three phases accumulate fatigue damage. However, it is expected that the initial phase will have the most significant contribution. This is due to the heavy drilling configuration, including the BOP-stack, which will excite large forces and moments to the wellhead. In order to conclude if the well has enough fatigue capacity it is necessary to obtain a complete overview of fatigue damage that is accumulated during the well's lifetime, all phases must be analysed and weighted for their expected duration.

In Figure 9-3 there is a large variation in fatigue life between the various hot spots. According to (Berge, 2015) this is normal in fatigue calculations. It is unexpected that the lack of cement results in a longer fatigue life for the critical hot spot. The figure in Appendix C is intended to support and make the following explanation easier to understand. Based on Figure 9-3 the lack of cement extends the fatigue lifetime for hot spots 10_1 and 10_2, which are the welds located on the wellhead. The lack of cement reduces the fatigue life for hot spots 20_1 and 20_2, which are the welds located on the conductor housing. Based on this observation, it may be assumed that the lack of cement causes the wellhead to defect laterally and "rest" on the conductor housing. Therefore, the conductor housing is exposed to larger forces when there is lack of cement between the 20" and 30". Figure 9-3 also demonstrates that hot spot 11_1, located at the connector, gives a significant reduction of the fatigue lifetime when there is a lack of cement. In case_0_0, the cement supports the area around the connector. When there is no cement around the connector (case_31_0), there will be larger stresses in the connector. It should also be mentioned that there is a negligible difference in fatigue lifetime for hot spot 21_1 in the two cement cases because this hot spot is located below the cement shortfall and is supported by cement in both cases.

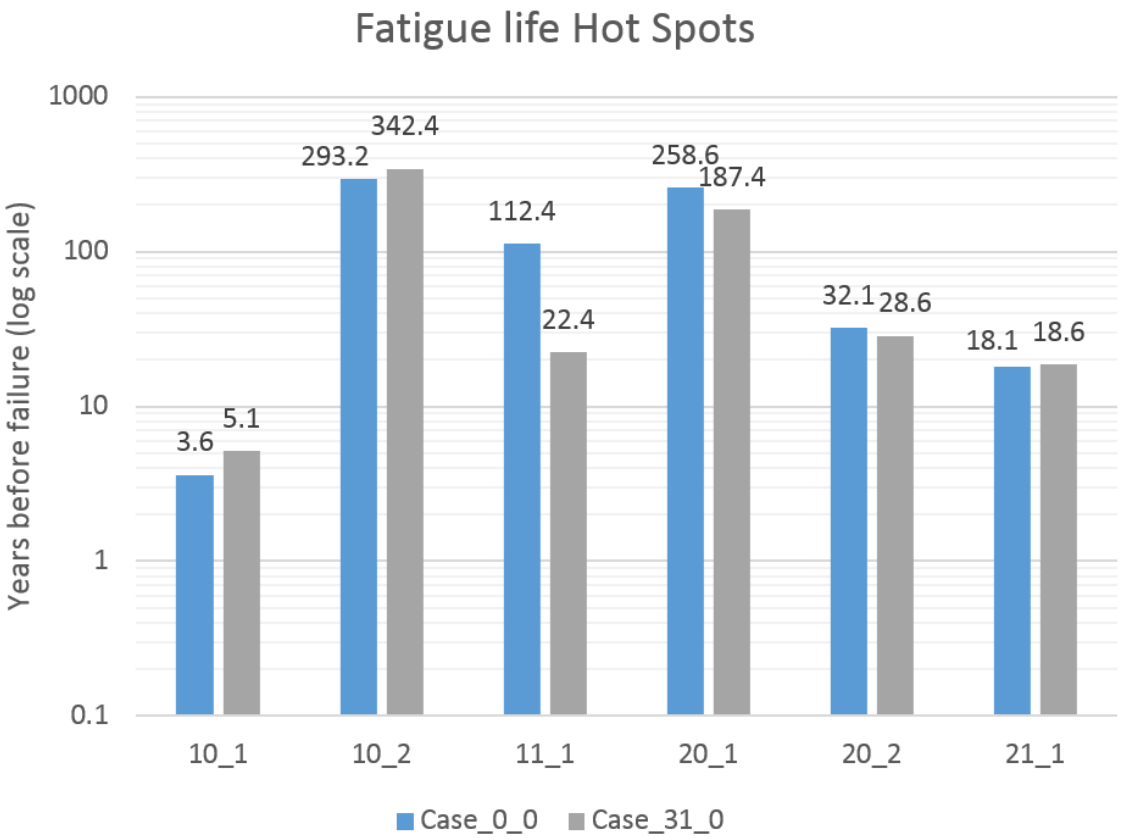

Figure 9-3 Fatigue life hot spots for two cement levels. Note that the diagram shows the fatigue life for a continuous drilling operation until fatigue failure occurs.

9.3 Study of Bending Moment Variations for Casing Depth

The excited moment due to environmental loads and the moment from the weight of the BOP-stack will increase with the lateral distance from their excitation point. In order to hold the well stable, restoring moments from the soil counteracts the moment. This counteracting moment will increase with the distance below the mud line due to the spring configuration illustrated in Figure 8-7. Thus, the highest bending moments do not necessarily occur at the wellhead datum but typically occur metres below the mud line.

In Figure 9-4, the moment envelope curve is plotted for the well line. Both the minimum and maximum moments that occur during a twenty-minute period are plotted for each of the four sea states. The top of the wellhead is located at 16 metres, while 0 metres corresponds to the soil node that is located 16 metres below the top of the wellhead. It can be seen that the extreme values for all four sea states are located at 11.68 metres, which corresponds to 4.32 metres below the wellhead. Both the maximum and minimum moments occur 4.32 metres below the top of the wellhead.

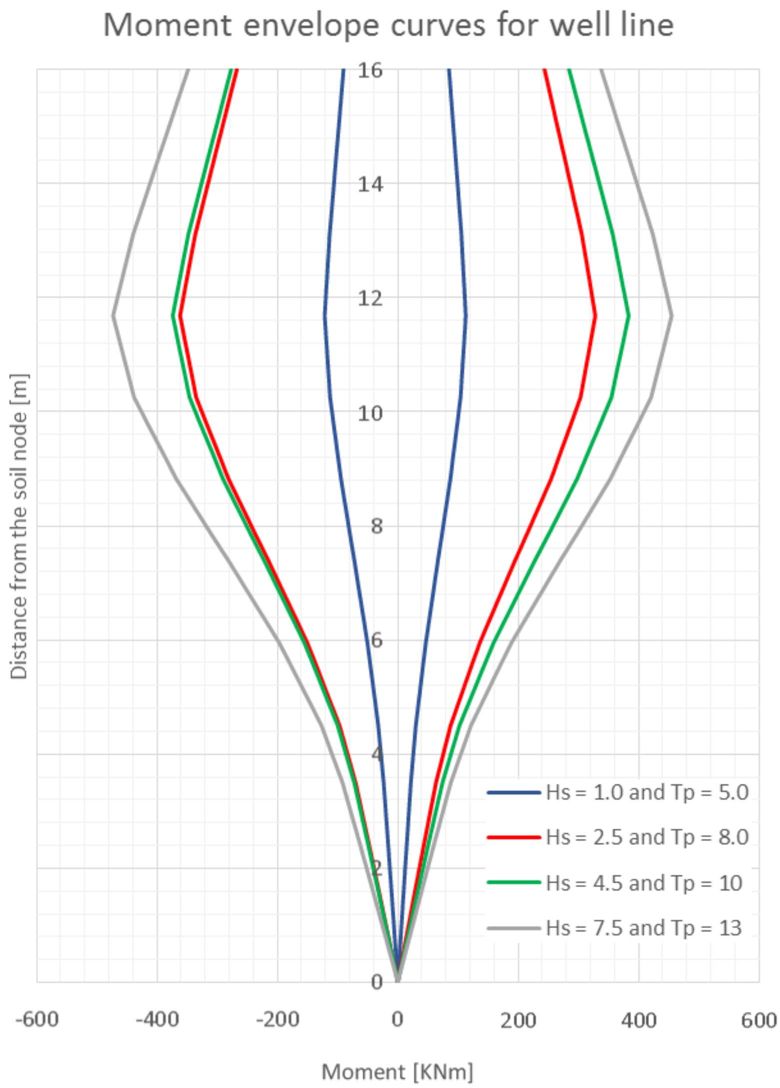

Figure 9-4 Envelope bending moment as a function of well depth.

9.4 Convergence Study

The purpose of a convergence study is to discover the required number of elements in order to attain reliable results. Few elements will give inaccurate results, and a high number of elements will result in a long processing time. Therefore, it is desirable to find a balance between accuracy and the processing time. In this study, the first focus is on the elements in the riser and then the element size in the upper part of the well. Since the riser ranges all the way through the water column, this part will take up most of the hydrodynamic forces. It is expected that a smaller element size in the riser section will provide a better representation of the hydrodynamic forces. The upper part of the well is chosen because it is where the forces and moments are monitored. Therefore, it is interesting to study how the element size in this region affects the results.

The maximum bending moment on the wellhead occurrence during a time series is compared. The environmental conditions for this study are set to irregular sea with significant wave height Hs=6.0 and peak period Tp=12.0. The seed number is kept constant to ensure that the results are comparable.

9.4.1 Element Length in the Riser Section

The default number of elements in the riser column was set to 167 elements. These elements are distributed into four sections. The upper and lower sections, which are the pup joints, have an element size that is slightly smaller than the elements size in the middle sections. These areas have a larger force gradient and need to be described in more detail. The default ratio of element size between the different sections is held as constant as possible during the study, while the total number of elements varies from 33 to 218. This corresponds to a variation in element length from 10 to 1.5 metres, where the default value in the example is approximately two metres. The results are given in Figure 9-5.

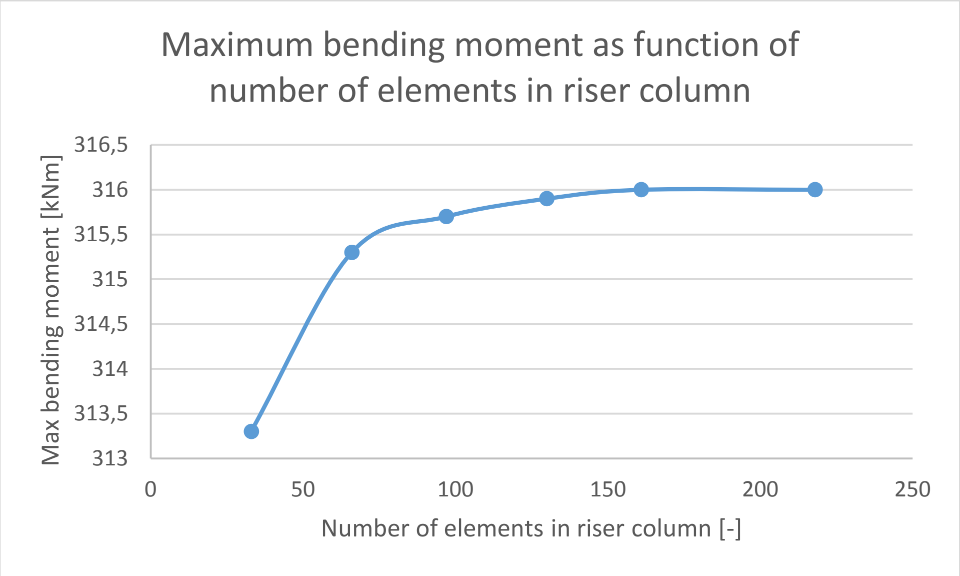

Figure 9-5 Convergence study of required number of elements in the riser column.

Based on the results, there is a significant drop in accuracy when the element size is larger than five metres, which corresponds to 65 elements on the graph. However, to obtain an acceptable accuracy, the results should converge to a certain value. By studying the graph, it appears that the results converge to 316 kNm. This indicates that the default value of the elements, 157, gives a fault of 0.9 kNm, which corresponds to 0.15%. This must be considered acceptable in such an analysis, as there are many parameters that need to be simplified compared to the real world.

9.4.2 Element Length in the Wellhead Section

It is expected that the element size in the area close to the wellhead is important in order to attain an accurate description of the moments because this is where the moments are monitored. Hence, it was decided to do a convergence study of the elements in the lowest segment of the BOP and the upper segment of the well. The interaction between these segments corresponds to the wellhead datum. The lowest segment on the BOP is two metres long and the upper segment on the well is 0.5 metres long. Each of these segments was, by default, divided into two elements. In this study, it is investigated whether reducing or increasing the number of elements in these two segments will affect the maximum bending moment on the wellhead datum. The results are plotted in Figure 9-6.

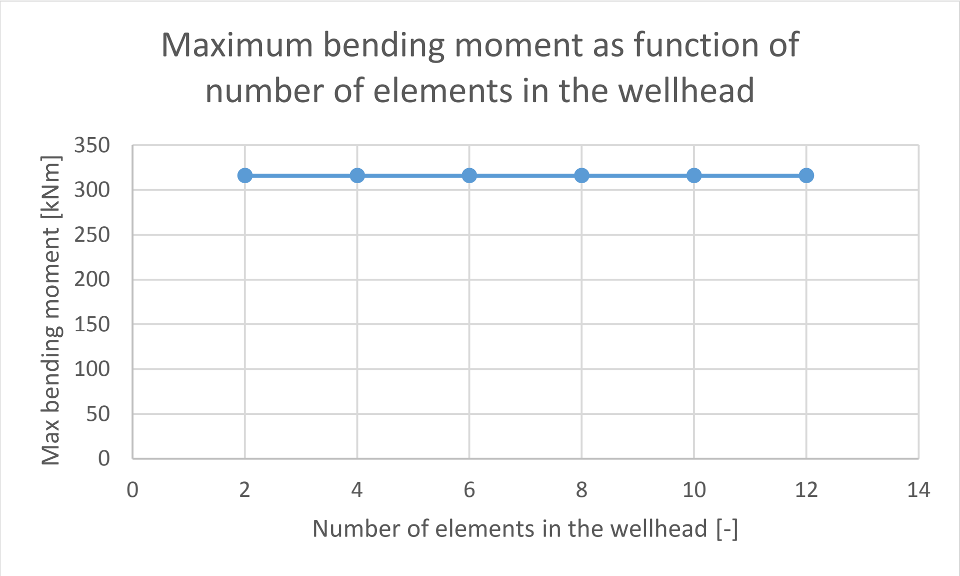

Figure 9-6 Convergence study of required number of elements in the region around the wellhead datum.

The graph shows a flat curve, which means that the results already converge with one element in each segment. If the number of elements in each segment is increased to six, the results are still the same. This is not expected since there are large moments in this area. However, an explanation for this may be that the soil well model is very stiff and short. This results in small lateral delta deflection of the wellhead datum.

9.4.3 Convergence Time Convergence

It is expected that with decreasing time steps there will be a corresponding increase in the accuracy of the dynamic calculations because the incremental stiffness is updated after each time step. Decreasing time steps will result in smaller errors based on the theory presented in Section 3.4. The plot in Figure 9-7 shows that the time steps 0.05, 0.1, and 0.25 provide very similar results. When increasing the time step to 0.5 seconds, the error will grow to approximately 1.6% compared to a time step of 0.1 seconds.

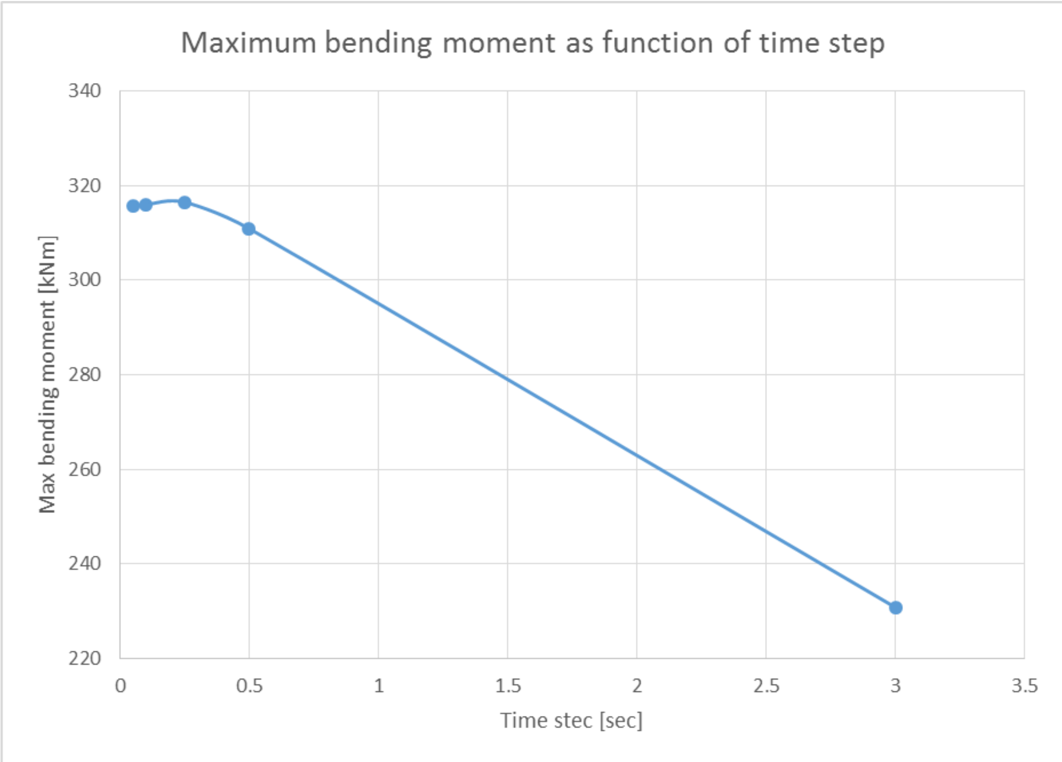

Figure 9-7 Convergence study of the time step.

9.5 Axial Force in the Riser Column

In Figure 9-8, the effective tension in the riser column is plotted. The plot is based on data with a zero MODU offset and a top tension of 1730 kN. The effective tension at the top of the riser column is roughly 1600 kN. The effective tension decreases with increasing depth due to the weight of the riser column. Generally, the slope or gradient of the curve can be related to the submerged weight per unit length of the equipment. A steep gradient indicates a heavy section, while a flat gradient indicates a lighter section. In the area where the BOP and LMRP are located, the gradient is relatively steep. The well ranges from zero to 16 metres, and the axial force (compression) at the bottom of the well is 82.5 kN higher than at the top of the well. This is due to the weight of the well. The axial force is between 16 and 23 metres, where the BOP and LMRP are located changes from approximately 600 kN to -500 kN. This corresponds to the submerged weight of the BOP and LMRP, which is 100.7 tonnes.

The difference between the minimum (min) and maximum (max) curve can be related to dynamic effects. In the well section, the difference between the max and min is approximately 50 kN. This indicates that there is cyclic axial loading on the well with load amplitude of up to

25 kN. This was not taken into account in the fatigue assessment of the well. This may be a non-conservative simplification.

It is important that the tension at the top of the LMPR stays on the positive side because negative tension (compression) in the riser can cause buckling. A typical requirement is that if one of the six tensioners fails, there should still be sufficient top tension to avoid negative tension in the riser. It is noted that the minimum effective tension at the top of the LMPR is 500 kN. If one of the tensioners fails, the top tension is reduced by 16.7%, which corresponds to a 288 kN reduction in the tension along the riser line. There will still be positive tension at the top of LMRP.

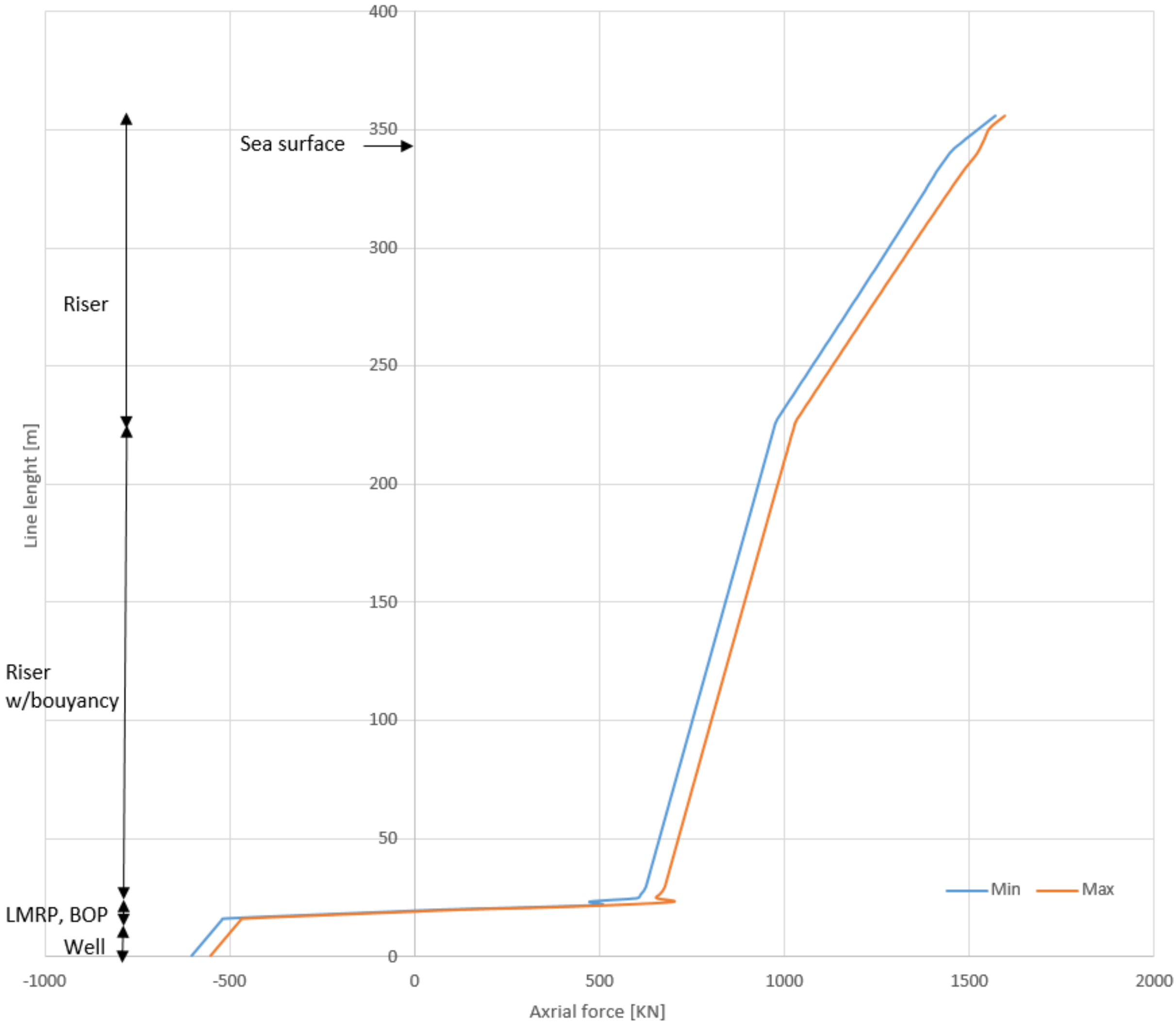

Figure 9-8 Axial force in the riser system.

10 Parameter Studies

10.1 Support of the Well

The well model that is presented in Section 8.5 is the case studied in this thesis. This is a relatively stiff model and, in this parameter study, a softer soil model is studied. Based on discussions with (Grytøyr, 2015a), a model that is just 15 metres into the soil may be too short if the soil is softer. How deep the well should be modelled depends on the stiffness of the soil surrounding the well. It is desirable that the well is modelled far enough into the soil such that all the moments are absorbed before reaching the bottom node. That means when the supporting soil is very soft, the well may need to be deeper compared to when the soil is stiff. The consequence of a too-short well model is that a misplacement of the lower boundary leads to artificial increased stiffness at the wellhead datum. To determine whether the well model is modelled far enough into the soil, the boundary conditions at the bottom of the well can be changed from free in all directions with respect to rotations to completely fixed in all rotational directions. If there is still any moment present at the lower end, it indicates that the well is not sufficiently deep in the soil such that all of the moments are absorbed. Based on this, the well line is extended in RIFLEX to 60 metres into the soil and uses soil properties (Appendix B) that are typical for the North Sea.

10.1.1 Description of New Soil Model

Soil data for the 20 soil layers is specified in Appendix B, and the PY curves are plotted in Figure 10-1. The support contribution from each soil layer is represented with a spring, which is placed in the specified midpoint of the soil layer. The soil resistance is given as stress and does need to be converted into force in order to be input into RIFLEX. This is done by multiplying the stress by the projected area of the conductor with cement. Force-displacement of the 20 springs is illustrated in Figure 10-2. Details on the calculation can be found in submitted attachment (zip-file).

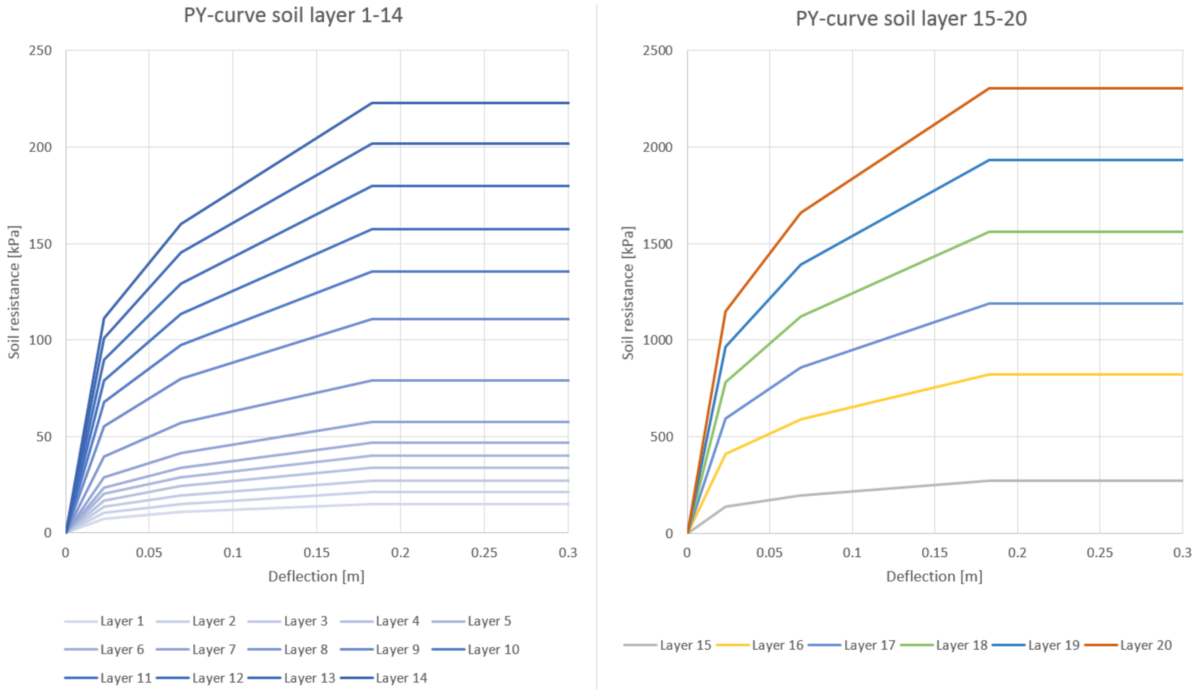

Figure 10-1 PY-curve for soil layers.

Figure 10-1 shows that the soil resistance increases with deeper layers. This agrees with our physical understanding that soil layers are harder (tightly packed) when moving deeper under the mudline.

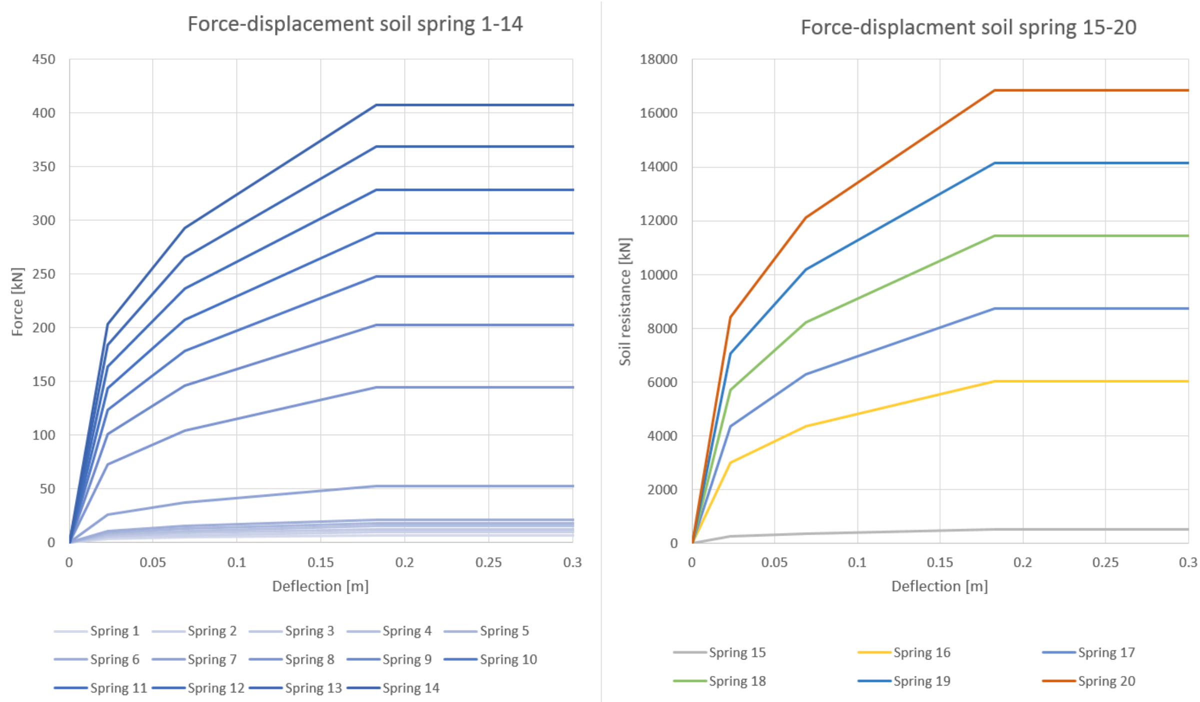

Figure 10-2 Force-displacement soil springs.

Springs 1 to 14 are located along the upper 15 metres of the well, while springs 15 to 20 are located along the 45-metre lower part of the well (details in Appendix B). By comparing the upper most 15 metres of both well models, it is seen that the soil in the initial soil model is much stiffer than the soil in this parameter study (springs 1 to 11 in Figure 8-8 are supporting the same distance as springs 1 in 14 in Figure 10-2).

10.1.2 Results

In Figure 10-3, the first 200 seconds of the wellhead moment time series for the two soil models are compared. The sea state is the same for both, significant wave height Hs=6.0, and peak period Tp=12.0. The seed number is kept constant to ensure that the results are comparable.

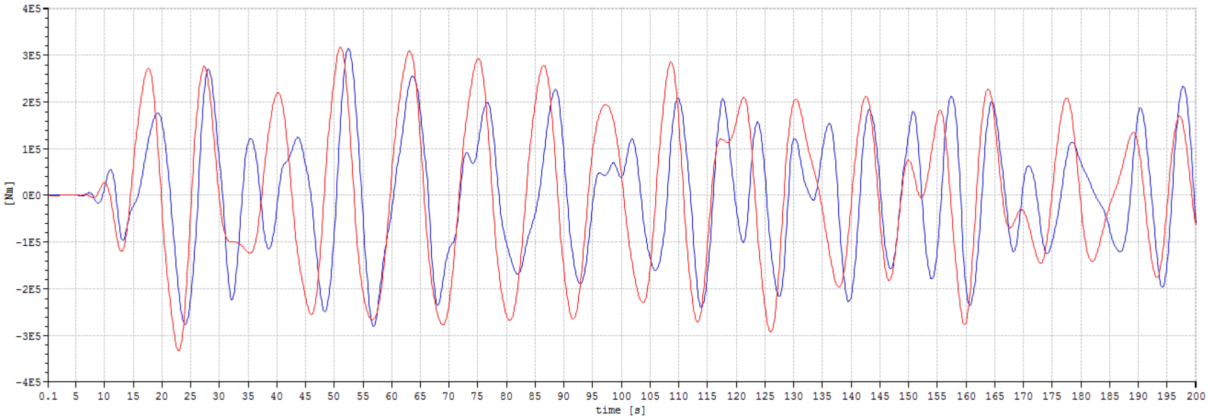

Figure 10-3 Comparison of wellhead moment time series - stiff soil model (blue) vs. soft soil model (red).

There seems that the soft soil model causes a small increase in the moment range and a smoother alternation between peaks and valleys.

The same fatigue assessment of the hot spots is performed with the new well soil model. The results are shown in Figure 10-4. By comparing Figure 10-4 with Figure 9-3, it can be seen that the softer soil model results in longer fatigue life for all the hot spots. After a discussion in a meeting with the supervisor, this is a bit unexpected. In general, it is expected that higher soil stiffness would result in a longer fatigue lifetime because the lower soil stiffness causes greater lateral deflection at the wellhead datum. Hence, the effect from the axial force due to the BOP weight will be larger. An explanation for these unexpected results may be that the soft soil model changes the eigenperiod of the system and causes dynamic amplification. Therefore, this should be investigated further and is a topic for further work.

Compared with the stiffer soil model, the softer soil model demonstrates an increase in fatigue lifetime from 63% to 189% for all the hot spots. The fatigue life of the critical hot spot 10_1 increases from 3.6 years with the stiff soil model and to 10.4 years with the soft soil model.

There are some limitations in the method modelling that cause the clear relationship between softer soil and longer fatigue life. This may not be the case in real-world scenarios. This is will be further discussed in Section 11.1.

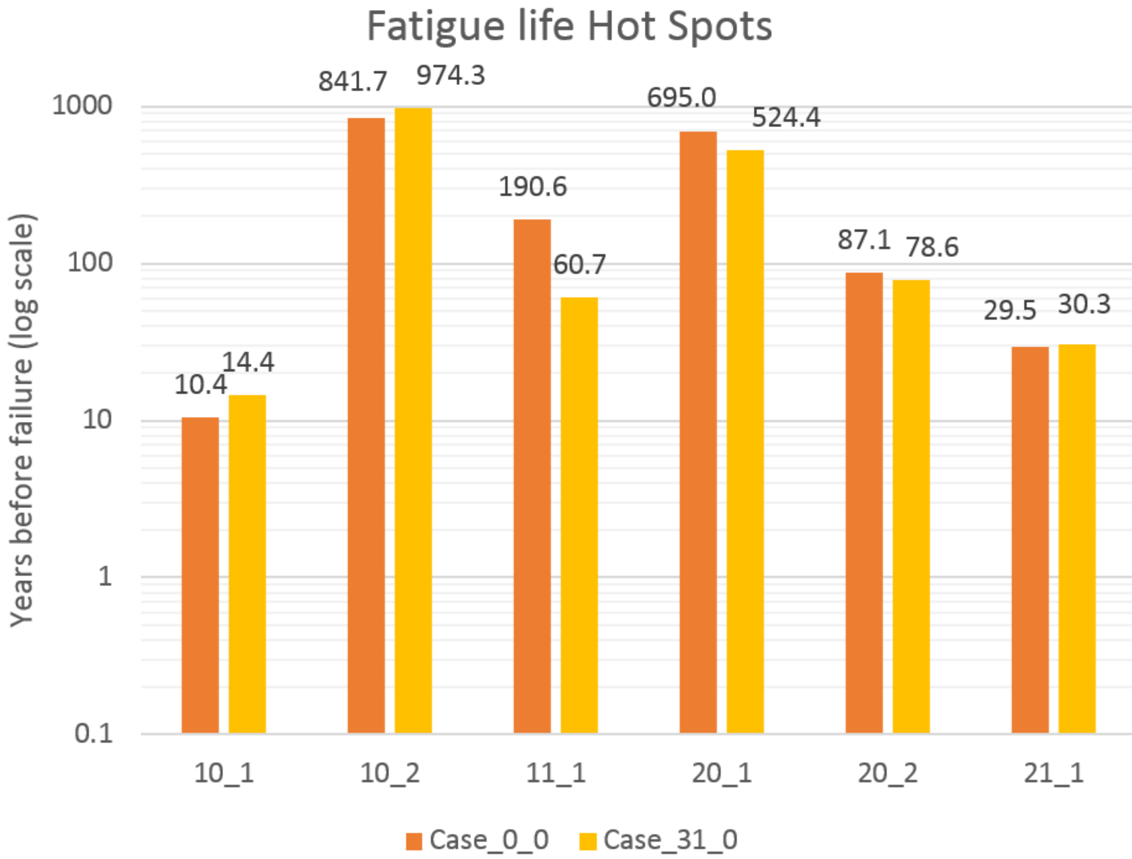

Figure 10-4 Fatigue life hot spots (soft soil). Note that the diagram shows the fatigue life for continuous drilling operation until fatigue failure occurs.

10.2 Current

In this parameter study, the effect of the current is studied. The two current profiles that are studied are shown in Figure 10-5. Current profile 1 is a uniform current profile with a velocity of 0.25m/s. Current profile 2 has a velocity of 1 m/s at the water surface, and the velocity rapidly decays with water depth.

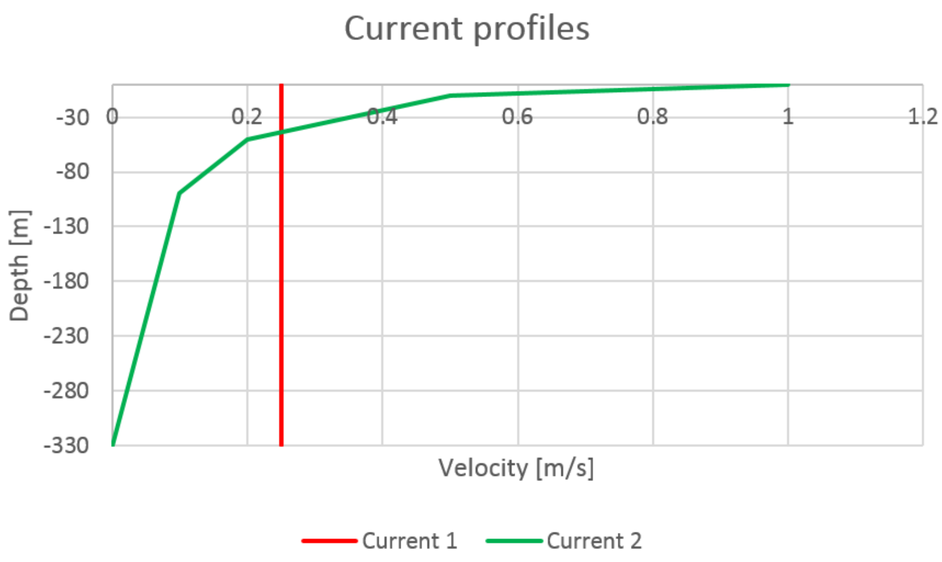

Figure 10-5 Current profiles.

In Figure 10-6, the first 200 seconds of the wellhead moment time series are compared for no current (blue), current profile 1 (red), and current profile 2 (green). For the current profiles, the mean value of the graph moves from zero to below zero. The moment ranges are somewhat reduced compared to no current, especially for current profile 1. This may be because the current increases the hydrodynamic damping for the riser column, which causes the excitations to lower. Based on the graph, the current may cause larger extreme values of the moment. However, the moment range (which is smaller) is the governing load effect for fatigue damage. Therefore, it is expected that the current will reduce the fatigue damage and hence increase the fatigue life.

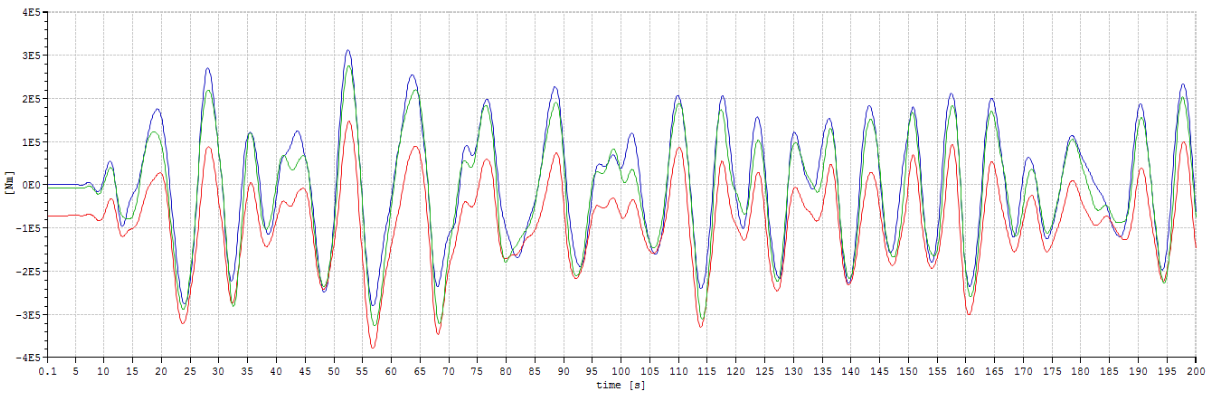

Figure 10-6 Comparison of wellhead moment time series. No current (blue), current 1 (red) and current 2 (green).

In Figure 10-7, the fatigue life of the critical hot spot 10_1 is compared for the three current scenarios. It can be seen that including the current in the analysis increases the fatigue life. Based on the results, which are presented in Figure 10-6 and discussed above the same figure, this was expected.

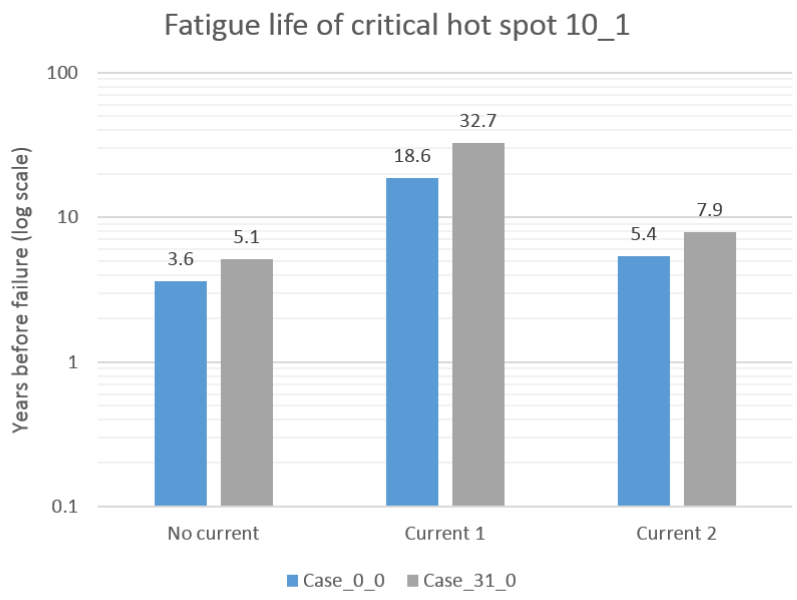

Figure 10-7 Fatigue life of hot spot 10_1 (current variations). Note that the diagram shows the fatigue life for continuous drilling operation until fatigue failure occurs.

10.3 BOP-weight

The BOP-weight is expected to have a significant effect on the forces on the wellhead datum and hence the fatigue life of the well. The BOP that initially is used in the calculation is 128 tonne, which is relatively light today. According to (Sangesland, 2014), a modern BOP-stack has a submerged weight from 270-365 tonnes. Therefore, how an increase in the weight of the BOP-stack will influence the fatigue life, bending moments, and axial tension will be investigated. The height of the BOP-stack is kept constant in order to attain results that are more comparable. In this study, three BOP-stacks, which are given in Table 10-1, are studied.

Table 10-1 Parameter study: Weight of BOP-stack

Parameter study BOP/LMRP mass							
BOP-stack	Weight in air [ton]	Submerged weight [ton]	Height [m]	Fatigue life HS 10_1 [years]	[days]	Max bending moment at WH-datum [kNm]	Max axial tension at WH-datum [kN]
Light	128	100.7	7.9	3.614	1319	316	-468.5
Medium	256	228.7	7.9	3.305	1206	323.3	-1777
Heavy	346	318.4	7.9	3.143	1147	325.8	-2604

The light BOP-stack is used in the case study in this thesis. The result of using a medium BOP-stack, which is twice the weight of the light BOP-stack, is an increase in the bending moments at the wellhead datum. The fatigue life is reduced by 8.5%. It can also be seen that the axial force at the wellhead increases due to the increased weight.

When using a heavy BOP-stack, the bending moments and axial force at the wellhead increase even more due to the larger weight. The result is a reduction in fatigue life of 13% compared to the light BOP-stack.

The results of increasing the weight of the BOP-stack show the tendencies that were expected. However, a larger variation in fatigue life was expected between a light, medium, and heavy BOP. One reason may be the moderate water depth, which is 330 metres. It may be that the effect of a heavier BOP-stack is more significant in shallower water because there are more riser-induced forces in shallower waters. Another reason may be that, since the soil is very stiff, the lateral BOP movement is small. These topics can be investigated in further work.

.

11 Discussion

The results from the fatigue assessment concluded in this thesis, are highly dependent on the results provided from Statoil. Another point is that the results form Statoil are constant during the parameter studies. The parameters are only varied in the global model in the parameter studies. This is a limitation factor since the local and global model should be consistent in order to attain valid results.

11.1 Well and Soil Model

The comparison of the stiff and soft soil models shows that the softer soil results in a longer fatigue life for all the hot spots. Based on discussions with Andreas Amundsen, this is not necessarily the case in reality. In reality, softer or harder soil properties may initially cause critical hot spots to change to a new location.

The reason the results show a correlation between softer soil properties and longer fatigue life is that the soil models were only implemented in the global model. Therefore, only the time series of the bending moment on the wellhead is updated according to the soil model. A change in soil properties will also influence the results from the local analysis, such as moment-to-stress functions; hence, the local model must also be updated with the same soil properties as the global model. Since the author was given just the results from the local analysis and not the local FE-model itself, this was not done. The consequence is that the only difference in the two fatigue assessments for the two soil-models is the time series of wellhead moment.

11.2 Environment

For drilling operations, there is typically an operation limit on significant wave height. According to (Nielsen, 2007), a typical operation limit for drilling with semisubmersibles is Hs = 4 metres. This limit may be even higher for modern semisubmersibles. The operation limit should have been taken into account when estimating the fatigue life for the hot spots. This could have been done by excluding sea states outside the operation limits and weighting the remaining sea states so that the total probability is equal to one. However, according to Figure 9-2, most of the damage is accumulated for Hs below 4.5 metres. Therefore, excluding the sea states above the limit may not have a significant effect on the fatigue life if the limit is above 4.5 metres. The results will be more conservative; therefore, it should not be a concern with respect to safety to not include the operation limit in the calculations.

11.3 Fatigue assessment

Considering that a drilling operation typically lasts one month or so, the fatigue lifetime of 3.6 years during continually drilling is not devastating. However, the well must be strong enough to prevent failure during the three phases of its lifetime. Without a full overview of the expected accumulated fatigue damage for other phases, it is difficult to evaluate whether the wellhead is under-dimensioned or not. It also depends on how long the well is expected to produce and the number of intervention and workover operations needed.

In general, fatigue calculations involve many uncertainties. No answer book can provide an exact fatigue life. Therefore, some degree of engineering judgment is necessary in order to progress in the calculations. Small variations in the input parameters cause large variations in fatigue life. Thus, it is necessary to evaluate the uncertainties involved and ensure that the results are on the conservative side. The best result that can be obtained is a conservative estimate of the fatigue life.

Examples of uncertainties in this thesis are as follows:

- Environmental conditions,
- Loading and how the loads are applied in the model,
- FE modelling of both global and local models,
- Soil-properties and the modelling of the soil,
- Calculation of the local stresses,
- The choice of SN-curves and SCF,
- Temperature variations,
- Initial defects in material, and
- Non-linearities.

The stiff soil model resulted in a fatigue life of 3.6 years, and the soft soil model resulted in a fatigue life of 10.4 years.

In order to extend the fatigue life of an existing well, the following actions should be considered:

- Use a lightweight BOP.
- Use supporting arms that support the BOP and counteract the moments on the wellhead.

- Use alternative methods when possible. An example is the riserless light well intervention (RLWI) that uses a wireline and lubricator system instead of a riser and BOP. This reduces the loading on the wellhead.

In order to extend the fatigue life of a well that is in the planning phase the following actions should be conducted:

- Use a wellhead with a high fatigue capacity.
- Install sensor technology and associated software that can monitor the structural status of the well.

12 Conclusion

The thesis work performed, is based on input data provided by two separate sources. A global model of the drilling system, based on examples provided by MARINTEK, is established in RIFLEX. Results from a local model of the well are provided by Statoil. The results from the local and global model are both important input parameters to the fatigue assessment analysis used for estimating the fatigue life of the wellhead.

Raw data for existing oil wells and drilling rigs are typically confidential information. For this reason, it was particularly challenging to collect realistic input data for the analyses. However, MARINTEK and Statoil provided the author with some examples used for educational purposes. This data may not be exact but is based on typical values. In a real case, such analyses require input data of a higher degree of accuracy. In order to attain results that are as accurate as possible, it is necessary to have realistic and relevant data for the specific case study.

Since this thesis only investigates the fatigue damage accumulated from the drilling operation, it is hard to evaluate whether the well is under-dimensioned or not. In order to do so, it is necessary to have a full overview of the expected accumulated fatigue damage for the residual phases of the well lifetime. If it turns out that the well does not have sufficient fatigue capacity after having investigated all the phases of the well lifetime, a suggestion is to perform measurements. In order to extend the fatigue lifetime, a solution can be to use an improved wellhead with higher fatigue capacity. However, this is only possible in the design phase and not for an existing well. For an existing well, a more feasible solution is to reduce the loading on the wellhead. This can be done by e.g. using a lightweight BOP or supporting arms that counteract the BOP movement.

In these studies, it is important to validate and verify that the results are accurate. In order to verify if the RIFLEX model of the riser and wellhead is able to produce accurate results, convergence studies on both element size and time steps are performed. An element size that gives an acceptable balance between accuracy and processing-time is chosen. There is also an uncertainty involved due to the fact that the fatigue assessment is based on two independent models, the local and global model. It is important that the specifications of the drilling system, well, and soil are consistent in both models. It is a limiting factor that the author did not have access to the local model, which is only valid for the specific case considered. This may have led to unrealistic tendencies in the results from the parameter studies.

The knowledge obtained from the work performed in this thesis is not the results themselves. The results will differ for different cases. In the real world, no cases will be identical. There will always be some variation in the input parameters which will make each case unique. The results obtained in this thesis are therefore valid for just this specific case. However, the method of wellhead fatigue analysis is the same for other cases. This makes the basic understanding of the method and the training in the simulation software the most important pieces of knowledge obtained from this thesis.

12.1 Further Work

12.1.1 Local Model

This thesis focused on the global modelling. Statoil provided the local model results, however, updating the local model is necessary for consistent parameter studies.

12.1.2 Extreme Response Studies

Extreme response studies of the riser system are important in order to dimension the system. This is not investigated in this thesis.

12.1.3 Verify the Results

The results obtained in this report should be compared with similar case studies in order to verify that the results are reliable.

12.1.4 Fatigue During the Entire Well Lifetime

The lifetime of a well comprises many phases. The first phase is the construction phase; in this phase, the drilling rig is connected to the well. It is expected that most of the fatigue damage occurs in this phase. The next phase is the production phase. During this phase, a number of maintenance operations or upgrades are conducted. These operations require a workover or completion configurations that are connected to the well. Lastly, when the well is finished producing, the well is plugged and abandoned. These three phases accumulate fatigue damage to the well and wellhead. A fatigue assessment, including the accumulated damage from the entire lifetime, should be investigated.

The moment-to-stress function for the conductor casing connector weld were missing. Therefore, these hot spots were excluded from the fatigue assessment. These hot spots should be investigated further.

The fatigue assessment is conducted without an operation limit on Hs. This may lead to overly conservative results. The effect of including an operation limit could be interesting to examine.

12.1.5 Resonance

A semi-submersible has typically a high eigenperiod. This makes the semi-sub sensitive to slowly varying forces. The riser system may have resonance periods in the range as typical wave force periods. However, the hydrodynamic damping for the riser is typically very large, which reduces the excitations. The results of the parameter study of soil stiffness give unexpected results. BOP dynamic response is a possible reason for this behaviour. The softer soil stiffness and increased length of the well may trigger cantilever type eigenmode of the BOP (DNV, 2011). This should therefore be further investigated.

12.1.6 VIV

Vortex-induced vibration (VIV) should be investigated. The VIV motions can accumulate fatigue damage to the riser system.

12.1.7 MODU Offset

The MODU offset can imply larger moments on the wellhead. Drift off loss of position due to the failure of the dynamic positioning system or mooring lines can also be investigated.

12.1.8 Parameter Studies

- Modelling of the flex joints.
- Investigate how a scatter diagram from another area will affect the results.
- The number of casing installed will affect the hang down weight on the wellhead. In this study, just the surface casing was installed. If more casings are installed, the hang down weight on the wellhead will be larger.
- Water depth.
- Lack of grout around the wellhead may be modelled by removing the upper most soil spring.

13 References

API, A. P. I. (2010). Recommended Practice on Procedures for Testing Casing and Tubing Connections (Third Edition ed., Vol. API RP 5C5): Global Standards.

ASTM. (2011). Standard Practices for Cycle Counting in Fatigue Analysis *ASTM E1049-85(2011)e1* (Vol. E1049-85). ASTM: West Conshohocken.

Bergan, P. G., Larsen, P. K., & Mollestad, E. (1981). *Svingning av konstruksjoner* (2 ed.). Trondheim: Tapir forlag.

Berge, S. (2006). *Fatigue and Fracture Design of Marine Structures*. NTNU.

Berge, S. (2015) *Conversation and discussion with Stig Berge*.

Cameron. (2012). Subsea wellhead system. In S.-T. D. D. H.-C. S. W. System (Ed.). offshore-mag.

DNV-GL. (2014). SIMA. from http://www.dnv.com/services/software/products/sesam/sesam_marine/sima.asp

DNV. (2010). Dynamic Risers *Fatigue Limit State* (Vol. DNV-OS-F201).

DNV. (2011). Wellhead Fatigue Analysis Method. In S. JIP Structural Well Integrity, Marathon, Lundin, Eni, Total, ExxonMobil, BP, BG Group, (Ed.), (Rev 01 ed.). DNV web page: DNV.

DNV. (2012). Fatigue Design of Offshore Steel Structures (Vol. DNV-RP-C203, pp. 178). http://www.dnv.com: DNV.

DNV/MARINTEK. (2004). *RIFLEX*. Paper presented at the SESAM, MARINTEK. https://www.sintef.no/upload/MARINTEK/PDF-filer/FactSheets/RIFLEX.pdf

DNVGL. (2015). Wellhead fatigue analysis *Recommended practice* (Vol. DNVGL-RP-0142).

Faltinsen, O. M. (1990). *Sea loads on ships and offshore structures*. United Kingdom: Cambrigde university press.

Fedem, & Berbu, A. (2015, 21.05.2015). [Email].

Grytøyr, G. (2015a) *Conversation and discussion with Guttorm Grytøyr from Statoil*.

Grytøyr, G. (2015c). [E-mail: Local model WH-fatigue].

iHS. (2014). Offshore drilling and production vessels.

Langen, I., & Sigbjornsson, R. (1979). *Dynamisk Analysis of Marine Structures*: Tapir.

Larsen, C. M. (2005). DRAG FORCES IN DYNAMIC ANALYSIS *Dynamic analysis of marine structures*.

Lylund, A. (2015). *Analysis of riser-induced loading on wellhead.* (Project thesis), NTNU, Trondheim.

MARINTEK. (2014a). *RIFLEX Theory Manual*.

MARINTEK. (2014d). RIFLEX User guide.

MECF. (2014). DISCHARGE OF DRILLING MUD INTO THE GULF OF MEXICO FROM DEFECTIVE EQUIPMENT. LOWER MARINE RISER PACKAGE (LMRP) CONNECTOR FAILURE

Moan, T. (2003). *Finite Element Modelling and Analysis of Marine Structures*.

Nielsen, F. G. (2007). *Lecture Notes in Marine Operations*. Paper presented at the Marine Operations, Trondheim.

Norsk-Standard. (2009). Petroleum- og naturgassindustri Bore- og produksjonsutstyr *Del 1: Konstruksjon og drift av marint stigerørsutstyr* (Vol. ISO 13624-1:2009).

PetroWiki. (2013, 23.08.2013). MODU Types. from http://petrowiki.org/MODU_types

Roylance, D. (2001). Introduction to Fracture MechanicsDepartment of Materials Science and Engineering. Cambridge, MA 02139: Massachusetts Institute of Technology. Retrieved from http://ocw.mit.edu/courses/materials-science-and-engineering/3-11-mechanics-of-materials-fall-1999/modules/frac.pdf.

Sangesland, S. (2014). Drilling and Completion of Subsea Wells - An Overview - (Rev. 1. ed.). Powerpoint presentaion.

Schlumberger. (2014). Blowout preventer. *Oil field Glossary.* from http://www.glossary.oilfield.slb.com/en/Terms/b/blowout_preventer.aspx

Statoil (Writer). (2014). Subsea Seminar Part 8 - How is wellhead fatigue handled by industry standards?

Sævik, S. (2015) *Questoins to Svein Sævik*.

Wikipedia. (2013). Drilling riser.

Appendix A Local Model Data

Local model data		
Variable	**Value**	**Unit**
Mudline level	0	m
Wellhead datum level above mudline	4	m
Depth of Conductor below mudline	70	m
Friction coefficient between steel parts	0.15	-
Friction coefficient between steel and cement	0	-
Steel Young's modulus	210	GPa
Steel Poisson's ratio	0.3	-
Cement Young's modulus	3.5	GPa
Cement Poisson's ratio	0.3	-
Conductor OD	30	inch
Conductor ID	28	inch
Surface Casing OD	21.12	inch
Surface Casing ID	18.50	inch
BOP height (WH datum to FLJ axis)	10.651	m
BOP+LMRP submerged weight	217	tonnes
Riser tension on top of BOP (flex joint)	124	tonnes
Weight of surface casing	20	Tonnes
Cement shortfall from mud line	0 to -15 every 1	m

Appendix B Typical Soil Data North Sea

Depth of soil segment (m)																		
top	mid point	bottom	disp (m)	PY stress (kPa)	disp (m)	PY stress (kPa)	disp (m)	PY stress (kPa)	disp (m)	PY stress (kPa)	disp (m)	PY stress (kPa)	disp (m)	PY stress (kPa)	disp (m)	PY stress (kPa)	disp (m)	PY stress (kPa)	disp (m)	PY stress (kPa)
0	0.3	0.5	-914.4	-14.96	-0.183	-14.96	-0.069	-10.77	-0.023	-7.481	0	0	0.023	7.481	0.069	10.77	0.183	14.96	916.4	14.96
0.5	0.8	1	-914.4	-21.01	-0.183	-21.01	-0.069	-15.13	-0.023	-10.51	0	0	0.023	10.51	0.069	15.13	0.183	21.01	916.4	21.01
1	1.3	1.5	-914.4	-27.23	-0.183	-27.23	-0.069	-19.61	-0.023	-13.62	0	0	0.023	13.62	0.069	19.61	0.183	27.23	916.4	27.23
1.5	1.8	2	-914.4	-33.62	-0.183	-33.62	-0.069	-24.21	-0.023	-16.81	0	0	0.023	16.81	0.069	24.21	0.183	33.62	916.4	33.62
2	2.3	2.5	-914.4	-40.18	-0.183	-40.18	-0.069	-28.93	-0.023	-20.09	0	0	0.023	20.09	0.069	28.93	0.183	40.18	916.4	40.18
2.5	2.8	3	-914.4	-46.9	-0.183	-46.9	-0.069	-33.77	-0.023	-23.45	0	0	0.023	23.45	0.069	33.77	0.183	46.9	916.4	46.9
3	3.5	4	-914.4	-57.3	-0.183	-57.3	-0.069	-41.26	-0.023	-28.65	0	0	0.023	28.65	0.069	41.26	0.183	57.3	916.4	57.3
4	5	6	-914.4	-79.23	-0.183	-79.23	-0.069	-57.05	-0.023	-39.62	0	0	0.023	39.62	0.069	57.05	0.183	79.23	916.4	79.23
6	7	8	-914.4	-110.8	-0.183	-110.8	-0.069	-79.79	-0.023	-55.41	0	0	0.023	55.41	0.069	79.79	0.183	110.8	916.4	110.8
8	9	10	-914.4	-135.5	-0.183	-135.5	-0.069	-97.54	-0.023	-67.73	0	0	0.023	67.73	0.069	97.54	0.183	135.5	916.4	135.5
10	11	12	-914.4	-157.6	-0.183	-157.6	-0.069	-113.5	-0.023	-78.79	0	0	0.023	78.79	0.069	113.5	0.183	157.6	916.4	157.6
12	13	14	-914.4	-179.7	-0.183	-179.7	-0.069	-129.4	-0.023	-89.84	0	0	0.023	89.84	0.069	129.4	0.183	179.7	916.4	179.7
14	15	16	-914.4	-201.8	-0.183	-201.8	-0.069	-145.3	-0.023	-100.9	0	0	0.023	100.9	0.069	145.3	0.183	201.8	916.4	201.8
16	17	18	-914.4	-222.7	-0.183	-222.7	-0.069	-160.3	-0.023	-111.3	0	0	0.023	111.3	0.069	160.3	0.183	222.7	916.4	222.7
18	19	20	-914.4	-271.9	-0.183	-271.9	-0.069	-195.7	-0.023	-135.9	0	0	0.023	135.9	0.069	195.7	0.183	271.9	916.4	271.9
20	24	28	-914.4	-822.2	-0.183	-822.2	-0.069	-592	-0.023	-411.1	0	0	0.023	411.1	0.069	592	0.183	822.2	916.4	822.2
28	32	36	-914.4	-1192	-0.183	-1192	-0.069	-858.5	-0.023	-596.2	0	0	0.023	596.2	0.069	858.5	0.183	1192	916.4	1192
36	40	44	-914.4	-1562	-0.183	-1562	-0.069	-1125	-0.023	-781.2	0	0	0.023	781.2	0.069	1125	0.183	1562	916.4	1562
44	48	52	-914.4	-1932	-0.183	-1932	-0.069	-1391	-0.023	-966.2	0	0	0.023	966.2	0.069	1391	0.183	1932	916.4	1932
52	56	60	-914.4	-2303	-0.183	-2303	-0.069	-1658	-0.023	-1151	0	0	0.023	1151	0.069	1658	0.183	2303	916.4	2303

Appendix C Illustration of Case_0_0 and Case_31_0